Impedance and Electromechanical Vibration Measured in the Organ of Corti up to 50 kHz: New Insights for Cochlear Amplification

Dissertation
zur Erlangung des Grades eines Doktors
der Naturwissenschaften
der Fakultät für Mathematik und Physik
der Eberhard-Karls-Universität zu Tübingen

vorgelegt von

Marc Philippe Scherer
aus Tettnang

2005

Tag der mündlichen Prüfung:	4. Oktober 2005
Dekan:	Prof. Dr. P. Schmid
1. Berichterstatter:	Prof. Dr. A.W. Gummer/Prof. Dr. H. Ruder
2. Berichterstatter:	Prof. Dr. D. Kern
3. Berichterstatter:	Prof. Dr. Ch. Steele

Contents

Abbreviations

BM	Basilar membrane
CF	Characteristic frequency
HeC	Hensen's cell
IHC	Inner hair cell
IPC	Inner pillar cell
ISC	Inner sulcus cell
OC	Organ of Corti
OHC	Outer hair cell
OPC	Outer pillar cell
OT	Outer tunnel
RL	Reticular lamina
TM	Tectorial membrane
ToC	Tunnel of Corti

Summary

To elucidate mechanisms of cochlear amplification, an *in-vitro* preparation of the cochlear partition from the guinea-pig inner ear without tectorial membrane and with clamped basilar membrane was developed. Subsequently, the organ of Corti was characterized at up to 9 radial positions (between inner sulcus cells and Hensen's cells) in terms of a Norton equivalent circuit: as a force source in parallel with a load impedance, both acting between the clamped basilar membrane and the reticular lamina.

Three types of results are presented here: the mechanical point impedance and the electrically evoked velocity were measured in the ranges 0.48–50 kHz and 0.48–67 kHz, respectively. From these two quantities, the associated source force was calculated. Characteristic filter parameters were extracted from the frequency responses of all three quantities.

Firstly, an innovative method was developed to measure the mechanical driving point impedance of biological structures up to at least 50 kHz. The technique employs an atomic force cantilever with a ferromagnetic coating and an external magnetic field to apply a calibrated force to the cantilever. Measurement of the resulting cantilever velocity using a laser Doppler vibrometer yields the impedance. A key feature of the method is that it permits impedance measurements on biological tissues in physiological solutions at acoustical frequencies.

As a prerequisite for the impedance measurement, existing models of the high-frequency dynamical response of atomic force cantilevers in viscous fluids were extended, and a method was developed to confirm experimentally the validity of the theory up to 67 kHz in air and CCL_4. The theory permits calibration of these cantilevers in fluid above their first resonant frequency. This is important for general applications such as dynamic AFM modes and dynamic mechanical measurements on biological tissues.

The measured mechanical impedance of the organ was described by a generalized Voigt-Kelvin viscoelastic model, in which the stiffness was real-valued and independent of frequency, but the viscosity was complex-valued with positive real part, which was dependent on frequency and negative imaginary part, which was independent of frequency. There was no evidence for an inertial component. The magnitude of the impedance was greatest at the tunnel of Corti, and decreased monotonically in each of the radial directions.

Secondly, the velocity of the upper surface of the organ resulting from the electromotile action of the outer hair cells was measured with a laser Doppler vibrometer at the same radial positions as the impedance. Displacement was calculated from velocity. Displacement amplitudes (normalized to electric current density) were constant up to about 10–20 kHz, above which they decreased with 12 dB/oct. Two phase reversals were observed – one at the tunnel of Corti and the other at the outer tunnel. Upon administration of sodium salicylate, amplitudes decreased by a factor of two, independent of frequency, with no change in phase. Similar results were obtained with a chloride channel blocker, anthracene-9-carboxylic-acid, the amplitudes decreasing 5-fold. Furthermore, a pharmacological block of the conductances in the outer hair cell stereocilia had no significant effect, whereas blocking all cation channels in the outer hair cell basolateral

membranes reduced amplitudes 2-fold. These pharmacological experiments showed that 1) the electrically induced vibration of the organ of Corti derives from the electromechanical action of the outer hair cells and 2) the electric current enters the cell through the basolateral membrane.

Thirdly, the force acting on the reticular lamina was calculated for each of the radial positions from the velocity and the impedance of the organ of Corti. Force on the cuticular plates of the outer hair cells exhibited a broad amplitude maximum at 7–20 kHz with Q_{3dB} of 0.6–0.8, followed by a first-order low-pass characteristic at higher frequencies. The force response on the inner hair cells was similar to that on the outer hair cells, but with reversed phase. However, the low-frequency amplitude was smaller than for the outer hair cells by up to 15 dB.

The following implications of these results for cochlear amplification are suggested: 1) the purely viscoelastic behavior of the organ broadens the frequency response of the displacement compared to that for an inertial load: its filter function is that of a first-order low-pass rather than a second-order resonant filter. The relevance of the point measurements lies in the fact that the tectorial membrane is attached to the reticular lamina through the stereocilia of the outer hair cells, so that force is exerted on quasi-discrete points. 2) Localized amplification of the basilar-membrane travelling wave cannot be accounted for by a place specific displacement resonance of the organ of Corti, but a putative second resonance can occur only at the tectorial-membrane level. 3) The reticular lamina does not move as a rigid plate, but exhibits phase reversals at two radial locations. 4) For extracellular stimulation, the bandwidth of electrically evoked force and vibration is always greater than or equal to the characteristic frequency of a certain cochlear place. 5) The force maximum is consistent with the recent proposal of a piezoelectric resonance of the outer-hair-cell lateral wall. 6) The data show that the force can compensate the amplitude attenuation – but not the phase lag – caused by electrical low-pass filtering of the receptor potential. 7) In the experimental configuration used here, extracellular current enters the outer hair cells through their basolateral membrane rather than their stereocilia. 8) The observed low-frequency attenuation of the inner hair cell force indicates that the mechanical coupling between outer and inner hair cells is high-pass filtered. This supports the view that the organ of Corti is essentially an elastic, fluid filled tube, in which radial coupling is dominated by hydrodynamical forces.

These results experimentally elucidate previously unknown micromechanical details of cochlear amplification.

Chapter 1. Introduction

This chapter gives an overview of the mechanisms involved in peripheral sound processing and the capabilities of the auditory system. The importance of a better understanding of the micro-electromechanical processes in the cochlea for improving diagnosis and therapy of hearing impaired patients is pointed out. The concept of experiments and evaluation procedures carried out in this study is outlined.

1.1 Motivation

Notwithstanding the more than 100 years of auditory research, the understanding and treatment of diseases of the auditory system is far from being satisfactory. This is of particular relevance since hearing impairment is one of the most frequent diseases in the industrial societies. In Germany, 12–15 million patients (15–19% of the population [89]) suffer from inner ear disorders. Hearing loss and/or tinnitus occur spontaneously, congenitally, and through exposition to chemicals (also medication), and intense noise (work-related or during recreational activities) [129]. The German army alone produces 40 noise trauma *per day*, half of which remain irreversible [181]. Most importantly, speech recognition performance, especially in background noise, degrades strongly even upon mild damage to the inner ear. This has enormous consequences for the affected patients: maintaining their normal social and professional environments often becomes impossible. The associated economic loss, both for the individual and the society, is significant.

One reason why to date treatment of inner ear disorders is very limited is the lack of knowledge about the detailed micro-electromechanical mechanisms within the cochlea. Despite the considerable worldwide efforts and the large number of publications in the field, the small size, inaccessibility, and vulnerability of the cochlea have impeded clarification of cochlear function. Therefore, more basic research and a better understanding of the details is a prerequisite for improved diagnosis and therapy of inner ear diseases.

Recent modelling studies [38, 50, 87] have emphasized the lack of reliable experimental data on the mechanical and electromechanical properties of the most important structure of the cochlea – the cochlear partition. This work is intended to fill some of the gaps by providing the compressional mechanical impedance of the organ of Corti and the mode of deformation of the organ of Corti when the outer hair cells (OHCs) generate a mechanical force via their electromechanical transduction mechanism.

1.2 Signal processing capabilities of the ear

In order to give an impression of the high degree of perfection to which the auditory system of mammals has evolved, its technical specifications are outlined in the following.

1.2.1 Sensitivity

Sound level is usually measured in units of dB SPL (decibel sound pressure level), defined as [7]

$$\mathrm{SPL} \;=\; 20\log_{10}\frac{p_{eff}}{p_{ref}}\;\;[\mathrm{dB}] \tag{1.1}$$

where p_{eff} is the effective RMS (root mean square) variation of pressure as a sound signal propagates in air and $p_{ref} := 2 \times 10^{-5}$ Pa is a reference pressure. p_{ref} is chosen so that 0 dB SPL corresponds to the human threshold of hearing at 1 kHz. The highest sensitivity of -3 dB SPL in humans is reached at 4 kHz [202]. The associated energy can be estimated as follows: sound intensity (energy flow per unit area) of a plane or spherical sound wave in air is [7]

$$I = \frac{p_{eff}}{\rho_0 c} \quad \left[\frac{\mathrm{J}}{\mathrm{sm}^2}\right] \tag{1.2}$$

where $\rho_0 \approx 1.18$ kg/m^3 is the mean (static) density of air and $c \approx 344$ m/s the speed of sound (both depending on pressure and temperature). Only part of the total area of the tympanic membrane is relevant for sound transmission: the so called pars tensa with an area of 55 mm^2 [14]. This gives an energy flow into the auditory system of 1.9 pJ/s at -3 dB SPL. Deflection of the stereocilia (see Sec. 1.3) at these sound levels is estimated to be 0.1–1 Å [162], while Brownian motion already causes RMS deflections of 1 Å [9].

Hearing threshold decreases with stimulus duration and reaches an asymptotic value at durations greater than 200 ms [54], so that an acoustic energy of about 0.4 pJ is necessary to elicit sound perception.

In comparison, the human visual system is most sensitive in the scototopic (dark-adapted) state at a wavelength of 507 nm [193]. Contrast is perceivable at light intensities greater than 5×10^{-3} cd/m^2 ≈ 7.3 μW/m^2 [8]. With a pupil diameter of 7.1 mm [11] this corresponds to an energy flow of 290 pJ/s into the eye. The integration time of the rod cells is about 100 ms, so that a picture looms above an optical energy of 29 pJ.

1.2.2 Frequency resolution

A psychoacoustic measure of frequency resolution is the so called 'frequency difference limens' defined as the difference in frequency Δf between two sinusoidal tones of equal sound level that can just be detected by a test person. In humans the best relative frequency resolution $\Delta f/f \approx 1.5 \times 10^{-3}$ occurs at $f \approx 2$ kHz [105]. If the duration of the tone is decreased from 200 ms to 6.25 ms, $\Delta f/f$ degrades to 5×10^{-3}. The best frequency resolution is achieved at sound levels of 20–30 dB SPL.

The highest frequency resolution of all animals is achieved by bats. In *rhinolophus ferrumequinum*, a bat using constant frequency sounds for echolocation, a value of $\Delta f/f \approx 5 \times 10^{-4}$ at the second harmonic of the emission frequency can be estimated from the tuning curves of single neurons in the nucleus cochlearis (the central terminal of the auditory nerve) [91].

In humans the loss of frequency discrimination is associated with difficulties in speech recognition, especially in the presence of background noise [202]. Therefore, the high frequency resolution of the auditory system is an essential prerequisite for normal social interaction of humans and its deprivation cannot be compensated by a hearing aid. This is one of the reasons why a causal therapy of inner ear diseases is of paramount importance.

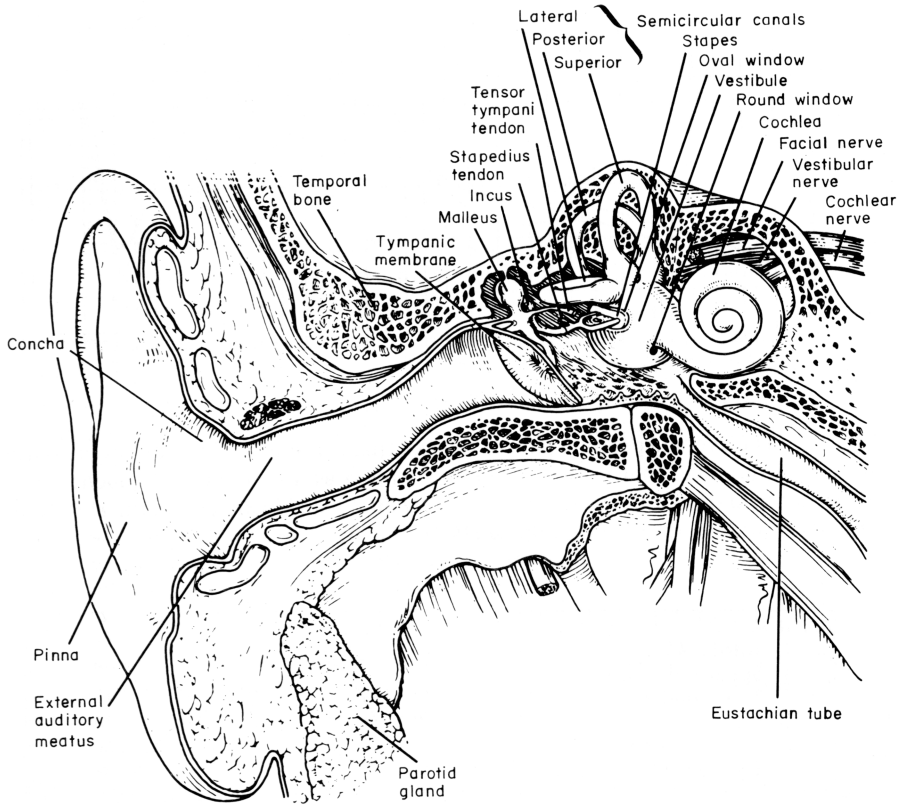

Figure 1.1: *Overview of the human auditory periphery. Sound is transmitted to the cochlea via the tympanic membrane and middle ear ossicles (malleus, incus, and stapes). Figure taken from Pickles [128].*

1.2.3 Intensity resolution

The human ear can process sound levels between 0–120 dB SPL, a range of six orders of magnitude [25]. The intensity resolution, that is the ability to discriminate two tones at different levels, does not quite obey Weber's law $\Delta p/p = \text{constant}$, which is typical for sensory systems, but instead

$$\frac{\Delta p}{p} = \frac{1}{4}\left(\frac{p}{p_0}\right)^{-\frac{1}{6}} \tag{1.3}$$

for sinusoidal tones (p_0 is the threshold at the respective frequency, p the stimulus level and Δp the just resolvable difference) [54].

1.2.4 Temporal resolution

The ability to detect transient changes in amplitude or frequency of a sound signal depends strongly on its envelope. Typically, above 30 dB SPL, it is on the order of several milliseconds [187]. Towards threshold temporal resolution degrades.

1.3 Anatomy of the inner ear – the cochlea

Most likely, not all readers of this text are familiar with the anatomy of the ear. Therefore, a description of the relevant structures is included. Some of this section follows parts of chapter three of the book by Pickles [128].

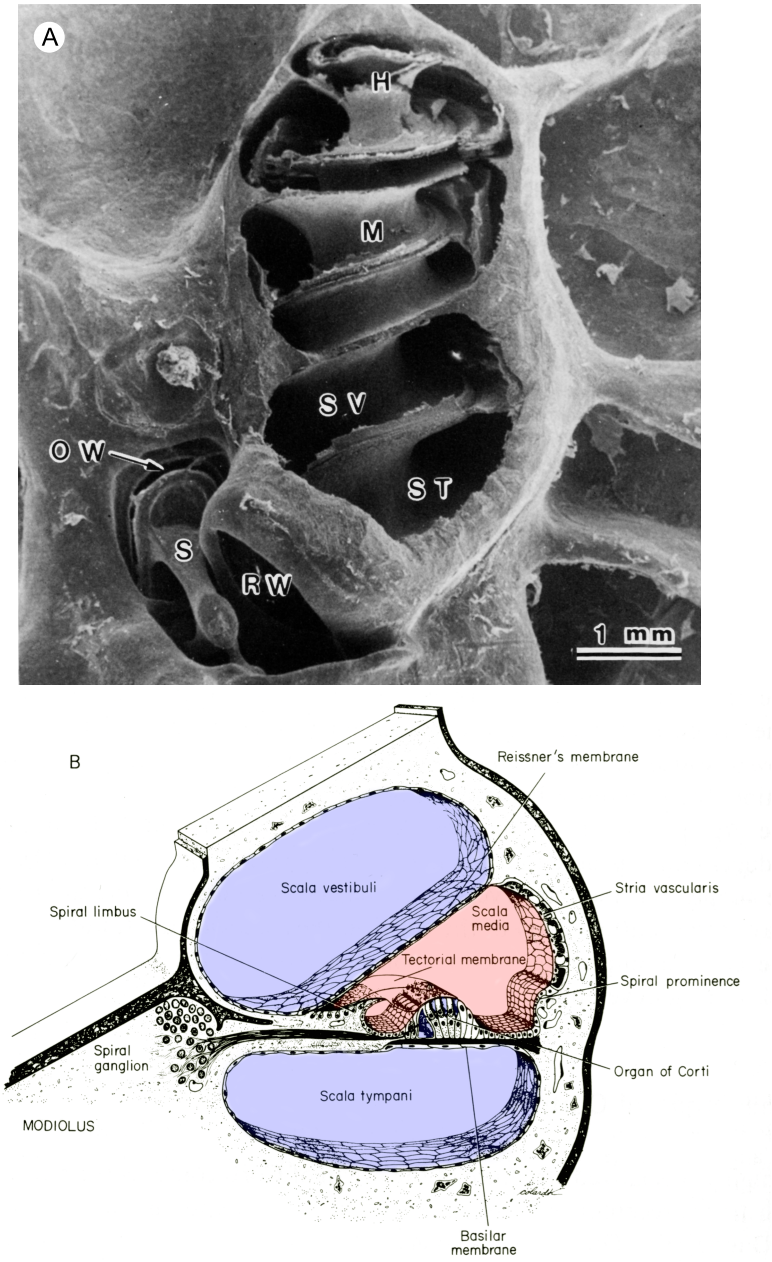

Figure 1.2: *Two views of the coiled cochlear duct. A: electron micrograph of the opened gerbil cochlea. SV: scala vestibuli; ST: scala tympani; M: modiolus; H: helicotrema; S: stapes; OW: oval window; RW: round window (Figure taken from Jahn and Santos-Sacchi [75]). B: cartoon depicting the three fluid filled compartments and their separating membranes. Endolymph is colored red and perilymph blue. The organ of Corti, sitting on the basilar membrane, is the primary sensory epithelium. The so-called cochlear partition includes basilar membrane, organ of Corti, and tectorial membrane. The auditory nerve follows a cavity inside the modiolus (Figure adapted from Pickles [128]).*

1.3.1 General Anatomy

Anatomy and electrophysiology of the auditory periphery are very similar among mammals, the structures differing mainly in size. It seems justified, therefore, to assume that the cochlear mechanisms found in guinea pig, gerbil, chinchilla, mouse, or cat (typical animal models for auditory research) are much like those in humans.

Fig. 1.1 shows the position of the human cochlea in relation to the other structures of the ear. It is embedded deep in the temporal bone. In man (guinea pig), the cochlea is about 10 (5) mm wide and 5 (5.5) mm from base to apex. It consists of a coiled, fluid filled channel running from the oval and round windows (the base of the cochlea) to the end of the spiral (the apex, Figs. 1.2 and 1.3). This channel has bony walls and is separated into three fluid compartments: scala vestibuli, scala media, and scala tympani. The former are separated by Reissner's membrane and the latter by the cochlear partition including the basilar membrane (Fig. 1.2). The basilar membrane is 35 (18.5) mm long. Total fluid volume within the cochlea is 192.5 (20.9) μL [15, 44, 168, 189]. The auditory nerve and the blood vessels enter the cochlea by way of a central cavity, the modiolus.

The fluids in the three compartments are of different ionic compositions: while scala vestibuli and scala tympani are filled with perilymph, scala media is filled with endolymph. The composition of perilymph is very similar to that of normal extracellular fluid in the body, while the composition of endolymph is similar to that of intracellular solutions. The ionic composition of endolymph is maintained by stria vascularis, a secretory structure at the outer perimeter of scala media. The fluid in scala media is at a potential of +80 mV (the endocochlear potential) with respect to the perilymphatic space. The sign of the endocochlear potential is opposite to that of the Nernst-potential between the two fluids. Consequently, the observation that upon anoxia the endocochlear potential quickly (within 2 min) changes from +80 mV to -40 mV [88] led to the conclusion that the endocochlear potential is highly dependent on metabolism. Although the details of its generation remain obscure, the endocochlear potential is likely produced by ion transporters in stria vascularis [154, 176, 190, 191].

Scala vestibuli and scala tympani are joined at the apical end of the cochlea by an opening known as the helicotrema. Cross section of cochlear duct decreases from base to apex with the spatial relations between the scalae remaining approximately constant [189]. However, the basilar membrane tapers in the opposite direction: it is narrow at the base and broad at the apex.

Reissner's membrane consists of only one or two cell layers and is thought to have no influence on fluid mechanics within the duct [29, 98, 113]. Presumably, its main purpose is to maintain separation of endolymph and perilymph. In contrast, the cochlear partition is an extremely specialized structure which is central to the transduction of a pressure wave to a neural signal. It is here that the auditory nerve terminates.

Sound is transferred to the cochlea via vibration of the footplate of the stapes, the innermost of the middle ear ossicles. It is in contact with the oval window, a membraneous window opening into scala vestibuli. The conservation of volume in the cochlea is achieved by a second membraneous window opening into scala tympani, the round window. Therefore, motion of the stapes is not primarily leading to a compression of the cochlear fluids, but to displacement of cochlear partition and round window membrane. This deflection is initiated at the base of the cochlea and propagates to the apex in a manner similar to a surface wave (Fig. 1.4). It is called the travelling wave [189].

The amplitude of the travelling wave is not uniform along the cochlea. Instead, for sinusoidal stimulation, basilar-membrane displacement increases monotonically from base to apex, reaches a maximum, and then decreases quickly. The longitudinal place of the maximum depends on frequency: it is near the base for the highest audible frequencies and near the apex for the lowest ones. Therefore, since deflection of the basilar membrane is closely related to generation of a neural signal at that place (see Sec. 1.3.2), the cochlea essentially behaves as a frequency analyzer. The frequency which elicits a maximum displacement at a particular longitudinal place is called the characteristic frequency (CF) of that place.

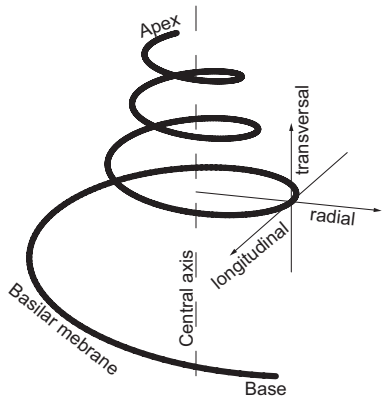

Figure 1.3: *Coordinate system used in this study (and in the literature). The thick line depicts the basilar membrane. The base of the cochlea is the part adjacent to the round window and the apex is the opposite end. Longitudinal: along a tangent of the spiral (distance is measured from the base); radial: outward from the central axis of the spiral; transversal: perpendicular to the plane of the basilar membrane, from scala tympani to scala media.*

1.3.2 Cochlear partition

The cochlear partition includes the basilar membrane, the overlying organ of Corti, and the tectorial membrane (Figs. 1.2 and 1.5).

The basilar membrane is a fibrous structure with the fibers leading from its inner suspension, the osseous spiral lamina, to the outer suspension in the cochlear wall.

The highly specialized structure of the organ of Corti contains the inner and outer hair cells (IHC and OHC). One end of these cells (the apical end) is integrated in the upper surface of the organ of Corti, the reticular lamina. From this end small hairs (the stereocilia) protrude into the scala media fluid space.

The IHCs are the primary sensory cells: deflection of their stereocilia leads to an intracellular potential change and to the generation of an action potential in the afferent[1] nerve fiber terminating at their basal pole. The innervation of OHCs is predominantly efferent. Consequently, they are believed to be of importance for the local mechanical properties in a way that can be controlled by the brain (see also Sec. 1.4). In man, there is one row of IHCs and three (basally) to five (apically) rows of OHCs (guinea pig: three rows). There are about 4000 IHCs in the human cochlea.

The organ of Corti is given rigidity by an arch formed by inner and outer pillar cells (IPC and OPC) extending between basilar membrane and reticular lamina. These cells are assumed to be relatively stiff since they contain densely packed, axially running microtubules [179]. The arch is surrounded by phalangeal cells; that is, by cells with processes which end in a plate in the reticular lamina. The inner phalangeal cells completely surround the IHCs. On the modiolar side of the IHCs, there is a number of soft supporting cells (the inner sulcus cells).

The outer phalangeal cells, called Deiters' cells, form cups holding the basal ends of the OHCs and extend from there to the basilar membrane. They send fine processes (the phalanges) up to the reticular lamina. External to the OHCs there is a row of soft supporting cells called Hensen's cells (HeC).

It is noteworthy that the volume of the organ of Corti is not completely filled by cellular structures. In the tunnel of Corti (spanned by the inner and outer pillar cells), around the OHC, and in the outer tunnel (between OHC and HeCs) there are spaces

[1] In contrast to electrical cables, nerve fibers transmit action potentials only in one direction: *afferent* fibers from the periphery to the central nervous system and *efferent* fibers in the opposite direction.

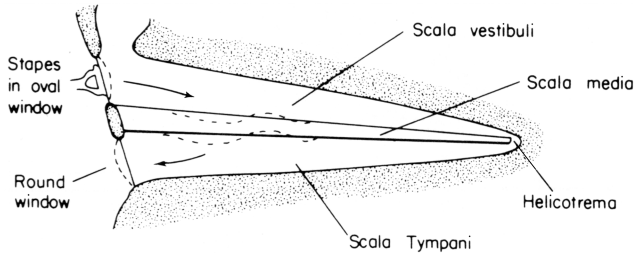

Figure 1.4: *Schematic view of the uncoiled cochlea. An indentation of the oval window membrane by the stapes footplate leads to an outward motion of the round window and, for frequencies above a few Hertz, to a displacement of the cochlear partition which propagates from base to apex – the so-called travelling wave. Figure taken from Pickles [128].*

filled with perilymph. Most importantly, the border between endolymph and perilymph is the *upper* surface of the organ of Corti, that is the reticular lamina. Consequently, inner and outer hair cell stereocilia are bathed in endolymph while their cell somata are surrounded by perilymph (see also Sec. 1.4).

The organ of Corti is covered by a gelatinous and fibrous flap, the tectorial membrane (Fig. 1.5). The tectorial membrane is fixed only on its inner edge, where it is attached to the limbus. There is disagreement in the literature as to whether or not it is joined to the reticular lamina by small trabeculae or processes and by a so-called marginal net [48, 85, 96, 97, 172, 186].

The longest OHC stereocilia are shallowly but firmly embedded in the under-surface of the tectorial membrane [41]. The IHC stereocilia are probably not embedded and might fit loosely into a raised groove known as Hensen's stripe on the under surface of the tectorial membrane [48, 96, 97, 172, 175, 186]. Therefore, it is usually concluded that shearing *displacement* between tectorial membrane and reticular lamina is the stimulus for bending the OHC stereocilia, while at acoustic relevant frequencies shearing *velocity* provides the driving force for bending of the IHC stereocilia via the fluid drag [147, 164, 172].

1.4 State of the art

It has been shown that the ear's outstanding sensitivity and frequency selectivity found both in auditory nerve signals and psychoacoustic experiments are already established at the mechanical level of the travelling wave on the basilar membrane [20, 83, 112, 140, 142, 145, 148, 162, 163].

The sharp basilar-membrane tuning observed in the living animal depends on a normal physiological condition of the cochlea: it disappears upon pharmacological alteration of the endocochlear potential (Sec. 1.3) [43, 143, 165], acoustic trauma [20, 127, 144, 162], and death of the animal [20, 120, 140, 145, 162]. These observations, together with theoretical considerations [86, 188] led to the postulation of a physiologically vulnerable mechanical feedback mechanism operating at acoustic frequencies, which enhances the deflection of the basilar membrane, particularly at the location of the characteristic frequency [28, 31, 77, 114, 205]. In this concept, electrochemical energy provided by the different ionic compositions of endo- and perilymph is converted to mechanical energy amplifying the travelling wave. Indeed, analyses of the power flux along the cochlear duct has shown amplification in sensitive cochleae and no amplification in insensitive ones [12, 36, 37].

The putative actor element for this feedback are the OHCs embedded in the organ of Corti. It has been shown that their length changes in response to a variation of electrical potential across their basolateral membrane [5, 13, 199]. This so-called electromechanical

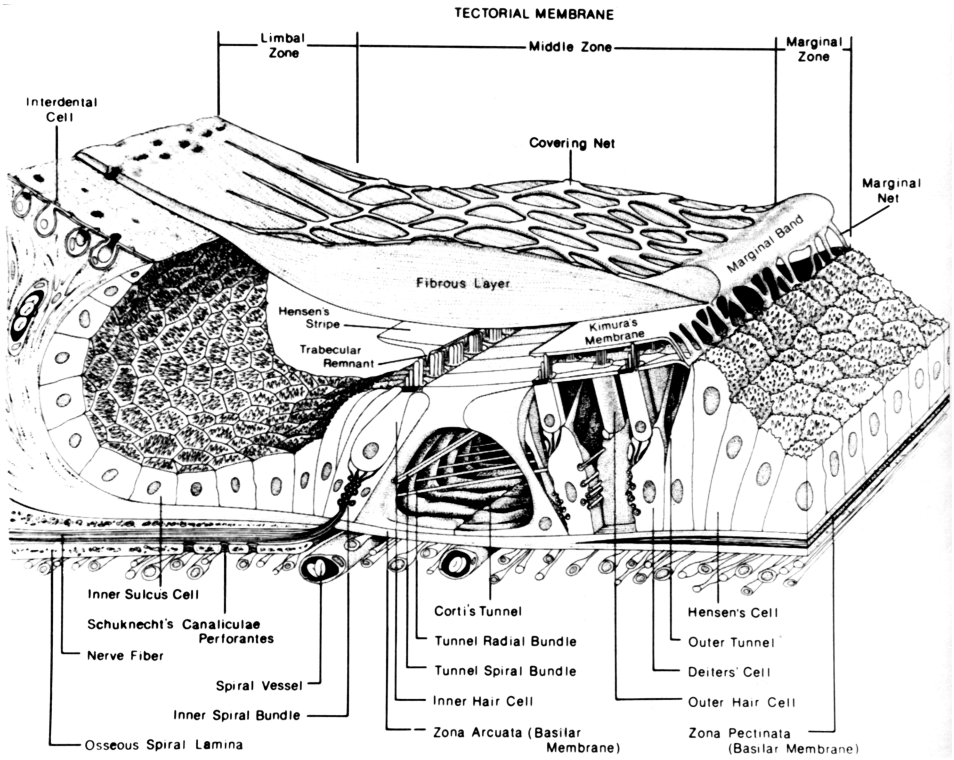

Figure 1.5: *Detailed view of the cochlear partition, including basilar membrane, cellular structures of the organ of Corti, and tectorial membrane. Displacement of the basilar membrane in the transverse direction leads to shearing between reticular lamina (the upper surface of the organ of Corti) and tectorial membrane and to a deflection of the stereocilia. The extracellular spaces of tunnel of Corti, around the outer hair cell somata, and outer tunnel are filled with perilymph. Figure taken from Lim [96].*

transduction works up to at least 79 kHz [46]. The mechanism involves a voltage sensitive protein (prestin) [94, 99, 157, 200] which is located in the basolateral membrane of the cell [27, 155] in extremely high density [79]. There is evidence that intracellular Cl^- is bound to the prestin and acts as voltage sensor [123]. A change in transmembrane voltage is assumed to alter the conformation of the prestin leading to a change of the area occupied by the molecule in the plasma membrane. Due to the high density of prestin in the membrane this leads to a macroscopic variation of cell surface area. Presumably, this area change is converted to a cell length change by the specialized cytoskeleton of the OHCs. The deformation response of isolated OHCs in the microchamber configuration does not exhibit a resonance peak, but appears to be second-order low-pass filtered [46]. This agrees with the theoretical result that the fluid load on isolated OHCs leads to a highly damped, non-resonant system, if the electric stimulus is kept constant [180].

The sensor element of the feedback loop is the stereocilia bundle at the apical end of the OHCs. The stereocilia contain mechanosensitive non-selective cation channels (so-called transducer channels) which open upon deflection of the bundle in the direction of the tallest stereocilium. It is essential for cochlear amplification that there are two different fluid compartments surrounding the OHCs: the stereocilia are contained within endolymph, whereas their somata are surrounded by perilymph. The main difference between these fluids are the concentrations of Na^+ (perilymph: 145 mM, endolymph: 1.3 mM), K^+ (perilymph: 6 mM, endolymph: 157 mM), and Ca^{2+} (perilymph: 0.6 mM, endolymph: 0.023 mM). In addition to the endocochlear potential of +80 mV (see Sec. 1.3.1), the intracellular potential of the OHCs is -60 mV (relative to the surrounding perilymph), so that the potential difference between endolymph and OHC cytosol is 140 mV. In response to opening of the transducer channels, K^+ flows into the

cell, driven by the electrochemical gradient. Consequently, the potential within the cell changes. This deviation from the resting potential is called the receptor potential. The process of converting (mechanical) deflection of the stereocilia into a receptor potential is called mechanoelectrical transduction. In the physiologically relevant deflection range of the stereocilia tips (0.1–10 nm), the relation between deflection and receptor potential is linear to a good approximation.

Thus, the coaction of mechanoelectrical and electromechanical transduction converts a minute force on the stereocilia into a much stronger, measurable force generated by the OHC somata, with energy provided by an electrical battery. It is conceivable that such an electromechanical 'transistor' is the key element for a cochlear amplifier. Indeed, experiments with prestin knock-out animals strongly suggest that this is the case [94].

An open question is whether the receptor potential is low-pass filtered due to the RC-element formed by the transducer resistance and cell membrane capacitance. In isolated cells, the corner frequency of the corresponding low-pass characteristic is 50–500 Hz [65, 130]. However, to account for the physiological frequency range of up to 100 kHz, the cochlear amplifier has to function far above these corner frequencies. Possibly, an electromechanical resonance in the OHC lateral wall might (partially) compensate the presumed potential attenuation at high frequencies [171, 192].

Alternatively, Hudspeth [70] has proposed that the electromechanical feedback at high frequencies is derived from motors in the stereocilia, that are driven by calcium entering the stereocilia through open transducer channels.

OHC stereocilia are mechanically connected to the lower side of the tectorial membrane. Therefore, shearing between reticular lamina and tectorial membrane is the determining factor for a deflection of the OHC stereocilia. At low frequencies this shearing occurs, because reticular lamina and tectorial membrane rotate about two separate pivots, namely spiral lamina and the attachment of the tectorial membrane to the spiral limbus, respectively [16, 49, 137, 185]. The lever ratio between transverse basilar-membrane displacement and radial stereocilia deflection is approximately unity in this case [26]. As yet, it is not clear how the organ vibrates at high frequencies.

Since OHCs *in vivo* are part of the sophisticated mechanical structure of the organ of Corti, the question arises as to how the forces generated by the OHCs are coupled into the cochlear partition in a way that leads to amplification of the travelling wave. Recent theoretical investigations have emphasized the importance of experimental data about the pattern of deformation within the organ of Corti in order for cochlear models to require less a priori assumptions and to permit the estimation of the number of degrees of freedom within the organ of Corti [38, 50, 87].

One way to experimentally ascertain the deformation of the organ of Corti is to measure the radial pattern of deflection of the basilar membrane in the direction perpendicular to the basilar membrane. *In-vivo* measurements of acoustically evoked basilar-membrane displacements showed that while in the dead cochlea the basilar-membrane deflection phase is constant across its entire width, in the healthy cochlea the phase can vary across the basilar membrane [116, 117] (guinea pig). However, Cooper [19] (guinea pig and gerbil) found only small phase shifts in a similar experiment. Rectangular electric current pulses applied to the organ of Corti *in vivo* led to a counterphasic motion of zona arcuata and zona pectinata of the basilar membrane [121] (guinea pig). The relative motion of basilar membrane and reticular lamina was examined in the apical turn of the cochlea *in vivo* [101] (guinea pig): DC electrical stimulation *in vivo* led to a counterphasic motion between basilar membrane and reticular lamina above Hensen's cells. Motion of the reticular lamina in the radial direction during electrical stimulation *in vitro* [135] (guinea pig) and a resonant vibration of the tectorial membrane during sound stimulation *in situ* [57] (guinea pig) are further observations on the local mechanics of the organ of Corti and are thought to be essential for the normal function of the mammalian cochlea [4, 57, 64, 106, 110, 207].

Besides being fundamental for the cochlear amplification process, complex vibration modes induced by the electromotile response of the OHC could account for the complex and level-dependent electrical response pattern of the inner hair cells *in vivo* [18, 24, 106, 150]. Another important question, related to the cochlear amplifier, is if the OHC transmembrane potential, which is the driving stimulus for the electromotility [156], is low-pass filtered *in situ* due to the properties of the cell membrane [65, 130]. From the experiments mentioned above, little information about the relative motion of the constituents of the organ of Corti, in particular about the relative motion of basilar membrane and reticular lamina, could be obtained.

1.5 Purpose of this study

In order to elucidate the detailed mode of operation of the cochlear amplifier, the mechanical and electromechanical properties of an essential subsystem of it – the organ of Corti – were investigated *in vitro* (for preparation see Fig. 2.1). The analysis of only a subsystem is justified by the complexity, vulnerability, and inaccessibility of the complete system – the cochlea. It is important to note that in my preparation the basilar membrane is mechanically clamped and the tectorial membrane is removed (see Sec. 2.1). Therefore, the mechanics of the organ itself is exclusively observed.

It is also the purpose of this work to describe the organ of Corti abstractly by an equivalent (electrical or mechanical) circuit and to specify its characteristic parameters. There are two reasons for this approach.

Firstly, the mechanical and electrochemical structure of the organ of Corti is very complex, so that a detailed model necessarily incorporates a great many degrees of freedom. Consequently, implementation of a such a model (e.g. with the finite element method), as well as the numerical handling (computing time) is cumbersome and time consuming. Most likely however, for a complete understanding of the micro-electromechanics in the inner ear, inclusion of these many degrees of freedom is neither necessary nor beneficial. Therefore, reduction of the model to a few degrees of freedom stands to reason.

Secondly, considering the coding of sound information in the auditory nerve, it would be helpful to describe the properties of this coding by the theory of transmission systems. For this purpose a representation of the inner ear as block diagram with known parameters is desirable. Applications like the implementation of artificial inner ears and the investigation of the influence of parameter variations on the transmission properties would profit from such a representation. An equivalent circuit of the organ of Corti would be a natural part of this block diagram.

It is known from electric circuit theory that every linear circuit can be described by an associated Thévenin or Norton equivalent circuit. Therefore, as long as the *one-dimensional* motion of a single point of the upper side of the organ relative to the mechanically clamped basilar membrane is considered, even the complicated organ of Corti can be described by an equivalent circuit with two parameters. Since the OHCs correspond to a force source acting on the impedance of the surrounding organ, a Norton description appears most intuitive and is used in the following. Accordingly, the two parameters are the force source $F(\omega)$ and the mechanical impedance $Z(\omega)$, both depending on angular frequency ω (Fig. 2.4). The velocity of the upper surface of the organ, v, is given by $v = F/Z$.

The challenge of this study was to determine the two parameters $Z(\omega)$ and $F(\omega)$ experimentally. For this purpose, two linearly independent measurements are necessary *for every frequency*. For experimental reasons, measurement of Z and v was preferred and F was calculated. Since the parameters describe only one point on the upper surface of the organ, they were determined for 5–10 radial positions between inner sulcus cells

and Hensen's cells and three longitudinal regions corresponding to the first three cochlear turns.

The measurement of v was straight forward: an electric current was applied across the preparation and the velocity of the reticular membrane was measured with a laser Doppler vibrometer (LDV).

The measurement of Z, however, required the development of a novel technique which is described in detail in Chapter 2. This technique is based upon the ability 1) to determine the mechanical driving point impedance of an atomic force cantilever in fluid up to 50 kHz and 2) to determine the equivalent point force at the cantilever tip from an area force applied to the whole cantilever. This technique and the impedance measurements have recently been published in Biophysical Journal [160]. The description of electromechanical force and displacement is under review for publication in Proc. Natl. Acad. Sci. USA.

At the beginning of this work, no experimental method could be found in the literature to reliably calibrate the impedance of an atomic force cantilever in fluid above its first resonance frequency. Consequently, the theory of Sader [152] was extended to suit the present case and a method was developed to apply a Coulomb point force to the tip of the cantilever to validate the theory. This work was published in J. Appl. Phys. [159].

Chapter 2. Methods

In this chapter the experimental configurations and evaluation procedures for all three types of measurements (point force on the cantilever, impedance of the sample, and electrically evoked deformation of the sample) are described. The mathematical treatment of cantilevers in fluid as described by Sader [152] is summarized and extended.

2.1 Animal preparation

Preparations were made from the first three turns of the adult, pigmented guinea-pig cochlea, corresponding to distances of 3.8–13 mm from the round window [44, 189]). Young female animals were used, weighed 300–400 g, had a positive Preyer's reflex, and were killed by rapid cervical dislocation. The preparation included the modiolar bone, basilar membrane, and overlying organ of Corti of a half to a full turn (Figs. 2.1 and 3.4). The tectorial membrane was removed with an ultra-fine needle. Care and maintenance of the guinea pigs was in accordance with institutional and state guidelines. During preparation and experiment the sample was kept in Hanks' balanced salt solution (Sigma, supplemented with 4.1 mM $NaHCO_3$ and 10 mM HEPES buffer, adjusted to 310 ± 10 mOsm and pH 7.38 ± 0.02).

The organ of Corti was mounted on a custom-made support within the experimental chamber (Fig. 2.1). The design of the support was such that the basilar membrane was lying on a flat surface to the left and right of a 80 μm wide slit in the support allowing electric current to pass through the slit and the preparation. Hydrodynamic forces were expected to severely attenuate basilar-membrane motion in the transverse direction and this was confirmed by directly measuring basilar-membrane velocity with the interferometer during electrical and mechanical (with the cantilever) stimulation – it was below noise level (-30 dB). The mechanically 'clamped' configuration of the basilar membrane allowed the impedance and deformation of the organ of Corti to be investigated without the influence of the basilar membrane. For the deformation measurements, velocity of the reticular lamina was detected directly above the slit, whereas for the impedance measurements the cantilever tip was placed at the edges of the slit to ensure good support of the basilar membrane (Fig. 2.1).

Measurements typically began 40 min after sacrifice of the animal. An impedance measurement at one radial position required 4 min, a deformation measurement 2 min; 40 min were required for both measurements at all radial positions. In control experiments, impedance and electrically evoked deformation were repeatedly measured during a time span of 80 min – no significant change was observed. All experiments were carried out at controlled room temperature (20–22 °C).

2.2 Signal processing

The stimulus voltages were generated with an arbitrary waveform generator (AWG; Hewlett-Packard E1445A, Böblingen, Germany). Two signals were digitized simultaneously with a 4-channel, 16-bit resolution, 196-kHz sample rate analog-digital converter

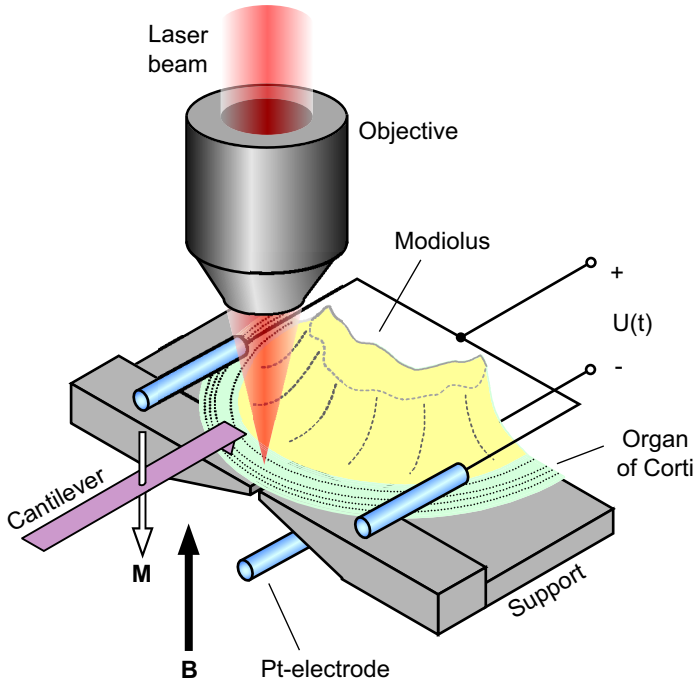

Figure 2.1: *Preparation and setup for the deformation and impedance experiments. The sample consisted of about one half of a cochlear turn, including modiolus bone (yellow), basilar membrane and overlying organ of Corti (green). The tectorial membrane was removed and the preparation was placed on a plastic support in such a way that the basilar membrane was lying flat on the support. The modiolar bone was fixed to the support with vaseline. Both experimental chamber and atomic force cantilever (purple) could be moved independently with motorized micromanipulators (Luigs & Neumann, Ratingen, Germany) to position the laser beam and to establish contact between organ of Corti and cantilever. For the deformation experiment, electric current was supplied to the bath medium via a ground electrode below the measurement site and two electrodes, which are electrically connected, above the preparation. At the measurement site, there was a 80 µm wide slit in the support allowing the current to pass through the cochlear partition and thereby evoke electromotile responses of the outer hair cells. The resulting deformation of the organ directly above the slit was detected by a laser Doppler vibrometer (LDV) coupled into the optical path of the microscope. The focus of the laser beam was in the focal plane of the microscope. For the impedance experiment, two measurements were made. Firstly ('contact measurement'), the cantilever tip was brought in contact with the upper surface of the organ of Corti slightly beside the slit and the cantilever (carrying a magnetic moment M) was stimulated by a magnetic field B generated by a coil below the support (not shown). Cantilever velocity was detected by the LDV. Secondly ('non-contact measurement'), the cantilever was retracted 13 µm from the reticular lamina and velocity was measured during magnetic stimulation.*

(ADC; Hewlett-Packard E1433A): voltage output of the LDV coding cantilever velocity on one channel and either 1) stimulus voltage between electrode and cantilever (for applying a point force to the cantilever), 2) voltage across the 0.9-Ω resistor coding stimulus coil current (for the impedance measurement), or 3) voltage across the 0.9-Ω resistor coding electric stimulus current through the bath (for the deformation measurement) on the second channel (Fig. 2.2). The data blocks had a size of 8192 samples. The beginning of data input and output was synchronized via trigger lines so that multiple data blocks could be averaged in the time domain. Between 100 and 600 averages were collected corresponding to effective averaging times of 4–25 s.

Both averaged input data blocks (velocity and stimulus) were fast-Fourier-transformed and saved to files. Velocity data were corrected off-line for the measured frequency response of the LDV and normalized with the stimulus.

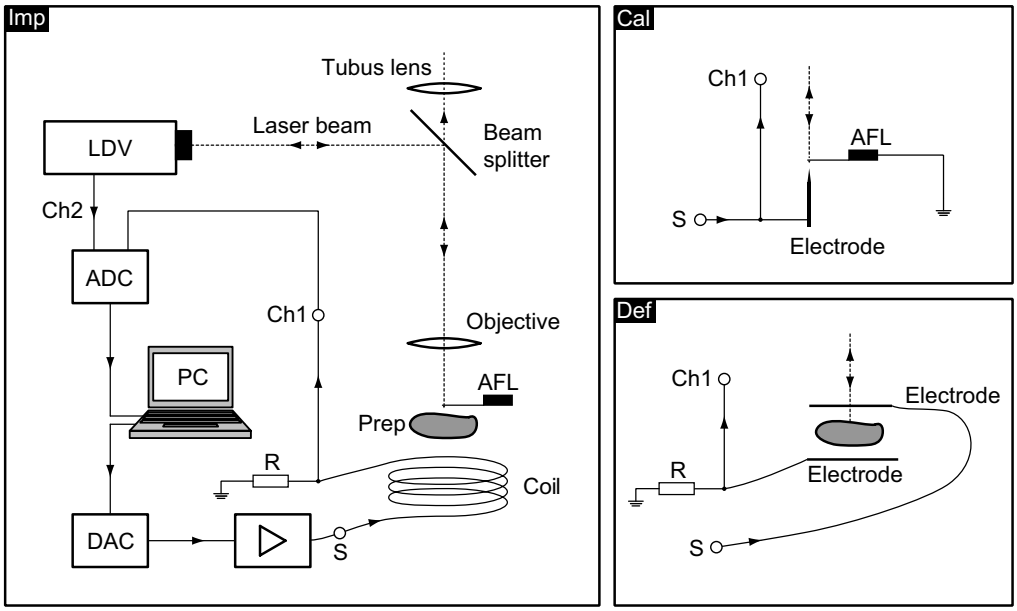

Figure 2.2: *Block diagram of electrical and optical signal flow. Left panel (Imp): impedance measurement. The beam from the laser Doppler vibrometer (LDV) was coupled into an upright microscope via a beam splitter, transparent below 590 nm, and focused on the atomic force cantilever (AFL). The tip of the AFL could be seen as a dark spot through the slightly transparent AFL, allowing the tip to be accurately positioned on its target. DAC: digital-to-analog converter for generating the driving voltage for the coil, amplified with a wide-band audio amplifier. A 0.9 Ω-resistor (R) was inserted between the coil and ground to monitor current. ADC: analog-to-digital converters for velocity and current data, channels 1 and 2 (Ch1, Ch2). Not illustrated is the second microscope used for measuring the indentation of the organ of Corti resulting from contact with the tip of the AFL; its optical axis was directed orthogonal to the plane of the drawing. Solid lines with arrows depict electrical connections, broken lines optical pathways. Lower right panel (Def): for the deformation measurement the coil is substituted by a pair of electrodes and the cantilever is removed (for connections Ch1 and S see left panel). The laser is focused on the upper surface of the organ, so that velocity of the reticular lamina could be measured during electrical stimulation. Upper right panel (Cal): configuration for applying an electrical point force to the cantilever. The stimulus voltage is connected to the sharp electrode and fed directly into the ADC. The Coulomb force acting on the grounded cantilever leads to motion of the tip detected by the LDV.*

The measurement software was written in VEE (Hewlett-Packard, Böblingen, Germany) and the off-line data processing software in Mathematica (Wolfram Research, Champaign, IL, USA). Nonlinear least mean square fitting was performed with the Levenberg-Marquardt algorithm. Fit parameters are given as mean±standard deviation. Tests of statistical significance were performed at the 95% confidence level.

Electrically and magnetically driven displacement of the cantilever and electrically evoked displacement of the reticular lamina were on the order of 1 nm and, therefore, a linear relationship between force and displacement (or velocity) could be safely assumed; this was also verified experimentally (Sec. 4.2.2). Consequently, instead of stimulating with a single frequency, stimuli were chosen to be multitone signals. They contained 9–81 frequency components between 50 Hz and 67 kHz, which were spaced almost logarithmically with a ratio of 1.07 between adjacent frequencies. The frequencies were shifted somewhat in order to exclude the coincidence of a stimulation frequency with one of the first four harmonics of a lower frequency, thereby reducing contamination of the measured velocity spectrum with harmonic distortion products. The exact stimuli are given in Secs. 2.5.4, 2.6.3 and 2.7.1, respectively. Frequencies were chosen so that an integer number of stimulus periods fell in the time window for data acquisition, as determined

by the ADC and DAC block size and sampling rate.

2.3 Velocity measurement

Velocity was measured with a laser Doppler vibrometer (LDV, OFV-302, wavelength 633 nm, power 1 mW) equipped with a demodulator (OFV-3000, bandwidth 100 kHz), both from Polytech (Waldbronn, Germany). The laser beam was focused on the sample by coupling it into the optical path of an upright microscope (Axioskop 2FS, Zeiss, Jena, Germany) via a beam splitter (AHF Analysentechnik, Tübingen, Germany), which was highly reflective only above 590 nm, but transparent for shorter wavelengths (Fig. 2.2). This allowed microscopic observation while the laser was focused on the sample. Since the reflectivity of the beam splitter for the laser wavelength was less than 100%, the laser spot could be seen through the ocular. The microscope objective was a water-immersion objective with magnification 40×, numerical aperture 0.8 and working distance 3.61 mm (Zeiss Achroplan, Jena, Germany). The laser spot had approximately a Gaussian profile, with full-width at $1/e^2$ of maximum power of 0.63 μm (quantified with a knife-edge method). By monitoring the amplitude of the laser heterodyne signal as a function of sample position, it was confirmed that the contribution of out-of-focus cellular structures to the reflected object beam was attenuated by at least 20 dB.

From the measured velocity, $v(t)$, the velocity spectrum $v(\omega)$ was obtained via fast Fourier transformation and the displacement spectrum calculated as $a(\omega) = v(\omega)/i\omega$. The velocity spectrum was corrected for the measured transfer function of the LDV. The noise floor of the measurement system, quantified as displacement amplitude, was derived from the cantilever velocity measured with the tip in contact with the support. The noise floor decreased from 10^{-2} nm at 480 Hz to 10^{-4} nm at 67 kHz (effective averaging time: 25 s).

2.4 Theory of atomic force cantilevers in fluid

In this section, the theory of a thin cantilever moving in an infinite fluid is summarized. The fluid forces on an infinitely long beam of arbitrary cross section moving in an incompressible viscous fluid have been treated by Tuck [183]. He developed an algorithm to calculate numerically the forces exerted by the fluid on an infinitely thin rectangular beam. Under the infinitely thin condition, he showed that the difference between the fluid forces exerted on a rectangular beam and on a circular beam, for which an analytical solution exists, never exceeds 15% for Reynolds numbers between 0.1 and 1000. Sader [152] has given a theoretical treatment for frictionless cantilevers immersed in viscous, inertial, incompressible fluids. He developed an expression for a correction function that allows approximation of the fluid forces on a rectangular beam without employing the time consuming numerical method of Tuck [183]. The theory as described in Ref. [152] is summarized in Sec. 2.4.1 for completeness and because I found important typesetting errors in his definition of the Fourier transform and in his derived Green's function; in fact, it was necessary for me to derive the Green's function anew. Moreover, I have extended the theory to a cantilever with internal friction [159]. Only deflections and forces normal to the flat side of the beam are considered.

2.4.1 General theory

The governing equation for the dynamic, small amplitude, lateral deflection $W(x,t)$ of a thin ($T \ll b \ll L$), isotropic beam of constant cross section (Fig. 2.3) subjected to an

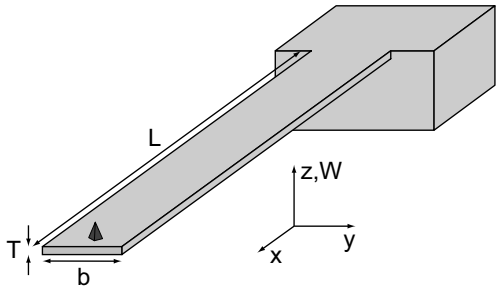

Figure 2.3: *The entire cantilever-system – composed of end block, cantilever and tip (darkened pyramid) – is manufactured from a single silicon crystal. The end block has dimensions of 3.4×1.6×0.3 mm^3. The dimensions of the cantilevers were in the ranges: length L = 125–450 μm, width b = 30–60 μm and thickness T = 1–5 μm. The values for L, T, and b were given on the data sheet supplied by the manufacturer with each cantilever. As a check on the theory and because the given T was not very accurate, T was also estimated as described in Sec. 3.1.1. The cantilevers had either rectangular or trapezoidal cross section with acute angle of 45°. The tip is a pyramid with a polygon-sided base, height 10–15 μm, and cone angle 50°. It is located 10–20 μm from the free end of the cantilever. x: distance along the cantilever from the end block. W: lateral displacement from the rest position (in the z-direction).*

applied force per unit length $F(x,t)$ is [59, 93]:

$$EI\frac{\partial^4 W(x,t)}{\partial x^4} + \beta EI\frac{\partial^4}{\partial x^4}\frac{\partial W(x,t)}{\partial t} + \mu\frac{\partial^2 W(x,t)}{\partial t^2} = F(x,t) \tag{2.1}$$

where E is Young's modulus along the longitudinal axis of the beam, I is the area moment of inertia with respect to the y-axis, β is the coefficient for the internal damping in the beam, μ is the mass per unit length of the beam, x is the spatial coordinate along the beam and t is time.

Although single-crystal silicon has cubic symmetry, rather than being isotropic, the use of a unidirectional value of E to describe the elasticity of the entire beam is justified because only compression along the longitudinal axis is considered. Young's modulus for silicon in the <011>-direction can be derived from the elasticity theory of crystal lattices [109] by applying a load per unit area in the <011>-direction and solving the linear equation system for the strain. Using the elastic moduli $C_{11} = 1.6578\times10^{11}\,\mathrm{N/m^2}$, $C_{12} = 0.6394\times10^{11}\,\mathrm{N/m^2}$, and $C_{44} = 0.7962\times10^{11}\,\mathrm{N/m^2}$ [95], I obtained $E = 1.6916\times10^{11}\,\mathrm{N/m^2}$.

For the trapezoid cross section of the some of the cantilevers used in this study with an angle of 45° (Fig.2.3), I is [178]:

$$I_{tr} = \frac{T^3}{36}\left(2b - 2T + \frac{b(b-2T)}{b-T}\right) \tag{2.2}$$

whereas in the case of a rectangular cross-section $I_{re} = BT^3/3$.

Internal damping was neglected in the formulation by Sader [152] but is required here for the analysis of vibrations in air. For the present application it was sufficient to assume that the stresses produced by internal damping are directly proportional to the rate of change of strain in the longitudinal direction, the (frequency-independent) proportionality constant being β.

If the mass and rotational moment of inertia of the AFM-tip are neglected, the boundary conditions on Eq. 2.1 for a beam clamped at $x = 0$ and free at $x = L$ are

$$W(x,t)|_{x=0} = \left.\frac{\partial W(x,t)}{\partial x}\right|_{x=0} = \left.\frac{\partial^2 W(x,t)}{\partial x^2}\right|_{x=L} = \left.\frac{\partial^3 W(x,t)}{\partial x^3}\right|_{x=L} = 0 \tag{2.3}$$

where the second- and third-order partial derivatives are proportional to the bending moment and shear force (at the free end), respectively.

The strategy to solve Eq. 2.1 for arbitrary $F(x,t)$ is to find a solution for its Fourier-transformed form in terms of a Green's function and to re-transform that solution into time space.

If the Fourier transform $\hat{W}$ of a time dependent variable W is defined as

$$\hat{W}(\omega) = \int_{-\infty}^{\infty} W(t) e^{i\omega t}\, dt \tag{2.4}$$

with ω denoting radial frequency, and the dimensionless spatial variable $\xi = x/L$ is introduced, then the Fourier transform of Eq. 2.1 becomes

$$\frac{EI(1-i\omega\beta)}{L^4}\frac{d^4\hat{W}(\xi,\omega)}{d\xi^4} - \mu\omega^2\hat{W}(\xi,\omega) = \hat{F}(\xi,\omega) \tag{2.5}$$

with the appropriate transformed boundary conditions.

The total force $\hat{F}(\xi,\omega)$ can be separated into the externally applied force $\hat{F}_{drive}(\xi,\omega)$ and the force exerted on the beam from the surrounding fluid $\hat{F}_{fluid}(\xi,\omega)$

$$\hat{F}(\xi,\omega) = \hat{F}_{drive}(\xi,\omega) + \hat{F}_{fluid}(\xi,\omega) \tag{2.6}$$

The hydrodynamic force can be calculated from the equations of motion of the fluid. For a rigid beam undergoing lateral oscillatory motion it has the general form [152]:

$$\hat{F}_{fluid}(\xi,\omega) = \frac{\pi}{4}\rho\omega^2 b^2 \Gamma(\omega)\hat{W}(\xi,\omega) \tag{2.7}$$

where ρ is the fluid density. The so-called 'hydrodynamic function' $\Gamma(\omega)$ is dimensionless and is obtained from the solution of the Navier-Stokes equations for incompressible fluids assuming small velocities:

$$\vec{\nabla}\cdot\vec{\hat{u}} = 0\,, \quad -\vec{\nabla}\hat{p} + \eta\nabla^2\vec{\hat{u}} = -i\rho\omega\vec{\hat{u}} \tag{2.8}$$

where $\vec{\hat{u}}$ and $\hat{p}$ are, respectively, the Fourier transformed velocity and pressure field, $\vec{\nabla} = (\partial/\partial x, \partial/\partial y, \partial/\partial z)$, and η is the viscosity of the fluid. $\Gamma(\omega)$ depends on the contour of the cross section of the beam [183]. Since for a beam with circular cross section and diameter b the mass per unit length is $\pi\rho(b/2)^2$, the real part of $\Gamma(\omega)$ specifies the so-called added mass, i.e. the ratio between the mass per length with fluid and the mass per length without fluid. Likewise, the imaginary part of $\Gamma(\omega)$ is proportional to the damping imposed on the beam by the fluid [183]. For a time dependence of the oscillation given by $\exp(-i\omega t)$, it is well-known that the exact analytical result for a circular cross section is [141]:

$$\Gamma_{circ}(\omega) = 1 + \frac{4i\,K_1(-i\sqrt{i\,\mathrm{Re}})}{\sqrt{i\,\mathrm{Re}}\,K_0(-i\sqrt{i\,\mathrm{Re}})} \tag{2.9}$$

where the Reynolds number, Re, is defined as

$$\mathrm{Re} = \frac{\rho\,\omega b^2}{4\eta} \tag{2.10}$$

and K_0 and K_1 are modified Bessel functions of the third kind [2]. An exact analytical solution was derived by Kanwal [80] for an infinitely thin, rectangular cross section and an algorithm for a numerical solution of the same problem is described in Tuck [183]. Since both methods require a significant amount of computation, an approximate correction function $\Omega(\omega)$ was presented in Sader (1998, his Eq. 21), which satisfies

$$\Gamma_{rect}(\omega) = \Omega(\omega)\,\Gamma_{circ}(\omega) \tag{2.11}$$

The $\Gamma_{rect}(\omega)$ calculated using $\Omega(\omega)$ from Sader [152] is accurate to within 0.1 % in the range $\mathrm{Re} \in [10^{-6}, 10^{4}]$.

Substituting Eqns. 2.6 and 2.7 into Eq. 2.5 yields

$$\frac{d^4\hat{W}(\xi,\omega)}{d\xi^4} - B^4(\omega)\hat{W}(\xi,\omega) = \hat{s}(\xi,\omega) \tag{2.12}$$

where

$$B(\omega) = \left[\frac{\mu\omega^2 L^4}{EI(1-i\omega\beta)}\left(1 + \frac{\pi\rho b^2}{4\mu}\Gamma(\omega)\right)\right]^{1/4} \tag{2.13}$$

and

$$\hat{s}(\xi,\omega) = \frac{L^4}{EI(1-i\omega\beta)}\hat{F}_{drive}(\xi,\omega) \tag{2.14}$$

Notice that internal damping simply causes the modulus of elasticity to become complex, where the relative value of the imaginary component, called the loss factor, is $\omega\beta$, the usual value for a Voigt-Kelvin viscoelastic material [22].

The general solution to Eq. 2.12 in terms of the appropriate Green's function $G(\xi,\xi',\omega)$ is

$$\hat{W}(\xi,\omega) = \int_0^1 G(\xi,\xi',\omega)\hat{s}(\xi',\omega)\,d\xi' \tag{2.15}$$

with $G(\xi,\xi',\omega)$ being constructed as described in standard mathematical textbooks with the boundary and continuity conditions given in Ref. [152] (his appendix A). I derived the following Green's function:

$$\begin{aligned}
G(\xi,\xi',\omega) = {} & \frac{1}{4B^3(1+\cos[B]\cosh[B])} \times \\
& \begin{cases}
(\cosh[B\xi] - \cos[B\xi]) \times \\
(\cosh[B(\xi'-1)]\sin[B] + \sin[B\xi'] - \cosh[B]\sin[B(1-\xi')] \\
\quad + \cos[B(\xi'-1)]\sinh[B] + \sinh[B\xi'] - \cos[B]\sinh[B(1-\xi')]) \\
\quad + (\sin[B\xi] - \sinh[B\xi]) \times \\
(\cos[B\xi'] + \cos[B(\xi'-1)]\cosh[B] + \cos[B]\cosh[B(\xi'-1)] \\
\quad + \cosh[B\xi'] + \sin[B(\xi'-1)]\sinh[B] + \sin[B]\sinh[B(1-\xi')]) \\
\qquad\qquad\qquad\qquad\qquad\qquad , 0 \le \xi \le \xi' \le 1 \\
(\sin[B(\xi-1)] + \sinh[B(\xi-1)]) \times \\
(-\cos[B(\xi'-1)] - \cos[B\xi']\cosh[B] + \cosh[B(\xi'-1)] \\
\quad + \cos[B]\cosh[B\xi'] + \sin[B\xi']\sinh[B] + \sin[B]\sinh[B\xi']) \\
\quad + (\cos[B(\xi-1)] + \cosh[B(\xi-1)]) \times \\
(\cosh[B\xi']\sin[B] + \sin[B(\xi'-1)] + \cosh[B]\sin[B\xi'] - \\
\quad \cos[B\xi']\sinh[B] - \cos[B]\sinh[B\xi'] + \sinh[B(1-\xi')]) \\
\qquad\qquad\qquad\qquad\qquad\qquad , 0 \le \xi' \le \xi \le 1
\end{cases}
\end{aligned} \tag{2.16}$$

2.4.2 Harmonic driving force

In this section the deflection of the cantilever in response to a harmonic point force and its resulting mechanical driving-point impedance $Z = F_{drive}/\dot{W}$ are calculated. It is emphasized that the theoretical treatment outlined in the previous section applies to a time dependence given by $\exp(-i\omega t)$; therefore, the external force per unit length acting upon the cantilever at $x = x_0$ with a radial frequency ω_0 is written as

$$F_{drive}(x,t) = F_0 \exp(-i\omega_0 t)\delta(x - x_0) \tag{2.17}$$

or

$$F_{drive}(\xi,t) = \frac{F_0}{L}\exp(-i\omega_0 t)\delta(\xi-\xi_0) \tag{2.18}$$

with F_0 being the frequency independent amplitude and δ the Dirac delta function. The Fourier transformed force is

$$\hat{F}_{drive}(\xi,\omega) = 2\pi\frac{F_0}{L}\delta(\xi-\xi_0)\delta(\omega-\omega_0) \tag{2.19}$$

Substituting Eq. 2.19 into Eqns. 2.14 and 2.15 gives

$$\hat{W}(\xi,\omega) = 2\pi\frac{F_0 L^3}{EI(1-i\omega\beta)}\delta(\omega-\omega_0)G(\xi,\xi_0,\omega) \tag{2.20}$$

and the inverse Fourier transformation gives

$$W(\xi,t) = \frac{F_0 L^3}{EI(1-i\omega\beta)}G(\xi,\xi_0,\omega_0)\exp(-i\omega_0 t) \tag{2.21}$$

If the deflection of the cantilever is measured directly at the location x_0 of the AFM-tip, the mechanical driving-point impedance of the cantilever at this location is

$$Z(\omega_0) = \frac{\int_{x_0-\varepsilon}^{x_0+\varepsilon} F_{drive}(x,t)\,dx}{\partial W(\xi_0,t)/\partial t} \tag{2.22}$$

Because F_{drive} is the force per unit length, it must be integrated over a small interval $[x_0-\varepsilon, x_0+\varepsilon]$ where the value of $\varepsilon > 0$ has no influence because of the Dirac delta function. Finally we obtain

$$Z(\omega_0) = \frac{EI(1-i\omega\beta)}{-i\omega_0 L^3 G(\xi_0,\xi_0,\omega_0)} \tag{2.23}$$

If the time dependence is given by $\exp(i\omega t)$, as opposed to $\exp(-i\omega t)$, the complex conjugate of the right hand side of Eq. 2.23 must be used.

2.5 Experimental validation of the cantilever theory

2.5.1 Generation of a point force

In order to exert a *point* force on the cantilever, a sharpened steel electrode was placed at a distance of about 10 μm from the end of the AFM-tip (Fig.2.2) and an electric field applied between them. The cantilever is electrically conductive. The steel electrode was etched to a tip diameter of about 1 μm by dipping a 0.5-mm stainless steel wire repeatedly in 2 M HCl while applying a voltage of 2 V between the wire and a Ag-electrode in the HCl. If the tip of the steel electrode is sharp enough and the distance between electrode and AFM-tip is sufficiently small, then the interaction between electrode and cantilever is dominated by the force on the AFM-tip, the force on the flat part of the cantilever being negligible. Since the cantilever is stiff along the narrow base of the pyramidal-shaped tip, a force acting on the tip is close to a *point* force on the cantilever.

2.5.2 Alignment of cantilever and electrode

The procedure for aligning the AFM-tip and the electrode relied on the fact that the cantilever is slightly transparent, so that the AFM-tip could be seen from the reverse side of the cantilever. The tip of the electrode was first brought into the focus plane of the microscope and was positioned to the center of the laser spot (Fig.2.2). It was then

retracted a short distance. Subsequently, the cantilever was brought into focus and the AFM-tip was centered in the laser spot. A diaphragm in the laser pathway was almost closed and the electrode was moved towards the cantilever until the diffraction pattern of the diaphragm seen on the back of the cantilever just started to change. At this position the electrode was assumed to be in contact with the AFM-tip. The electrode was then retracted by the desired distance.

2.5.3 Electrical contact to the cantilever

To establish a low-resistance electrical contact to the highly doped silicon of the cantilever, the SiO_2 surface layer of the cantilever was etched by placing a small droplet of HF (50%) for 10 min at the end of the chip supporting the cantilever. Indium was soldered to the 'clean' spot at 400°C and then contacted with silver paint (Agar Scientific, Stansted, U.K.). The electrical resistance across the contact obtained in this manner was typically several Ohms.

2.5.4 Coulomb force stimulus generation

The arrangement of cantilever and electrode surrounded by a dielectric fluid of permittivity ϵ has an electrical capacity, $C = \epsilon C_0$, where C_0 is the capacity in vacuum. When a voltage, U, is applied between the cantilever and the electrode, an electrical charge of magnitude $Q = CU$ is moved onto the cantilever and the electrode. The Coulomb force F between the two is proportional to Q times the electric field, E, between cantilever and electrode, which in turn is proportional to the applied voltage; thus $F \sim QE \sim \epsilon C_0 U^2$. (When the cantilever is deflected, the changing distance between the electrode and the AFM-tip causes a change in C and thus in F. However, this effect can be neglected for deflections much smaller than the tip-electrode distance.) In order to apply a *sinusoidal* force, the voltage must therefore be the root of a sinusoidally varying function. Since the force is always attractive, an offset voltage must be added, about which the force can alternate. If we choose U to be of the form

$$U(t) = U_0\sqrt{\sin\omega t + 1.2} \tag{2.24}$$

the Coulomb force exerted on the cantilever is

$$F(t) \sim \sin\omega t + 1.2 \tag{2.25}$$

The offset was set to 1.2 rather than 1.0, to avoid the occurrence of time points where $U(t)$ is not continuously differentiable, since this would have led to frequency components in the Fourier spectrum of $U(t)$, that were higher than the bandwidth of the voltage generator. The DC-offset had no influence on the measurement, because the differential equation for the cantilever is linear (see Sec. 2.4.1) and the solution for a sum of static and alternating forces is the superposition of the individual solutions for the static and alternating force components, respectively; that is, the cantilever deflection has a static component determined by the stimulus offset and an alternating component in response to the alternating part of the stimulus. Since the vibrometer was used in velocity rather than displacement mode, the static deflection component can be ignored.

Since with signal averaging it would have required at least two hours to measure the frequency response point by point, four multitone stimuli were used – they contained frequencies in the ranges of $50 - 400\,\mathrm{Hz}$ ($n = 31$), $50 - 960\,\mathrm{Hz}$ ($n = 46$), $0.4 - 67\,\mathrm{kHz}$ (n=81), and $40 - 67\,\mathrm{kHz}$ (n=9). During data analysis, the overlapping frequencies from the stimuli with more frequencies were discarded. Preference was given to the stimuli with fewer frequencies because they implied a larger force amplitude per frequency, resulting

in a higher signal-to-noise ratio. If f_i denotes the i-th frequency point, the multitone voltage stimulus can be expressed by

$$U(t) = U_0 \sqrt{H + \sum_i \sin(2\pi f_i t + \varphi_i)} \tag{2.26}$$

where the amplitudes were equal but the phases φ_i were randomly generated, with a uniform distribution in the interval $[0, 2\pi]$. The stimuli were generated once and saved to files so that the f_i and φ_i were the same for each measurement. The offset H was chosen 10% greater than the highest negative value of the sum of sinusoids to ensure that the expression under the root was always greater than zero. U_0 was set to give a peak voltage of $U(t)$ of 15 V, both for CCl_4 and air.

The amplitude of the force depends, via C and E, on the geometry of the arrangement and on the electrical permittivity of the surrounding medium. No attempt was made to calculate C or E. It is important, however, that even at 67 kHz the molecular relaxation processes in the liquid are much faster than the change in external electrical field [52]. Therefore, the permittivities of the media used in this study (air and CCl_4) equal their static values. This means that although the absolute magnitude of the force on the cantilever is unknown, it is independent of frequency.

The resistance across the cantilever contact, R, together with the capacitance of the electrode-cantilever system, C, forms a first-order low-pass filter. I have estimated a lower limit for the cut-off frequency of this filter according to $f_{3\mathrm{dB}} = 1/(2\pi RC)$, by assuming C to equal that of a plate capacitor with an area of $(20\,\mu\mathrm{m})^2$ and a plate-distance of $10\,\mu$m. With an upper limit for $R = 10\,\Omega$, I obtained $f_{3\mathrm{dB}} = 4.5 \times 10^{13}$ Hz in vacuum. The influence of this filter was therefore neglected.

2.5.5 Estimation of the mechanical driving point impedance

The mechanical driving-point impedance, Z, is defined as the ratio of the applied force, F_{drive}, at a particular location to the velocity $\partial W(t)/\partial t$ at the same location on the cantilever. However, the amplitude of Z at a stimulus frequency f_i can not be calculated from the measured velocity spectra because the amplitude of the driving-point force is unknown. However, since the phase φ_i of this force is known, the phase of the velocity is also known. Therefore, the mechanical driving-point impedance Z_i at the stimulus frequency f_i can be expressed as

$$Z_i = M \frac{\exp(i\varphi_i)}{v_i \exp(i\alpha_i)} \tag{2.27}$$

where v_i is the amplitude and α_i the phase of the velocity at f_i, as extracted from the scaled Fourier spectrum of the LDV signal. The (real) constant M is the unknown amplitude of the driving force. It is important, however, that M is independent of frequency because of the nature of the Coulomb force – its value was estimated by fitting the experimentally derived values Z_i (Eq. 2.27) to the values $Z(f_i)$ obtained from the model (Sec. 2.4.1) for frequencies in the range $0.4 - 1$ kHz. This upper frequency limit was chosen because the impedance of the cantilever below 1 kHz was dominated by its stiffness, the mass and the damping from the fluid being negligible. At these low frequencies it is assumed that the impedance derived from the model is correct. The lower frequency limit was chosen to ensure that the LDV output signal was about 20 dB above the noise floor in both air and CCl_4.

2.5.6 Embedding of the electrode in a flat surface

To simulate the situation for an AFM-tip near a flat, infinite surface, in a second set of experiments the electrode was embedded in epoxy glue in such a way that its tip was

level with the surface. A plastic ring with internal diameter about 4 mm and height little less than the electrode height served as a casting mould for the epoxy glue. The plastic ring was glued on the bottom of the experimental chamber with the electrode positioned somewhat off center. Since the epoxy glue shrinks during polymerization the mould was filled in two steps. First, it was filled with glue up to a level about 0.5 mm below the tip of the electrode. After curing, a second layer of glue was added in a way that the tip of the electrode was slightly ($20 - 60\,\mu$m) below the surface of the glue. The glue was liquid for about 2 h, allowing the surface to settle in its (flat) equilibrium shape. Gas bubbles in the glue were removed by placing the liquid glue in a vacuum chamber for several minutes before pouring into the mould. Finally, the cured epoxy glue surface was polished down to the level of the electrode-tip using a felt polishing plate and polishing paste.

2.6 Impedance of the organ of Corti

2.6.1 Measurement principle

For sufficiently small displacement amplitudes it is reasonable to assume a linear relationship between a point force F on the organ of Corti and the resulting displacement x (or velocity v) of that point in the same direction as the force; that is, $F = Kx$ or $F = Zv$, where K is the generalized complex stiffness, and Z is the impedance. For a harmonic time dependency, $v = i\omega x$ and, thus, $K = i\omega Z$. In order to find Z, or equivalently K, I determined experimentally the mechanical impedance: 1) of the free swinging tip of an atomic force cantilever, Z_{eq}, at a short distance (13 μm) from the preparation, and 2) of a system consisting of the same cantilever with its tip in contact with the specimen, Z_{cont} (Fig. 2.1). The impedances were found by applying a magnetic force to a ferromagnetic cantilever and simultaneously measuring the velocity of the cantilever tip. From the difference in impedance between the non-contact and the contact modes, I calculated the point impedance of the organ of Corti at the point of contact. In general, Z and K will depend on the frequency of the applied force – measurements were made in the range from 0.48–50 kHz. Above 50 kHz, standing acoustic waves formed between the measuring chamber and the objective, leading to an uncontrollable additional force on the cantilever.

The organ of Corti was described mechanically by an equivalent (Norton) point impedance, Z_{OC}, between the measured point on its upper surface and 'ground'. In the absence of electrical stimulation, the outer hair cells do not produce electromechanical force and, therefore, the organ of Corti does not contain a force source.

The mechanical stimulus with a magnetic area force applied to the cantilever was described by an equivalent point force source, F_{eq}, and an equivalent point impedance, Z_{eq}, connected between the tip of the cantilever and ground. A calibration procedure for F_{eq} and Z_{eq} is described in Sec. 2.6.5.

Since the cantilever tip is in contact with the organ of Corti at only one point, namely at the point for which the equivalent impedances and force are considered, Z_{eq} and Z_{OC} are independent of each other and do not change when contact is established. Therefore, the total impedance that is driven when the magnetic force is applied while the cantilever tip is in contact with the organ of Corti, is $Z_{cont} = Z_{eq} + Z_{OC}$. Since F_{eq} and Z_{eq} are known and $Z_{cont} = F_{eq}/v_{cont}$ can be found by measuring the velocity v_{cont} of the cantilever tip in the contact mode, Z_{OC} was calculated as $Z_{OC} = Z_{cont} - Z_{eq}$.

The signal-to-noise-ratio (SNR) for Z_{OC} is largest when the cantilever is soft compared with the sample; that is, when Z_{eq} is much smaller than Z_{cont}, because then the difference $Z_{cont} - Z_{eq}$ is large. In contrast, for a hard cantilever with $Z_{cont} \approx Z_{eq}$, the difference becomes small while the noise remains the same, and consequently the SNR

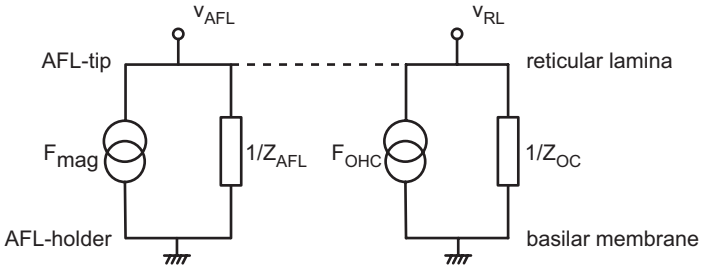

Figure 2.4: *Electrical equivalent circuit of the organ of Corti (OC) with or without contact (dashed line) to the atomic force cantilever (AFL). The velocities v of reticular lamina and AFL, respectively, were measured by a laser Doppler vibrometer. The equivalent magnetic point force F_{mag} acts on the tip of the cantilever (Sec. 2.6.1). Without contact between AFL tip and reticular lamina, F_{mag} drives only the equivalent point impedance of the AFL, Z_{AFL}. When contact is established, F_{mag} drives the sum of the impedances Z_{AFL} and Z_{OC}. When the AFL is retracted and the OC is stimulated electrically, the OHCs generate the force F_{OHC} acting on Z_{OC}, the impedance of the OC. Please note that in the electro-mechanical analogy used here, current corresponds to force and voltage to velocity. The electrical impedances are then reciprocal to the mechanical ones [7].*

is poor. Therefore, I used the softest cantilevers that I could obtain: one with a spring constant of 1.20 N/m for the first 21 preparations (1st and 2nd cochlear turns) and one with a spring constant of 1.59 N/m for the remaining 9 preparations (3rd cochlear turn).

2.6.2 Magnetic cantilevers

Atomic force cantilevers with a ferromagnetic cobalt coating are available commercially (type SC-MFM, Team Nanotec, Villingen-Schwenningen, Germany). The cantilevers, which were made of silicon, have a rectangular shape with length 215 μm, width 35 μm, and thickness about 2 μm; the Co-coating has a thickness of 50 nm. The tip-diameter of the cantilever was enlarged from the typical value of about 10 nm to about 0.5–2 μm by scratching the tip over a glass surface. The profile of the tip was examined in a separate set of experiments using an electron microscope (LEO 912, Oberkochen, Germany); the reproducibility of the profile and diameter of the enlarged tip was ensured by the crystalline structure of the Si; surface irregularities in the profile were less than 10 nm in magnitude. The cantilevers were slightly transparent when illuminated with white light in the experimental setup (Fig. 2.1), so that the tip appeared as a dark spot when viewed from the reverse side. This was used to position the tip precisely on the desired place (Fig. 3.4).

2.6.3 Magnetic stimulus generation

The cantilevers were magnetized with a strong NdFeB permanent magnet in the direction of their deflection (Fig. 2.1). The magnetic field was generated by a cylindrical coil (length 3 mm, diameter 4–10 mm, 120 windings of 0.22-mm varnished Cu wire), with the cantilever tip placed near the central axis of the coil at a distance of 2 mm from the end of the coil (Fig. 2.2). The magnetic moment of the cantilever thus experiences a dipole force in the magnetization direction.

The magnetic stimulus voltage, U_{drv}, contained 81 frequencies in the range 0.48–67 kHz (however, data were evaluated only up to 50 khz as mentioned in Sec. 2.6.1). If each frequency component has unity amplitude and random phase then

$$U_{drv}(t) = U_0 \sum_{k=1}^{81} \cos(2\pi f_k t + \varphi_k) \,, \tag{2.28}$$

where t is time, f_k is the k-th frequency, U_0 is a scaling factor, and φ_k is the randomly distributed phase of the k-th frequency component.

In order to maximize the SNR for the measured velocity at all frequencies, the cantilever response (resonance at 10–20 kHz in fluid) and the increased electrical impedance of the coil, Z^{el}_{coil}, at high frequencies (leading to smaller currents) was compensated for by weighting the stimulus with a function $W(\omega)$, which was similar to a resonator's impedance multiplied with Z^{el}_{coil}:

$$U_{drv}(t) = U_0 \sum_{k=1}^{81} W(2\pi f_k) \cos(2\pi f_k t + \varphi_k) \; . \tag{2.29}$$

For my cantilevers

$$W(\omega) = \left| 1 + i \left(\frac{\omega}{62998.4} - \frac{250}{\sqrt{\omega}} \right) \right| \; , \tag{2.30}$$

yielded a measured velocity that remained within one order of magnitude over the entire frequency range. The minimum value of $W = 1$, is at $\omega = 2\pi \times 10^4$ rad/s, the approximate resonance frequency of the cantilever in fluid. With this stimulus, the peak amplitude of the voltage signal was a factor of 53 greater than the amplitude of the frequency component with $W = 1$. U_0 was chosen so that the displacement amplitude per spectral point was about 1 nm.

The coil was driven by an audio amplifier (Onkyo A-905X) with a 3-dB bandwidth of 100 kHz. The RMS-current through the coil was set to 600 mA, corresponding to a peak current of 2 A, with the multitone driving voltage described above. Since the magnetic field strength is proportional to the coil current, the latter was measured via a 0.9-Ω resistor in the current path (Fig. 2.2). The voltage at the resistor was recorded simultaneously with the velocity signal (voltage output) of the LDV, so that the measured velocity could be normalized to coil current (and thus field strength). In this way, all measurements were truly comparable, irrespective of the amplifier gain.

By placing a second coil on top of the stimulation coil and monitoring the induced voltage, it was confirmed that filling the chamber with Hanks' balanced salt solution did not affect the frequency response of the generated magnetic field.

2.6.4 Determination of contact

Contact between the cantilever and the sample was established by bringing the reticular lamina – the upper surface of the organ of Corti – into microscope focus and then approaching the cantilever until a visible deformation of the reticular lamina just occurred. Typically, the indentation, had a depth of 1 μm, as measured from a direction perpendicular to the laser beam with a self-made second microscope; the objective was a W25×/∞ with NA of 0.45 described in Ref. [100]; the tubus lens had f=160 mm, and the ocular was 12.5× with f=20 mm. This allowed the sample indentation to be visualized whilst establishing contact. I attempted a second method to determine the instant of contact, namely by stimulating the cantilever magnetically and monitoring the velocity phase while the cantilever was approached. However, it was difficult to clearly identify the instant of contact by this method because there was no obvious phase jump upon contact; instead, because of fluid coupling to the surface of the organ of Corti, the phase changed only gradually as the surface was approached ($< 0.5°/\mu$m over a distance of about 17 μm before contact).

2.6.5 Equivalent impedance and force calibration

The magnetic force is an area force, because the ferromagnetic coating covers the entire tip side of the cantilever. The inhomogeneity caused by the tip coating was neglected.

Calibration was carried out after blunting the tip. In the case of a harmonic magnetic field with angular frequency ω, the force per unit length is given by

$$F_{drive} = \frac{F_0(\omega)}{L} \exp(-i\omega t)\,, \tag{2.31}$$

where F_0 is the total magnetic force on the magnetic moment of the entire cantilever, L is the length of the cantilever, and t is time. Introducing the Fourier transformed Eq. 2.31 into Eq. 2.14 and inverse-Fourier transforming Eq. 2.15, gives the deflection velocity v of the cantilever tip:

$$v(\xi_0, \omega, t) = \frac{-i\omega F_0(\omega) L^3}{EI(1 - i\omega\beta)} \int_0^1 G(\xi_0, \xi, B(\omega)) d\xi \, \exp(-i\omega t)\,. \tag{2.32}$$

$B(\omega)$ includes the fluid, inertial, and elastic forces on the cantilever and is given by Eq. 2.13 for the case of an infinitely extending fluid. The equivalent point impedance of the cantilever at its tip is given by Eq. 2.23:

$$Z_{eq}(\xi_0, \omega) = \frac{EI(1 - i\omega\beta)}{-i\omega L^3 G(\xi_0, \xi_0, B(\omega))} \tag{2.33}$$

and the equivalent point force is

$$\begin{aligned} F_{eq}(\xi_0, \omega, t) &= Z_{eq}(\xi_o, \omega) v(\xi_o, \omega, t) \\ &= F_0(\omega) \frac{\int_0^1 G(\xi_0, \xi, B(\omega)) d\xi}{G(\xi_0, \xi_0, B(\omega))} \exp(-i\omega t)\,. \end{aligned} \tag{2.34}$$

This means that $Z_{eq}(\omega)$ and $F_{eq}(\omega)$ can be calculated if $F_0(\omega)$ and $B(\omega)$ are known for the situation where the cantilever is near the organ of Corti. However, $B(\omega)$ is known from theory only if the cantilever is in air or is in an infinitely extending fluid. In my case, the organ is in a solution (Hanks' balanced salt solution) and the cantilever is near the sample. Therefore, the condition of an infinite fluid does not apply and the expression for $B(\omega)$ derived in Sec. 2.4 (Eq. 2.13) is not valid (as shown in Fig. 3.3). To resolve this issue a calibration procedure was developed to establish $F_0(\omega)$ and $B(\omega)$.

To find $F_0(\omega)$, the magnetically induced velocity of the cantilever tip in air was measured, with the cantilever in its usual position within the experimental chamber (200 μm above the support). This velocity spectrum, $v_{air}(\omega)$, together with the theoretical $B_{air}(\omega)$, were substituted into Eq. 2.32, which was then solved for $F_0(\omega)$. $F_0(\omega)$ depends only on the magnetic moment of the cantilever and on the magnetic field. Since the magnetic field doesn't change in the solution (see Sec. 2.6.3), $F_0(\omega)$ is the same in fluid and air.

To find $B(\omega)$ (and thus the fluid forces) in the case where the cantilever was near the surface of the sample, the velocity spectrum was measured in this position during magnetic stimulation. This velocity spectrum, $v_{free}(\omega)$, together with $F_0(\omega)$ as determined above, were substituted into Eq. 2.32, which was then solved numerically for $B(\omega)$.

Finally, equivalent impedance and force at the measurement position of the cantilever were calculated from Eqns. 2.33 and 2.34.

2.7 Electrically evoked deformation of the organ of Corti

2.7.1 Electrical stimulus generation

Electrical stimulation was provided via platinum electrodes in the bath below and above the sample (Fig. 2.1). The command voltage was a multi-tone complex including 81

frequencies in the range from 480 Hz to 67 kHz. If f_i denotes the i-th frequency and t_j the j-th time-point in the arbitrary waveform generator data block, the multitone voltage stimulus can be expressed by

$$U(t_j) = \frac{U_0}{23.61} \sum_{i=1}^{81} \cos(2\pi f_i t_j + \varphi_i) \tag{2.35}$$

where the individual amplitudes were equal but the phase offsets φ_i were randomly generated, with a uniform distribution in the interval $[0, 2\pi]$. The maximum value of the sum in Eq. 2.35 is 23.61 and therefore U_0 is the maximum voltage of the multi-tone complex. U_0 was typically set to 6–10 V.

2.7.2 Drug administration

Several pharmacological agents were applied to the preparation via the bath medium. They were intended to block electromotility (to confirm that the observed vibration truly originated from OHC electromotility) and to localize the electric current path through the OHCs. Details about the used substances are given in Sec. 3.3.6.

The experimental chamber was designed to have a more or less streamlined shape so that the whole bath fluid could be exchanged by supplying new medium at one end while draining away the present medium at the other end. The volume of the bath chamber was about 10 ml and 30–50 ml were typically rinsed through to exchange the medium. The fluid exchange took about 3 min. Washout was performed in the same way with fresh Hanks' medium. Care was taken that the temperature was the same for different media. The solutions obtained by adding drugs to Hanks' medium were adjusted to the same osmolarity and pH as normal.

Chapter 3. Results

Results from the three measurements are presented in this chapter: 1) application of a point force to the cantilever to confirm the cantilever theory, 2) impedance of the organ of Corti measured with magnetically actuated cantilevers, and 3) electrically evoked deformation of the upper surface of the organ. Finally, from impedance and deformation velocity, the force acting on the reticular lamina is calculated.

3.1 Validation of the cantilever theory

3.1.1 Determination of T and β

As a check on the accuracy of the model, T-values were calculated from the first resonant frequency of the cantilever and compared with the value provided by the vendor. For this purpose, a bisection algorithm was used that found the value of T that brought the calculated first resonant frequency within $\pm 10\,\mathrm{Hz}$ of the measured first resonant frequency. With T being determined in this way, the higher resonant frequencies were predicted by the model within the accuracy of the measurement.

The coefficient for internal friction, β, was chosen so that the calculated peak height of the first resonance in air equalled the measured value.

3.1.2 Comparison between model and data

Figs. 3.1 and 3.2 show the measured and the calculated impedance for a cantilever in air and immersed in CCl_4. The measurement in CCl_4 was performed at 10°C and the one in air at 20°C. The parameters were $\eta_{CCl_4} = 1.156\,\mathrm{mPa\,s}$, $\eta_{air} = 18.6\,\mu\mathrm{Pa\,s}$, $\rho_{CCl_4} = 1.610 \times 10^3\,\mathrm{kg/m^3}$, $\rho_{air} = 1.161\,\mathrm{kg/m^3}$ [95], $L = 385\,\mu\mathrm{m}$, $b = 59\,\mu\mathrm{m}$ and $x_0 = 360\,\mu\mathrm{m}$. η_{CCl_4} was linearly interpolated between the values given at 0°C and 25°C and ρ_{CCl_4} was calculated by correcting the value for 20°C with the thermal expansion factor. β was found to be $5 \times 10^{-8}\,\mathrm{s}$. Estimated T-values were $1.98\,\mu\mathrm{m}$ and $1.97\,\mu\mathrm{m}$ in air and CCl_4, respectively. These values are not only mutually consistent but also compare with the value of $2\,\mu\mathrm{m}$ provided by the vendor. In air, the measured velocity amplitude was $220\,\mu\mathrm{m/s}$, corresponding to a displacement amplitude of 1.98 nm, at the first resonant frequency of 17.62 kHz. In CCl_4 the velocity amplitude was $0.106\,\mu\mathrm{m/s}$, corresponding to a displacement amplitude of 0.50 nm, at the first resonant frequency of 3.41 kHz. The maximum velocity in response to the multitone was about 23-fold higher, depending on the choice of the stimulus phases φ_i. Thus the displacement amplitudes were at least two orders of magnitude smaller than the thickness of the cantilever; this justifies the linear description of stresses in the cantilever (Eq. 2.1).

Since the amplitude of the driving force is unknown, the experimental values were scaled as described in Sec. 2.5.5, yielding a value of $M = 84$ pN in CCl_4 and 30 pN in air for the amplitude of the driving force at each frequency. From the explanation given in Sec. 2.5.4 it is obvious that the ratio of the force amplitudes in different dielectric media should equal the ratio of their dielectric permittivities. The ratio of the force amplitudes was 2.8 compared with 2.2 for $\epsilon_{CCl_4}/\epsilon_{air}$ [95]. The difference can be explained by the

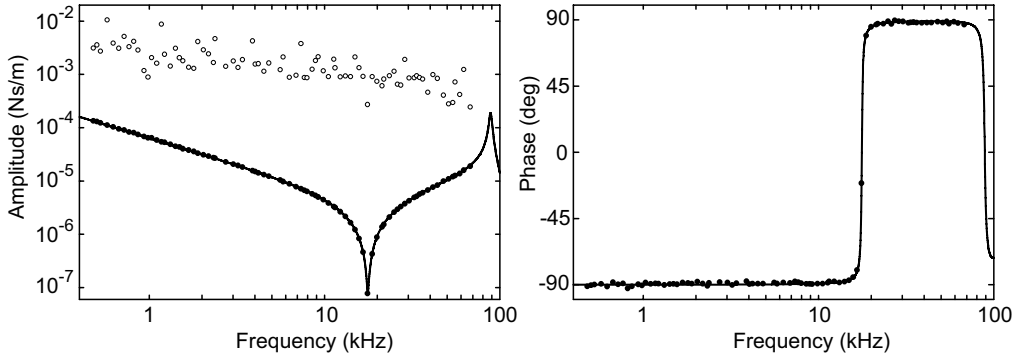

Figure 3.1: *Amplitude and phase of the mechanical driving-point impedance of an AFM cantilever in air. The filled circles are the values measured with a multitone force stimulus and the line is derived from the model (complex conjugate of Eq. 2.23). The parameters for the calculation were $\eta_{air} = 18.6\ \mu Pa\,s$, $\rho_{air} = 1.161\ kg/m^3$ [95], $L = 385\ \mu m$, $b = 59\ \mu m$ and $x_0 = 360\ \mu m$. T was determined to be 1.98 μm compared with the 2 μm given by the manufacturer. The scaling factor for the experimental values, which is equivalent to the amplitude of the applied force, M in Eq. 2.27, was 30 pN. The opened circles are the reciprocal of the noise floor measured on the cantilever in air without stimulation voltage, scaled with the same factor M as the measurement values. Since the points are proportional to the reciprocal of the measured velocity, a low noise floor in the velocity signal corresponds to a high noise floor in the impedance spectrum. Since signal averaging is performed in the time domain, a thermal noise excitation spectrum is absent. The coefficient for the internal friction of the cantilever, $\beta = 5 \times 10^{-8}\ s$, was set so that the calculated impedance at the resonant frequency of 17.62 kHz was the same as the experimental value.*

fact that the position of the steel electrode can be adjusted only with an accuracy of about 1 μm in all three directions. The geometry of the electrode-AFM-tip capacitor is therefore slightly different between two measurements, resulting in a different force for the same applied voltage.

The calculated impedance spectrum is in good agreement with the measured one over the entire frequency range. This was quantified with the mean relative difference between the measured and the calculated values as determined by

$$\Delta = \frac{1}{n} \sum_i \left| \frac{y_i - y(f_i)}{(y_i + y(f_i))/2} \right| \tag{3.1}$$

where y denotes either amplitude or phase, with y_i being the experimental values, $y(f_i)$ the calculated values and n the number of frequency points (115). For air, $\Delta = 0.013$ and $\Delta = 0.011$ for amplitude and phase, respectively. For CCl_4 the values are $\Delta = 0.052$ and $\Delta = 0.135$ for amplitude and phase, respectively. The assumptions of a point force and cantilever of infinite length and zero thickness can account for these small errors.

The spring constant, k, of the cantilever can be calculated using an expression derived by solving Eq. 2.1 for a static point force:

$$k = \frac{3\,EI}{x_0^3} \tag{3.2}$$

which agrees, of course, with the stiffness dominated, low-frequency part of the impedance, where $Z = k/(i\omega)$. The values are $k = 0.401\,\mathrm{N/m}$ in air and $k = 0.394\,\mathrm{N/m}$ in CCl_4. The small difference is due to the slightly different values of T obtained for the two cases.

When the stimulus contained only a single frequency, the velocity amplitudes of higher harmonics were at least an order of magnitude below the amplitude at the stimulus frequency. This was true even if a harmonic was situated at a resonant frequency of the

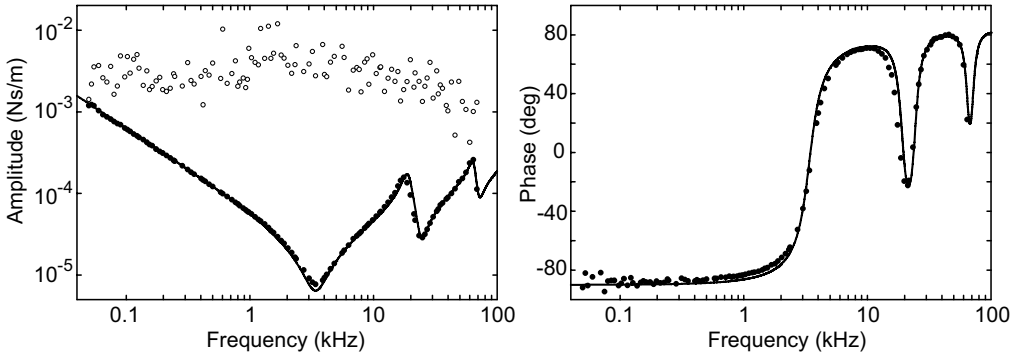

Figure 3.2: *Amplitude and phase of the mechanical driving-point impedance of the same cantilever as in Fig.3.1 in* CCl_4*. The filled circles are the values measured for a multitone force stimulus and the line is derived from the model (complex conjugate of Eq. 2.23). The parameters for the calculation were* $\eta_{CCl_4} = 1.156$ *mPa s,* $\rho_{CCl_4} = 1.610 \times 10^3$ *kg/m*^{3} *[95].* $\beta = 5 \times 10^{-8}$ *s, derived from the measurement in air.* T *was determined to be 1.97* μ*m. The scaling factor for the experimental values, which is equivalent to the amplitude of the applied force,* M *in Eq. 2.27, was 84 pN. The opened circles are the reciprocal of the noise floor measured on the cantilever in* CCl_4 *without stimulation voltage, scaled with the same factor* M *as the measurement values.*

cantilever. Since the highest stimulus frequency for which a harmonic can be detected is 35 kHz, my results show that the linearization of the Navier-Stokes equations is justified, at least up to 35 kHz for the velocity amplitudes used here.

With the free-standing electrode, the experimental setup simulated a situation where the fluid surrounding the cantilever is at rest infinitely far from the cantilever. The same was assumed in the theoretical treatment. However, if the AFM-tip is in contact with a flat extended surface, the fluid motion is restricted nearby the cantilever and the assumption is not necessarily justified. Therefore, the measurements were repeated with the steel electrode embedded in epoxy glue in such a way that the end of the electrode was level with the surface of the resin. In this configuration the AFM-tip was facing a flat plane extending infinitely far compared with the dimensions of the cantilever. The distance between the AFM-tip and the surface was set to about 1.5 ± 0.5 μm. Fig.3.3 shows the comparison between the free-standing and the embedded electrode. The resonant frequencies of the first and second mode were reduced by factors of 0.904 and 0.937, respectively, and the impedance increased by factors of 1.914 and 1.700 when the cantilever was near the surface. These changes can be understood qualitatively with an increase in damping and a change in added mass imposed by the fluid when its motion is restricted nearby the cantilever. In other words, the hydrodynamic function $\Gamma(\omega)$ in Eq. 2.7 will be different for different boundary conditions.

3.2 Impedance of the organ of Corti

Impedance was measured from 30 cochleae, each from a separate animal. One longitudinal location was examined in each cochlea. Measurements were made at up to eight radial positions (Fig. 3.4).

Data were pooled from three longitudinal regions along the cochlea: 3.8–4.5 mm (N=9), 7–8 mm (N=12), and 12–13 mm (N=9) from the round window. Figs. 3.5–3.7 show typical examples from these three longitudinal regions for impedances measured at three different radial positions on the reticular lamina.

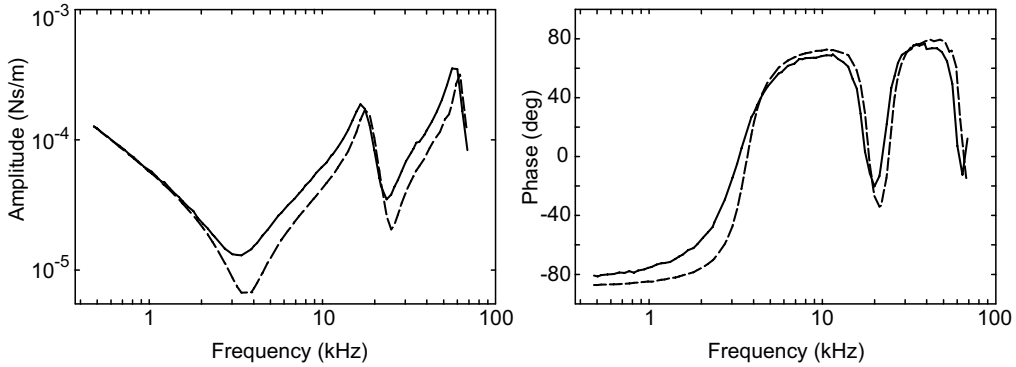

Figure 3.3: *Comparison between the cantilever impedance measured in CCl_4 above a flat surface and in the 'infinitely' extending fluid. The solid line was measured at a distance of 1–2 μm between AFM-tip and the electrode embedded in the surface and the broken line was measured with the same electrode standing free in the fluid and at approximately the same distance between AFM-tip and electrode. The decrease in resonant frequency is a factor of 0.904 for the first and 0.937 for the second mode relative to the case with the free-standing electrode. The increase in impedance amplitude is 1.914 and 1.700 for the first and second mode, respectively. The amplitudes were scaled to coincide with the theoretical (stiffness-dominated) value at 480 Hz.*

3.2.1 A Voigt-Kelvin viscoelastic description of impedance

Data from the organ of Corti could be consistently described by the impedance of a generalized Voigt-Kelvin viscoelastic material; that is with spring in parallel with a dashpot, for which $Z = k/(i\omega) + \mu$, with spring constant k and viscosity μ. The generalization was obtained by choosing the viscosity to be complex-valued, $\mu = \mu' - i\mu''$, such that real, $\Re$, and imaginary, $\Im$, components of Z have the following frequency dependence:

$$\begin{aligned} \Re(Z) &= \mu' = \frac{c_1}{\omega^2} + c_2 + c_3 \exp(-c_4\omega) \\ \Im(Z) &= -\frac{k}{\omega} - \mu'' = -\frac{k}{\omega} - c_5 \ , \end{aligned} \tag{3.3}$$

where $c_1 \ldots c_5$ and k are real-valued parameters, independent of frequency.

Obviously, the organ of Corti at any place along the cochlea is not as homogeneous as implied by this model: it is a mechanically complicated biological structure with fluid-filled channels (Fig. 3.4). Instead, the model is empirical, intended to mathematically describe the data in an analytical form, suitable for future development of biophysical models of the entire cochlea.

In the first step of the fitting procedure, the model Eq. 3.3 was fitted to the data with all parameters free. If one or more of the parameters c_1, c_2, k, or c_5 were not statistically significant, they were successively set to zero and the fitting algorithm repeated. If either or both c_3 or c_4 were not statistically significant, the exponential term was removed from the model in Eq. 3.3, and the fitting algorithm then repeated. This procedure prevented the occurrence of physically meaningless parameters. k and c_2 were always significant; c_1 and c_5 were significant with a few exceptions, and c_3 and c_4 were significant in about half of the cases around the tunnel of Corti, but zero otherwise. In the collated data given in Tables 3.1–3.3, the parameters that were not significant were treated as zero with the exception of c_4: if the exponential term was not used, c_3 was set to zero, but c_4 was excluded from the estimation of mean values. Average values of the fitted parameters for the three cochlear turns are plotted in Fig. 3.8.

In general, the impedance results can be characterized as follows. The real (or frictional) part exhibits a monotonic decrease proportional to ω^{-2}, followed by a region of

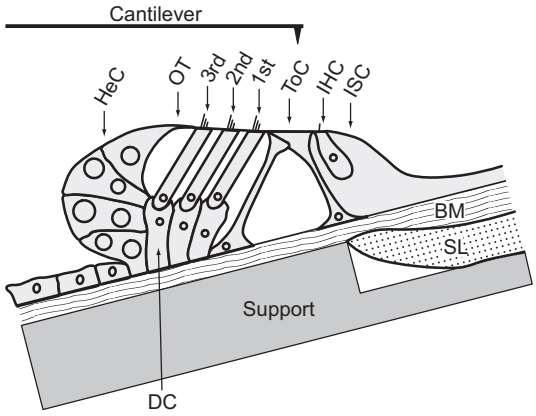

Figure 3.4: *Cross section of the organ of Corti (schematic, from the 2nd cochlear turn) showing the eight recording positions in the radial direction. ISC: inner sulcus cells; IHC: inner hair cell; ToC: tunnel of Corti; 1st – 3rd: rows of outer hair cells; OT: outer tunnel; HeC: Hensen's cells. The basilar membrane lies flat on the support, and is held in place by hydrodynamic forces. The support was tilted, so that the reticular lamina was approximately parallel to the focal plane of the microscope and the long axis of the cantilever. Cells within the ISC are not depicted. SL: Spiral lamina; DC: Deiters' cells. Non-shaded areas depict fluid spaces. The cantilever is drawn approximately to scale.*

reduced slope between 2–5 kHz (particularly evident in Fig. 3.6), and asymptotes to a constant positive value towards 50 kHz[1]. The exponential term in $\Re(Z)$ was introduced to model the region of reduced slope. Both the quadratic decrease and the region of reduced slope were most prominent at the tunnel of Corti and the adjacent positions (inner hair cells and 1st row outer heir cells), and were less obvious for recording locations away from the tunnel of Corti. The imaginary (or storage) part exhibits a decrease proportional to ω^{-1}, which asymptotes to a constant, (usually) negative offset at high frequencies. The proportionality constant of the former is equivalent to the spring constant, k, and the latter represents the imaginary component, μ'', of the viscosity.

3.2.2 Dominance of the real component near the characteristic frequency

At low frequencies, the magnitude of the imaginary component was larger than the real component; on average, a factor of 2.5, 2.8, and 2.9 larger at 500 Hz for outer hair cells of the 1st, 2nd, and 3rd turns, respectively. However, the ratio eventually reversed with increasing frequency, so that in the 1st and 2nd turns, at the characteristic frequency of the recording location, the real part was greater than the imaginary part; on average, 1.7 and 1.5 for outer hair cells of the 1st and 2nd turns, respectively. In the 3rd turn, at the characteristic frequency, the real part remained smaller than the imaginary part by a factor of 0.8. The cross-over frequency, where both have equal magnitude, was located 2.9 and 0.9 oct below the characteristic frequency for the 1st and 2nd turns, respectively, and 0.8 oct above the characteristic frequency for the 3rd turn.

This experimental result compares with a model [118] which proposes that enhanced frequency selectivity, particularly in the basal half of the cochlea, requires that at the characteristic frequency the viscous forces transmitted by Deiters' cells and outer hair cells are greater than the elastic forces.

[1] Here it should be emphasized that I use the word 'asymptote' rather liberally – it simply refers to the observation that the impedance component is constant at high frequencies, up to at least the maximum measurement frequency of 50 kHz. Assertions about a true asymptote would require measurements to at least an octave above the highest physiologically relevant frequency for the tissue; namely, at least 90 kHz for the extreme basal region of the guinea-pig cochlea.

	N	c_1	c_2	c_3	c_4	k	c_5
ISC	3	15.2	2.15×10^{-6}	0	$*$	0.0281	1.16×10^{-7}
IHC	11	180	1.39×10^{-5}	1.22×10^{-5}	$1.17_4 \times 10^{-4}$	0.219	3.94×10^{-6}
ToC	11	491	2.96×10^{-5}	8.44×10^{-6}	$8.04_4 \times 10^{-5}$	0.478	8.43×10^{-6}
1st OHC	9	168	9.72×10^{-6}	3.82×10^{-6}	$2.82_3 \times 10^{-5}$	0.195	3.99×10^{-6}
2nd OHC	9	57.1	6.54×10^{-6}	6.74×10^{-7}	$3.37_1 \times 10^{-5}$	0.112	1.42×10^{-6}
3rd OHC	9	59.6	5.27×10^{-6}	3.59×10^{-7}	$3.72_1 \times 10^{-5}$	0.0670	1.52×10^{-6}
OT	8	57.4	4.68×10^{-6}	0	$*$	0.0534	8.50×10^{-7}
HeC	6	40.0	1.33×10^{-6}	0	$*$	0.0354	0

Table 3.1: *Averaged fitted parameter values from 9 preparations from the region 3.8–4.5 mm from the round window – the basal turn of the cochlea. Radial locations are: inner sulcus cells (ISC), inner hair cells (IHC), tunnel of Corti (ToC), 1st to 3rd row outer hair cells (OHC), outer tunnel (OT), and Hensen's cells (HeC). N gives the number of measurements used for calculating the average. The subscript on the value of c_4 gives the number of measurements, for which both c_3 and c_4 were significantly different from zero, and the exponential term was consequently included. If the exponential term in Eq. 3.3 had to be omitted, c_4 is meaningless, which is indicated by $*$; c_3 was set to zero in this case. All units are SI.*

	N	c_1	c_2	c_3	c_4	k	c_5
ISC	10	45.8	5.99×10^{-6}	6.98×10^{-7}	$1.18_1 \times 10^{-4}$	0.0197	1.31×10^{-6}
IHC	13	194	1.76×10^{-5}	3.59×10^{-6}	$3.34_1 \times 10^{-4}$	0.174	5.46×10^{-6}
ToC	14	416	2.61×10^{-5}	1.04×10^{-5}	$8.49_4 \times 10^{-6}$	0.428	9.24×10^{-6}
1st OHC	13	90.7	8.69×10^{-6}	5.11×10^{-6}	$3.13_6 \times 10^{-5}$	0.149	2.52×10^{-6}
2nd OHC	15	20.8	6.59×10^{-6}	8.34×10^{-7}	$5.43_2 \times 10^{-5}$	0.0480	5.82×10^{-7}
3rd OHC	15	23.5	4.44×10^{-6}	1.00×10^{-6}	$1.55_1 \times 10^{-4}$	0.0326	5.92×10^{-7}
OT	10	16.1	4.47×10^{-6}	0	$*$	0.0296	5.44×10^{-7}
HeC	17	26.0	3.27×10^{-6}	0	$*$	0.0361	3.22×10^{-7}

Table 3.2: *Averaged fitted parameter values from 12 preparations from the region 7–8 mm from the round window – the 2nd turn of the cochlea. Acronyms and notations as in Table 3.1.*

3.2.3 Absence of an inertial component

Positive values for the imaginary component, which are indicative of an inertially dominated impedance at high frequencies, were found only in two cases: on the outer tunnel and Hensen's cells in the 3rd turn of the cochlea (Table 3.3). In all other cases, $\Im(Z) \leq 0$ up to 50 kHz. To verify that the measurement method can actually detect an inertial component, the impedance of a second cantilever was measured in place of the organ of Corti. The expected impedance with a positive imaginary (inertial) part at high frequencies was found. Therefore, I conclude that, except for the outer tunnel and Hensen's cells in the 3rd turn, the mass of the organ of Corti has physically insignificant effect on its dynamical behavior in the transverse direction up to at least 50 kHz.

3.2.4 Spatial dependence of the mechanical parameters

The magnitudes of both the real and the imaginary parts of the impedance were greatest above the tunnel of Corti and decreased towards Hensen's cells and the inner sulcus (Fig. 3.8). This radial position of maximum stiffness is consistent with the triangular structure of the pillar cells spanning the region between basilar membrane and reticular lamina, with their cytoskeletons reinforced by microtubules [170]. The stiffness of the basilar membrane is also known to be largest at the outer pillar cell [110].

The stiffness of the organ of Corti decreased from base to apex of the cochlea – the ratio of the stiffnesses was less than a factor of two (Fig. 3.8). This relatively small longitudinal variation of the compressional stiffness of the organ of Corti contrasts with the situation for the basilar membrane, where the (bending) stiffness decreases by two

	N	c_1	c_2	c_3	c_4	k	c_5
ISC	6	16.3	1.01×10^{-5}	0	$*$	0.0255	0
IHC	7	118	1.95×10^{-5}	0	$*$	0.191	3.46×10^{-6}
ToC	7	321	3.35×10^{-5}	4.23×10^{-6}	$2.22_1 \times 10^{-5}$	0.307	9.92×10^{-6}
1st OHC	7	99.3	1.36×10^{-5}	6.02×10^{-6}	$2.50_2 \times 10^{-5}$	0.201	3.54×10^{-6}
2nd OHC	7	51.4	8.35×10^{-6}	0	$*$	0.0795	1.02×10^{-6}
3rd OHC	6	11.6	6.84×10^{-6}	0	$*$	0.0551	1.25×10^{-7}
OT	6	0	6.22×10^{-6}	0	$*$	0.0190	-3.83×10^{-7}
HeC	7	47.1	4.81×10^{-6}	0	$*$	8.59×10^{-3}	-2.37×10^{-7}

Table 3.3: *Averaged fitted parameter values from 9 preparations from the region 12–13 mm from the round window – the 3rd turn of the cochlea. Acronyms and notations as in Table 3.1. Notice the negative values for c_5 on the outer tunnel and Hensen's cells – this indicates a measurable inertial component.*

orders of magnitude from base to apex [110, 189]. The stiffness of the organ of Corti measured at the tunnel of Corti (0.3–0.5 N/m in Fig. 3.8) is comparable to basilar-membrane stiffness at the outer pillar cells reported [110] for the apical region of the (gerbil) cochlea. In other words, the compressional stiffness of the organ of Corti does not contribute significantly to the mechanical impedance of the cochlear partition in the basal region of the cochlea. This result supports an assumption in a viscoelastic model [118], namely that the 'cochlear amplifier stiffness', k_m, defined in that paper, which is equivalent to the stiffness, k, measured by me at the outer hair cells, appreciably contributes to the cochlear partition stiffness only in the apical region of the cochlea.

When mean parameter values at different radial positions of one longitudinal region are compared, all pairs of c_1, c_2, k, and c_5 are highly correlated (Table 3.4). This implies that they might not be as independent as my empirical viscoelastic model suggests, but could be derived instead from a suitable physical model of the organ.

There was no significant correlation between parameter pairs from different preparations at the same radial and longitudinal recording locations. This is simply explained by the observation that the inter-animal scatter of parameter values was of the order of the standard deviations of the parameter estimates, which in turn were also small (e.g. for k, the coefficient of variation was typically 2–4% at the outer hair cells).

3.2.5 Qualitative observations

Apart from the quantitative results, the following qualitative observations were made: When the tunnel of Corti was compressed in the transverse direction by moving the tip of the cantilever 10 μm beyond the point of initial contact, the visually observable deformation of the reticular lamina extended radially from the inner hair cells to the 3rd row outer hair cells, and longitudinally along the tunnel of Corti for at least 50 μm. Since this is a static displacement, the coupling cannot be mediated by the fluid, but represents a property of the solid structure. This is in agreement with findings of other authors: Naidu and Mountain [111] displaced the basilar membrane with a point probe and measured deflection in the neighborhood of the probe. They found space constants for the longitudinal coupling of 16.7–56.9 μm from base to apex, respectively. Richter et al. [138] measured the response of the basilar membrane to a displacement pulse applied on a certain longitudinal position in the so-called 'hemicochlea' preparation. They found a longitudinal decrease in basilar-membrane vibration amplitude of 58 dB/mm, which corresponds to a space constant of 150 μm. Moreover, in my preparation, the further away (radially) the cantilever tip was situated from the pillar heads, the more local the deformation was. Inner sulcus and Hensen's cells were so soft that pushing the cantilever so far towards the reticular lamina that its tip penetrated the cell membrane and its flat part touched the cells, still led to an extremely localized deformation, extending less than

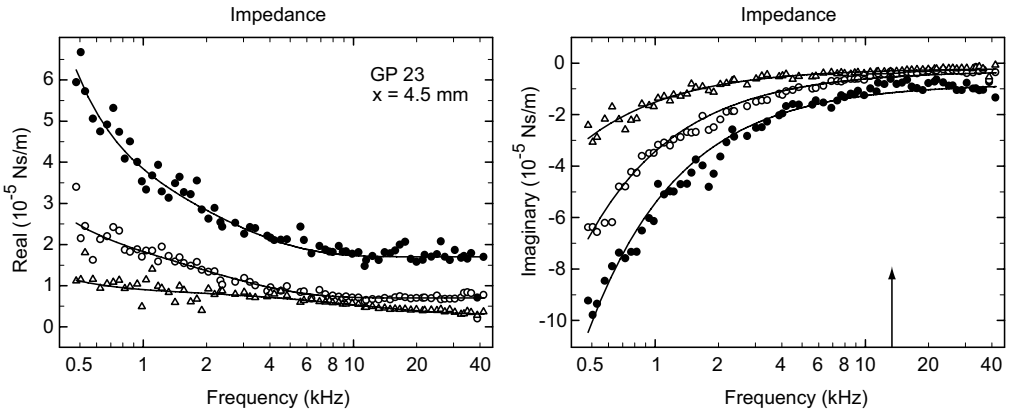

Figure 3.5: *Real and imaginary parts of the impedance of a preparation 4.5 mm from the round window at three radial locations: tunnel of Corti (filled circles), inner hair cell (open circles) and 1st row outer hair cell (open triangles). Notice that the magnitude of the impedance is greatest at the tunnel of Corti. The arrow indicates the characteristic frequency according to the map of Tsuji and Liberman [182]. The fit functions are given by Eq. 3.3. Parameters are (mean ± standard deviation): tunnel of Corti:* $k = 0.292 \pm 0.005$, $c_1 = 237 \pm 27$, $c_2 = (1.75 \pm 0.03) \times 10^{-5}$, $c_3 = (2.38 \pm 0.28) \times 10^{-5}$, $c_4 = (7.11 \pm 0.95) \times 10^{-5}$, $c_5 = (7.92 \pm 0.61) \times 10^{-6}$*; inner hair cell:* $k = 0.197 \pm 0.003$, $c_1 = 49.5 \pm 19.3$, $c_2 = (7.00 \pm 0.23) \times 10^{-6}$, $c_3 = (1.56 \pm 0.21) \times 10^{-5}$, $c_4 = (7.39 \pm 1.10) \times 10^{-5}$, $c_5 = (3.13 \pm 0.34) \times 10^{-6}$*; 1st row outer hair cell:* $k = 0.082 \pm 0.002$, $c_1 = 23.7 \pm 8.0$, $c_2 = (3.21 \pm 0.46) \times 10^{-6}$, $c_3 = (6.03 \pm 0.47) \times 10^{-6}$, $c_4 = (1.53 \pm 0.38) \times 10^{-5}$, $c_5 = (1.94 \pm 0.25) \times 10^{-6}$*. Stiffness of cantilever: 1.20 N/m. All units are SI.*

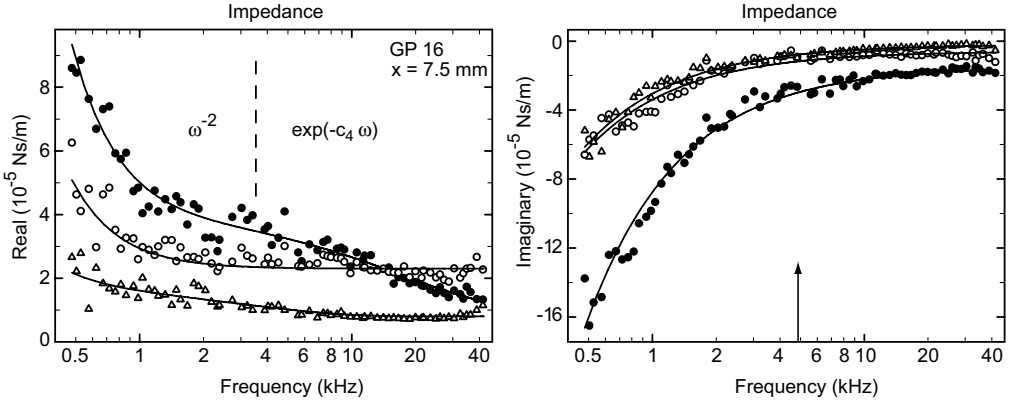

Figure 3.6: *Real and imaginary parts of the impedance of a preparation 7.5 mm from the round window at three radial locations: tunnel of Corti (filled circles), inner hair cell (open circles) and 1st row outer hair cell (open triangles). Dashed line separates the regions where the* ω^{-2} *and exponential terms of Eq. 3.3 dominate – at lower frequencies for* ω^{-2} *and at higher frequencies for the exponential. The arrow indicates the characteristic frequency according to the map of Tsuji and Liberman [182]. Fitted parameters are: tunnel of Corti:* $k = 0.456 \pm 0.009$, $c_1 = 502 \pm 29$, $c_2 = (9.57 \pm 3.20) \times 10^{-6}$, $c_3 = (2.86 \pm 0.27) \times 10^{-5}$, $c_4 = (8.52 \pm 2.17) \times 10^{-6}$, $c_5 = (1.46 \pm 0.10) \times 10^{-5}$*; inner hair cell:* $k = 0.176 \pm 0.005$, $c_1 = 253 \pm 17$, $c_2 = (2.35 \pm 0.04) \times 10^{-5}$, $c_3 = 0$, *c_4 is not used,* $c_5 = (5.65 \pm 0.54) \times 10^{-6}$*; 1st row outer hair cell:* $k = 0.179 \pm 0.004$, $c_1 = 53.7 \pm 20.5$, $c_2 = (7.68 \pm 0.39) \times 10^{-6}$, $c_3 = (9.01 \pm 1.65) \times 10^{-6}$, $c_4 = (4.57 \pm 1.33) \times 10^{-5}$, $c_5 = (1.54 \pm 0.48) \times 10^{-6}$*. Stiffness of cantilever: 1.20 N/m. All units are SI.*

15 μm around the cantilever, while the cells appeared to wrap around it. Therefore, it seemed as if the pillar cells form a rigid longitudinal beam, surrounded by tissue, which becomes increasingly softer in the radial direction.

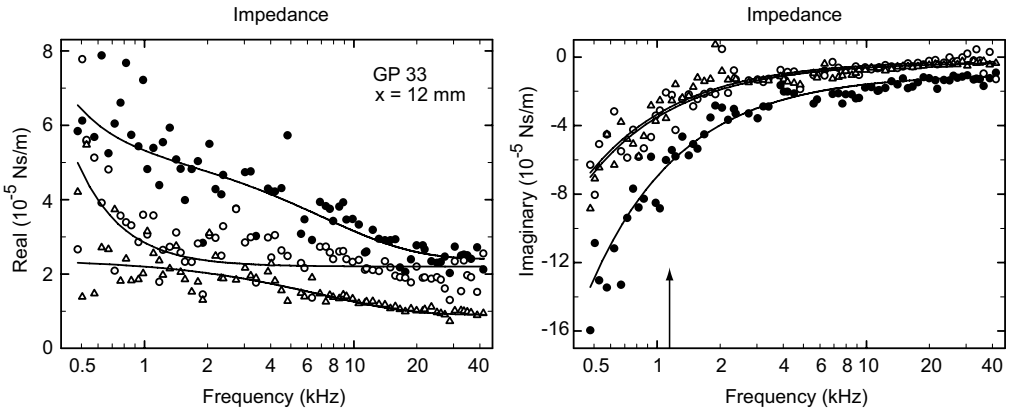

Figure 3.7: *Real and imaginary parts of the impedance of a preparation 12 mm from the round window at three radial locations: tunnel of Corti (filled circles), inner hair cell (open circles) and 1st row outer hair cell (open triangles). The arrow indicates the characteristic frequency according to the map of Tsuji and Liberman [182]. Fitted parameters are: tunnel of Corti:* $k = 0.375 \pm 0.010$, $c_1 = 122 \pm 48$, $c_2 = (2.41 \pm 0.16) \times 10^{-5}$, $c_3 = (2.96 \pm 0.28) \times 10^{-5}$, $c_4 = (2.22 \pm 0.52) \times 10^{-5}$, $c_5 = (1.04 \pm 0.11) \times 10^{-5}$*; inner hair cell:* $k = 0.198 \pm 0.009$, $c_1 = 254 \pm 36$, $c_2 = (2.19 \pm 0.08) \times 10^{-5}$, $c_3 = 0$, c_4 *is not used,* $c_5 = (2.37 \pm 1.01) \times 10^{-6}$*; 1st row outer hair cell:* $k = 0.202 \pm 0.008$, $c_1 = 0$, $c_2 = (9.39 \pm 1.15) \times 10^{-6}$, $c_3 = (1.47 \pm 0.15) \times 10^{-5}$, $c_4 = (2.29 \pm 0.68) \times 10^{-5}$, $c_5 = (2.68 \pm 0.88) \times 10^{-6}$*. Stiffness of cantilever: 1.59 N/m. At frequencies below about 2 kHz, the SNR was about half that for the more basal recordings in Figs. 3.5 and 3.6, because the cantilever was stiffer and, in addition, the magnetic force was 70% of that for the softer cantilever. All units are SI.*

3.3 Electrically evoked vibration of the organ of Corti

Data are presented here from 61 preparations, which appeared to be in normal morphological condition: 1) orderly arrangement of hair cells, supporting cells, and Hensen's cells, 2) cylindrical shaped OHCs, 3) alignment of the reticular lamina in the focal plane of the microscope. Typical displacement patterns from the first three cochlear turns are shown in Figs. 3.9 and 3.10.

Four characteristic properties of the displacement responses were quantified: the average low-frequency amplitude (at 0.48–1 kHz), A; the asymptotic high-frequency amplitude slope, s; the corner frequency at which the high-frequency amplitude decrease begins, f_c (defined as the intersection of regression lines below and above the cut-off); and the total phase shift in the range 0.48–67 kHz, $\Delta\varphi$. The values were averaged from subsets corresponding to the 1st, 2nd, and 3rd cochlear turn. Table 3.5 summarizes these parameters.

3.3.1 First and second row OHC

1st and 2nd row OHCs always moved in a very similar manner (Fig. 3.9): the displacement amplitude was independent of frequency below 2–4 kHz. In this frequency region a small decrease of a few dB occurred (thick arrows in Fig. 3.9), followed by a second frequency independent region up to about 10 kHz. Above that and in the high-frequency limit, the amplitude decreased linearly on a log-log scale. The displacement phase started at somewhat less than -180° at 480 Hz and shifted by -45° up to the 2–4 kHz, where the small down-step in amplitude occurred. The phase then decreased by a few degrees up to 10 kHz, and finally shifted down to -360° between 10–50 kHz. At higher frequencies a difference between 1st and 2nd row OHCs occurred: while the phase at the 1st row OHCs remained constant at about -360° above 40 kHz, the phase at the 2nd row OHCs continued to decrease.

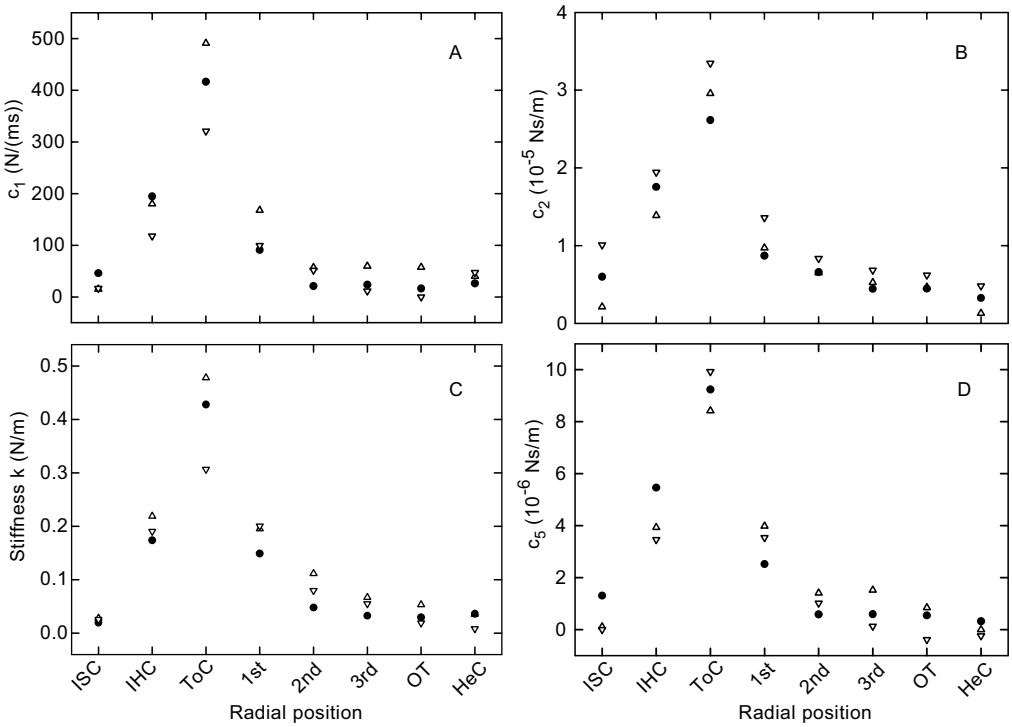

Figure 3.8: *Mean parameter profiles across the organ of Corti for the three longitudinal regions of the cochlea. Upward triangles: 3.8–4.5 mm, circles: 7–8 mm, downward triangles: 12–13 mm. A: c_1, the proportionality constant describing the quadratic decrease of $\Re(Z)$ at low frequencies; B: c_2, the high-frequency value of $\Re(Z)$; C: k, the stiffness; D: c_5, the high-frequency value of $-\Im(Z)$. In order to make the different regions comparable, the radial positions are set to equidistant intervals rather than true distance. Notice that the tunnel of Corti presents the stiffest component, and that its stiffness becomes progressively larger towards the base of the cochlea. Error bars are not shown because the standard deviations were in most cases smaller than the radius of the plot symbols. Acronyms as in Table 3.1.*

The direction convention for the interferometer is such that a positive velocity is directed towards the objective. Therefore, a phase of -180° means that the cells contract if the extracellular potential is positive at the apical end of the cells relative to that at the basal end, and that the reticular lamina moves towards scala tympani in this case.

The high-frequency amplitude slope, s, was approximately -12 dB/oct and the total phase shift, $\Delta\varphi$, was approximately -180° (Table 3.5). This means that the frequency responses were those of a second-order low-pass filter in the high-frequency limit. Although the response of the 1st and 2nd row OHCs is similar to an overdamped resonator, the amplitude step between 2 and 5 kHz indicates that the two-pole filter is not a resonant one, but a combination of two first-order low-pass filters with different corner frequencies. This view is consistent with the fact that the viscoelastic impedance of the organ presents one first-order low-pass filter to the applied force. Consequently, the second first-order low-pass filter must be in the generated force. The frequency response of the force is discussed in detail in Sec. 3.4.

The corner frequency, f_c, was similar to CF for the mean basal turn location (Table 3.5). It decreased with position along the cochlea (Fig. 3.11) but the decrease was much less pronounced than that of CF, so that in the 2nd and 3rd cochlear turns, f_c was at least two octaves above CF. In other words, so far as cochlear function is concerned, these filter functions for the OHCs are *effectively* all-pass functions. A similar conclusion was drawn for the electromechanical displacement of the isolated OHC [46].

	3.8–4.5 mm				7–8 mm				12–13 mm			
	c_1	c_2	k	c_5	c_1	c_2	k	c_5	c_1	c_2	k	c_5
c_1	1.00	0.987	0.989	0.979	1.00	0.982	0.982	0.991	1.00	0.960	0.911	0.986
c_2		1.00	0.992	0.981		1.00	0.957	0.994		1.00	0.928	0.974
k			1.00	0.990			1.00	0.968			1.00	0.957
c_5				1.00				1.00				1.00

Table 3.4: *Pearson's correlation coefficients for the mean values of c_1, c_2, k, and c_5. Pairs were taken from one longitudinal region and the correlation coefficient calculated for the 8 radial positions. Correlation matrices from all three longitudinal regions are included in this table. c_3 and c_4 are omitted because they describe a region of reduced slope, which was found mainly, although not exclusively, for recordings at the tunnel of Corti. All correlation coefficients are significantly different from zero. All units are SI.*

3.3.2 Third row OHC

The 3rd row OHCs moved with similar amplitudes as the 1st and 2nd row OHCs. However, they sometimes showed larger phase lags at higher frequencies (Fig. 3.10B) or even moved in reverse phase to the 1st and 2nd row OHCs (Fig. 3.10F). In the latter case, 3rd row OHCs were in phase with the OT and HeCs (see also Sec. 3.3.5).

3.3.3 IHC

Importantly, IHC displacement phases were in *counterphase* to the 1st and 2nd row OHCs over the whole investigated frequency range. They started at 0° at 480 Hz, and began to decrease above about 2 kHz to a saturation value of -180° at 40 kHz. Displacement amplitudes between 0.48 and 2 kHz were generally a few dB smaller than at the 1st and 2nd row OHCs. However, between 4 and 10 kHz IHC amplitudes exhibited a maximum similar to a broadly tuned resonant or band-pass filter, with amplitudes reaching the OHC values. In the high-frequency limit, frequency responses at the IHCs were approximately those of a second-order low-pass filter ($s \approx -12$ dB/oct, $\Delta\varphi \approx -180°$, see Table 3.5), as was the case for 1st and 2nd OHCs. The corner frequency separating the high-frequency roll-off from the low-frequency region decreased along the cochlea. It was near CF in the mean basal-turn location (Fig. 3.11), and at least two octaves above CF in the more apical turns.

3.3.4 Tunnel of Corti

The motion of the inner border of the inner pillar head was almost identical to that of the adjacent IHC cuticular-plate. The same was true for the outer border of the outer pillar head and the adjacent cuticular plate of the 1st row OHC (Fig. 3.10B and D). Since the IHCs move in counterphase to the 1st and 2nd OHCs, there must be a pivot point somewhere near the attachment of inner and outer pillar heads. In addition, displacement amplitude and phase at the attachment region were very sensitive to small radial changes in the measurement position and sometimes depended strongly on frequency (Fig. 3.10A, C, and E). It is, therefore, concluded that this pivot is radially located near the attachment between inner and outer pillar heads, and that its exact position changes somewhat with frequency.

3.3.5 Outer tunnel and Hensen's cells

The reticular-lamina surface of outer tunnel and Hensen's cells moved in opposite phase to the 1st and 2nd row OHCs. In some cases the 3rd row OHCs were in phase with

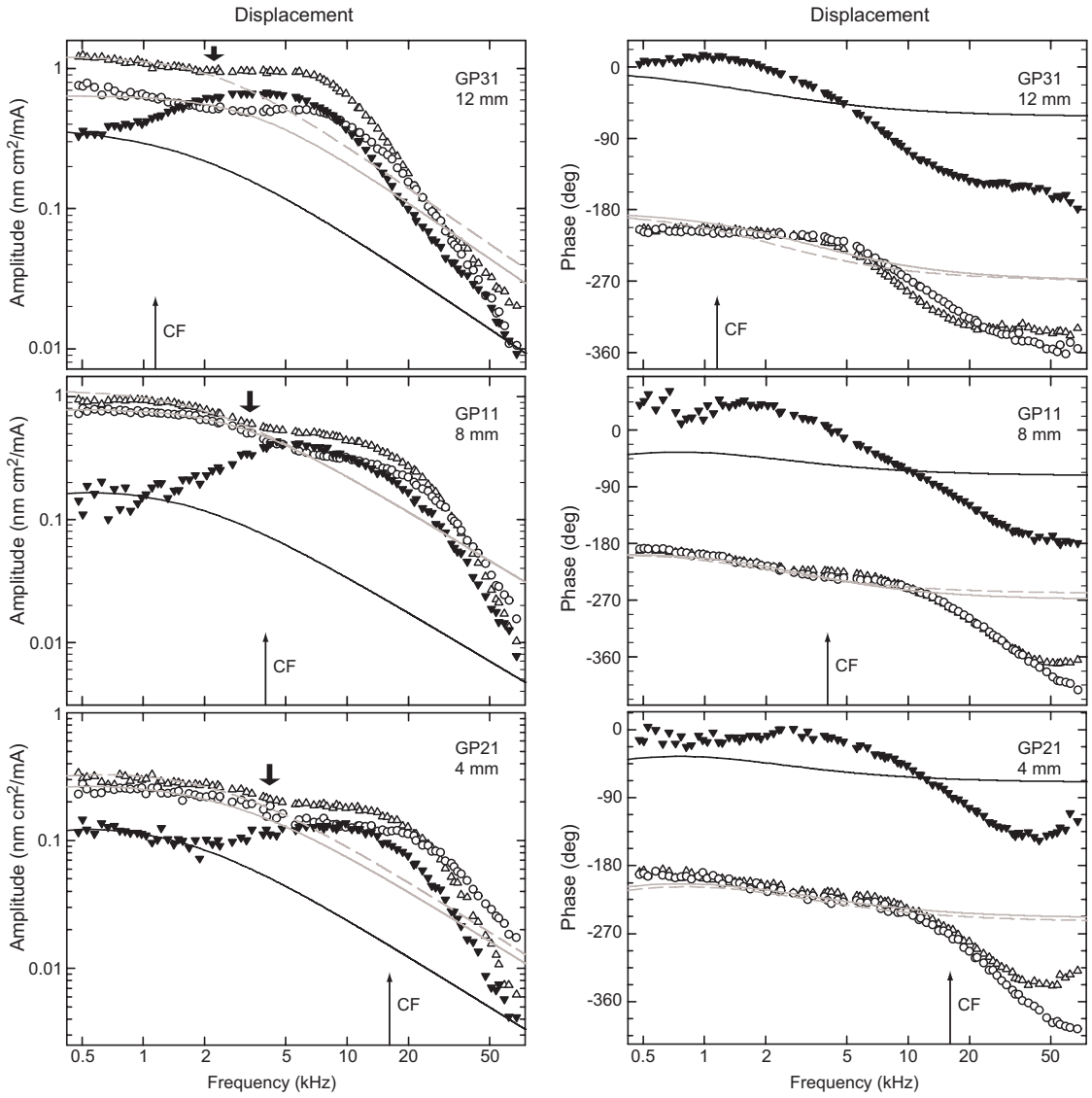

Figure 3.9: *Displacement amplitudes (left) and phases (right) for three preparations: upper panel: $x = 12$ mm ($CF \approx 1.2$ kHz); middle panel: $x = 8$ mm ($CF \approx 4.2$ kHz); lower panel: $x = 4$ mm ($CF \approx 15.2$ kHz). Filled triangles and black line: IHC; open circles and solid grey line: 1st row OHC; open triangles and dashed grey line: 2nd row OHC. Thin arrows: CF calculated from the tonotopic map of Tsuji and Liberman [182]. The lines give the (calculated) displacement responses to a hypothetical, frequency independent test force acting on the (measured) viscoelastic impedance at the respective position. They show the first-oder low-pass characteristic of the viscoelastic material. The amplitude of this test force is scaled arbitrarily to match the measured displacement amplitudes at 480 Hz. Note that there is a step in the measured amplitude response (thick arrows); this coincides with the cut-off frequency in the constant-force case and might suggest that it results from the material properties of the organ. Above 4–5 kHz for the OHC and 1-2 kHz for the IHC, the measured displacement is higher than what is expected for a constant force; this implies a force which increases with frequency. In the high-frequency limit, the measured frequency response corresponds to a second-order low-pass filter (Table 3.5)*

the outer tunnel (Fig. 3.10F), while in other cases they were in phase with the 1st and 2nd row OHCs (Fig. 3.10B and D). Therefore, another pivot point (besides the tunnel of Corti) occurs between 2nd row OHCs and outer tunnel, either inside or outside the 3rd row OHCs. In the 1st turn of the cochlea, the pivot was inside the 3rd row OHCs

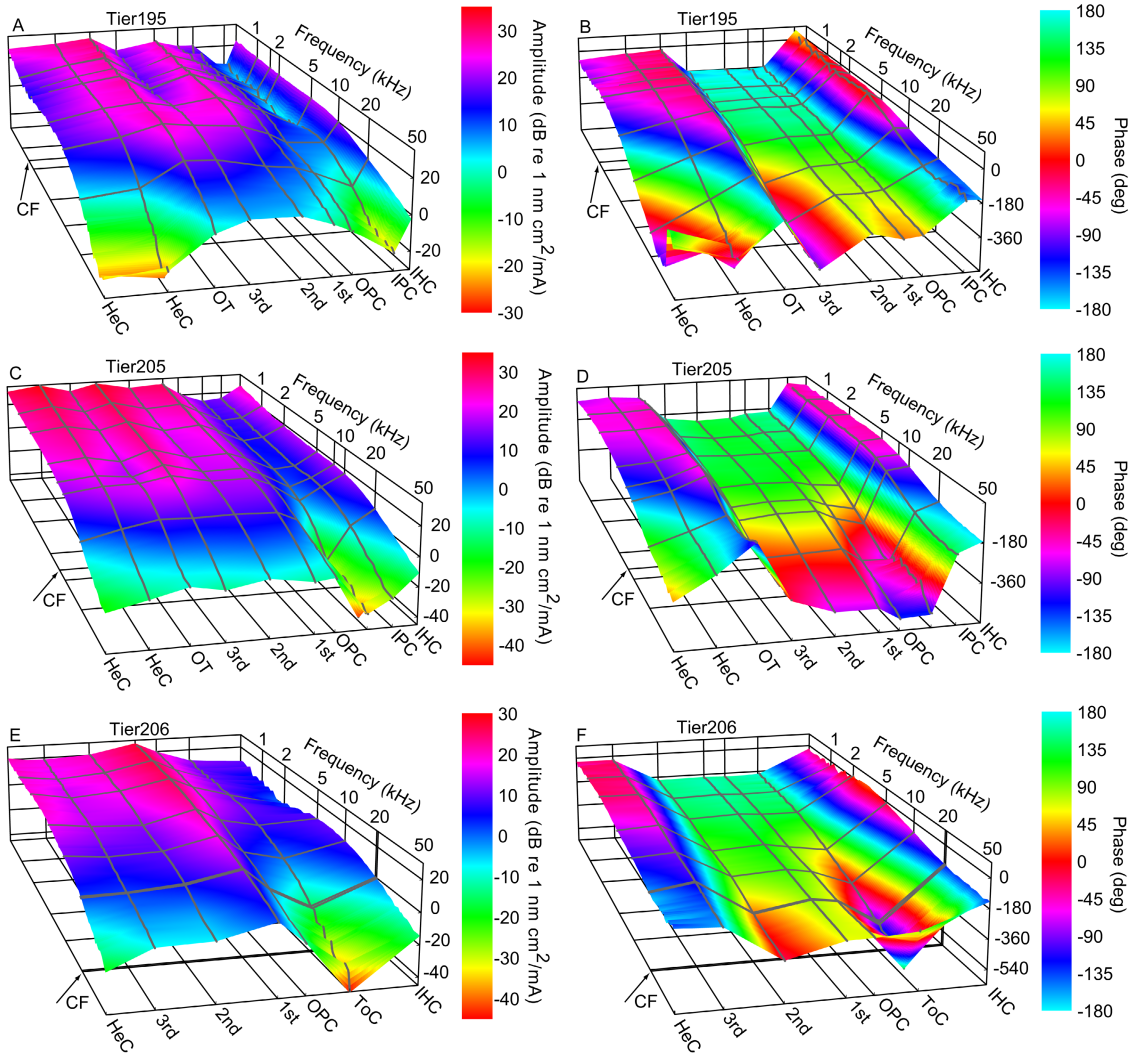

Figure 3.10: *Displacement amplitudes (left) and phases (right) as functions of frequency measured at different radial positions for three preparations. Upper panel: $x = 11$ mm ($CF \approx 1.6$ kHz); middle panel: $x = 6$ mm ($CF \approx 8$ kHz); lower panel: $x = 3$ mm ($CF \approx 20.9$ kHz). Radial positions are: inner hair cells (IHC); inner pillar cells (IPC); tunnel of Corti (ToC); outer pillar cells (OPC); 1st to 3rd row OHC; outer tunnel (OT); Hensen's cells (HeC). Arrows: CF calculated from the tonotopic map of Tsuji and Liberman [182]. Notice phase reversals between IPC and OPC and between 2nd OHC and OT (see Table 3.6). Displacement exhibits a low-pass characteristic with parameters given in Table 3.5. Note that phase jumps randomly when amplitudes approach the noise level (typically -30 to -40 dB).*

in almost half of the cases, while towards the apex of the cochlea, the pivot was more frequently outside of the 3rd row OHCs (Table 3.6).

3.3.6 Effect of drugs on displacement

In these experiments, all agents that affected the electrically induced displacement did so by attenuating the amplitude response independent of frequency, but without affecting the phase response. An example is given in Fig. 3.12.

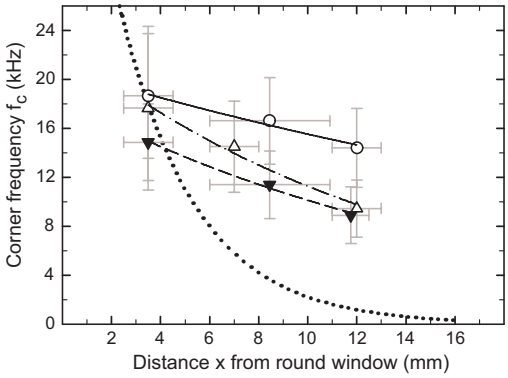

Figure 3.11: *Average corner frequencies of the displacement low-pass characteristic for three radial positions and three longitudinal regions. Filled triangles: IHC; open circles: 1st OHC; open triangles: 2nd OHC. Horizontal error bars give the range of longitudinal positions, x, included in the calculation of the average f_c, vertical error bars the standard deviation of f_c. The numbers of measurements from which each average was determined are in the range 51–116. For all three radial positions, the mean f_c are significantly linearly correlated with x. Exponential regression lines and Pearson's correlation coefficients, r, are: IHC: $f_c = (18.5 \pm 0.7) \times 2^{-x/(11.5\pm1.0)}$, $r = -0.9998$; 1st OHC: $f_c = (20.8 \pm 0.8) \times 2^{-x/(23.7\pm3.7)}$, $r = -0.9930$; 2nd OHC: $f_c = (23.0 \pm 1.4) \times 2^{-x/(9.7\pm1.2)}$, $r = -0.9995$. The dotted line gives the characteristic frequency according to the map of Tsuji and Liberman [182]: $CF = 54.7 \times 2^{-x/2.2}$.*

	x (mm)	N	A (dBnm)	f_c (kHz)	s (dB/oct)	$\Delta\varphi$ (deg)
1st OHC	2.5–4.5	19	0.5 ± 14.3	18.7 ± 5.1	-10.3 ± 2.4	-184 ± 68
	6–10.9	16	5.2 ± 11.9	16.6 ± 3.5	-13.4 ± 3.1	-230 ± 49
	11–13	16	-1.7 ± 8.2	14.4 ± 3.2	-11.2 ± 2.0	-135 ± 37
2nd OHC	2.5–4.5	30	-0.1 ± 13.7	17.7 ± 6.7	-11.2 ± 2.5	-198 ± 103
	6–8	63	13.4 ± 10.9	14.5 ± 3.7	-13.2 ± 3.0	-225 ± 79
	11–13	23	1.3 ± 7.8	9.5 ± 2.3	-10.1 ± 2.3	-157 ± 76
IHC	2.5–4.5	24	-9.5 ± 14.7	14.9 ± 3.1	-15.8 ± 2.5	-209 ± 84
	6–10.9	22	-1.3 ± 16.9	11.4 ± 2.8	-14.5 ± 3.2	-177 ± 44
	11–12.5	16	-4.1 ± 10.5	8.9 ± 2.3	-12.0 ± 2.0	-156 ± 38

Table 3.5: *Parameters extracted from the displacement spectra at the 1st and 2nd row outer hair cells (OHC) and inner hair cells (IHC). The longitudinal distances from the round window, x, were pooled in regions corresponding to the 1st, 2nd and 3rd cochlear turn. The actual range of x, from which preparations were included in the statistics, is given in column two. N is the number of measurements in this x-range; A the average low-frequency amplitude (at 0.48–1 kHz) normalized to current density in the chamber, given in units of dBnm := dB re 1 nm/(mA/cm^2); f_c the corner frequency for the low-pass characteristic; s the asymptotic high-frequency amplitude slope; $\Delta\varphi$ the total phase shift between 480 Hz and 67 kHz. Values are given as mean ± standard deviation.*

3.3.6.1 Blockers of electromechanical transduction

Non-specific electrically induced motion of the organ of Corti was tested by application of blockers of electromechanical transduction. First, sodium salicylate is known to reduce electromotility [146, 155], axial cell stiffness [146], and non-linear capacitance [155]. Within 5–10 min after perfusion with 0.2–10 mM, salicylate reversibly reduced displacement amplitudes, equally at IHCs and OHCs, by factors of 0.54±0.22 for 0.2 mM salicylate (N=13), 0.39±0.11 for 1 mM salicylate (N=6), and 0.34±0.08 for 10 mM salicylate (N=11). The mean attenuation for all concentrations was 0.44±0.20 (N=30). Second, since electromotility depends on intracellular Cl^- [123, 151], and since niflumic acid, a non-specific anion channel inhibitor, reduces nonlinear capacitance [151], we tested the two chloride channel blockers anthracene-9-carboxylic acid (9-AC [82]) and tamoxifen [35]. Within 3–5 min of perfusion, 9-AC of concentration 0.2-1 mM reversibly

x (mm)	2.5–4.5	6–10.9	11–13
3rd in phase with 2nd OHC	13/24 (54%)	29/32 (91%)	16/17 (94%)

Table 3.6: *Number of cases where 3rd row OHCs moved in phase with 2nd row OHCs, implying that the phase reversal occurred between 3rd row OHCs and outer tunnel, at three different longitudinal regions of the cochlea. Given is also the total number of measurements and the percentage.*

reduced displacement amplitudes by a factor of 0.24±0.05 (N=8). 50–100 μM tamoxifen had no significant effect (N=5). Taken together, the experiments with these two effective blockers unequivocally demonstrate that the electrically induced vibration of the organ of Corti derives from the electromechanical action of the OHCs, and not from electrophoretic fluid drag or from surface charges.

3.3.6.2 Blockers of channels in the stereocilia

To examine the possibility of current flow through channels in the OHC stereocilia, we perfused with a mixture containing 600-μM dihydrostreptomycin (DHSM) for the mechanosensitive transducer channels [76], 600-μM suramin for the P2X-receptors [34], and 10-μM carboxyeosin for Ca^{2+}-ATPase [197]. Moreover, KCl was replaced with CsCl to block potassium currents. This mixture had no significant effect on vibration (N=3), as examined over a period of 20 min after perfusion. These results suggest that current through channels in the OHC stereocilia is negligible under our experimental conditions.

3.3.6.3 Blockers of channels in the basolateral cell membrane

To examine the possibility of current flow through channels in the OHC basolateral cell membrane, we perfused with a mixture containing the above stereocilia channel blockers and blockers of cation channels in the cell wall: 100-nM tetrodotoxin for the Na^{+}-channels [17], 200-μM linopirdine for the KCNQ4-channels [102], 10-μM paxilline for the BK-channels [167], and 30-μM tubocurarine for the α-9 receptors [10]. This mixture reversibly reduced the displacement amplitudes by a factor of 0.55±0.06 (N=3), within 3–5 min after perfusion. As a test of the significance of this block, in a further set of experiments we augmented this mixture with a combination of 200-μM 9-AC, which we have shown to block electromechanics, and 10-μM tamoxifen. This mixture reversibly reduced the displacement amplitudes by a factor of 0.14±0.02 (N=3), within 3–5 min after perfusion. This suggests a multiplicative effect of the blockers of electromechanics and cation channels in the cell wall. Taken together, these results unequivocally demonstrate that, in this experimental configuration, current enters the OHC through the basolateral cell membrane.

3.4 Force generation in the organ of Corti

Data are presented here for 30 preparations for which both velocity on the reticular lamina, v, and compressional mechanical impedance of the organ of Corti, Z, were measured up to 50 kHz in the same preparation on the same radial positions. The force, F, acting on the measured point on the upper surface of the organ of Corti was calculated as $F = Zv$. This F is the Norton equivalent point force which needs to be applied to the equivalent impedance Z in order to produce the velocity v at this point of the reticular lamina. Typical force data for the first three cochlear turns are shown in Fig. 3.14. Quantitative properties of the force spectra are collected in Table 3.7.

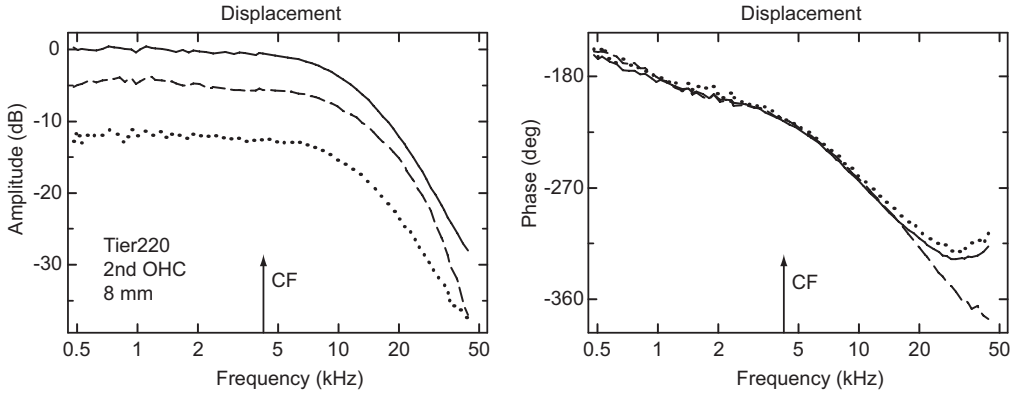

Figure 3.12: *Effect of 9-AC on electrically evoked displacement at a 2nd row OHC. Solid line: control; dotted line: 5 min after perfusion with 500-μM 9-AC; dashed line: 5 min after washout. The washout was not perfect due to flow constraints in the chamber. Amplitude is scaled to the control value at 480 Hz of 2.4 nm/(mA/cm^2).*

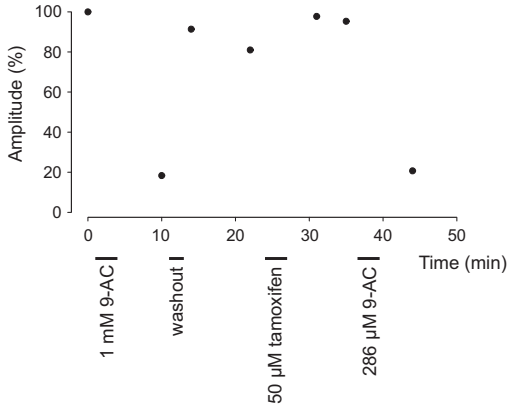

Figure 3.13: *Effect of 9-AC and tamoxifen on the low-frequency displacement amplitude. The rinsing duration and content of different bath media are indicated below the time axis. 9-AC leads to a reversible amplitude attenuation to less than 25% for concentrations of both 0.28 and 1.00 mM. In contrast, application of 50 μM tamoxifen was followed by a statistically insignificant amplitude increase. Both effects were observed within 5 min after application.*

3.4.1 First and second row OHC

Force amplitudes between 0.48–2 kHz were 30–100 pN cm^2/mA. At higher frequencies they exhibited a broad maximum. Average quality factors, Q_{3dB}, defined as the reciprocal of the relative 3-dB-width of this peak, were 0.6–0.8; there was no statistical difference between values from the different cochlear turns. Peak amplitudes were 5–10 dB above the low-frequency values (r_p in Table 3.7). The phase at the peak was roughly -90°. Mean peak frequencies, f_p, decreased from 17.0 to 12.6 kHz from the 1st to 3rd cochlear turn (Fig. 3.15) for the 1st row OHCs; the range was 17.4 to 9.5 kHz for the 2nd row OHCs. While in the 1st turn they were similar to the characteristic frequency, in the higher turns they were several octaves above the characteristic frequency. Amplitude slopes s at the highest frequencies, above the peak, were -3.5–8.4 dB/oct. Average total phase shifts $\Delta\varphi$ between 0.48–50 kHz were in the range 96°–180° with relatively large standard deviations. Considering the fact that the asymptotic limit might not have been fully reached, these values of s and $\Delta\varphi$ are indicative of a system of order between one and two (or between 2/3 and 5/3 based on the high-frequency amplitude slopes).

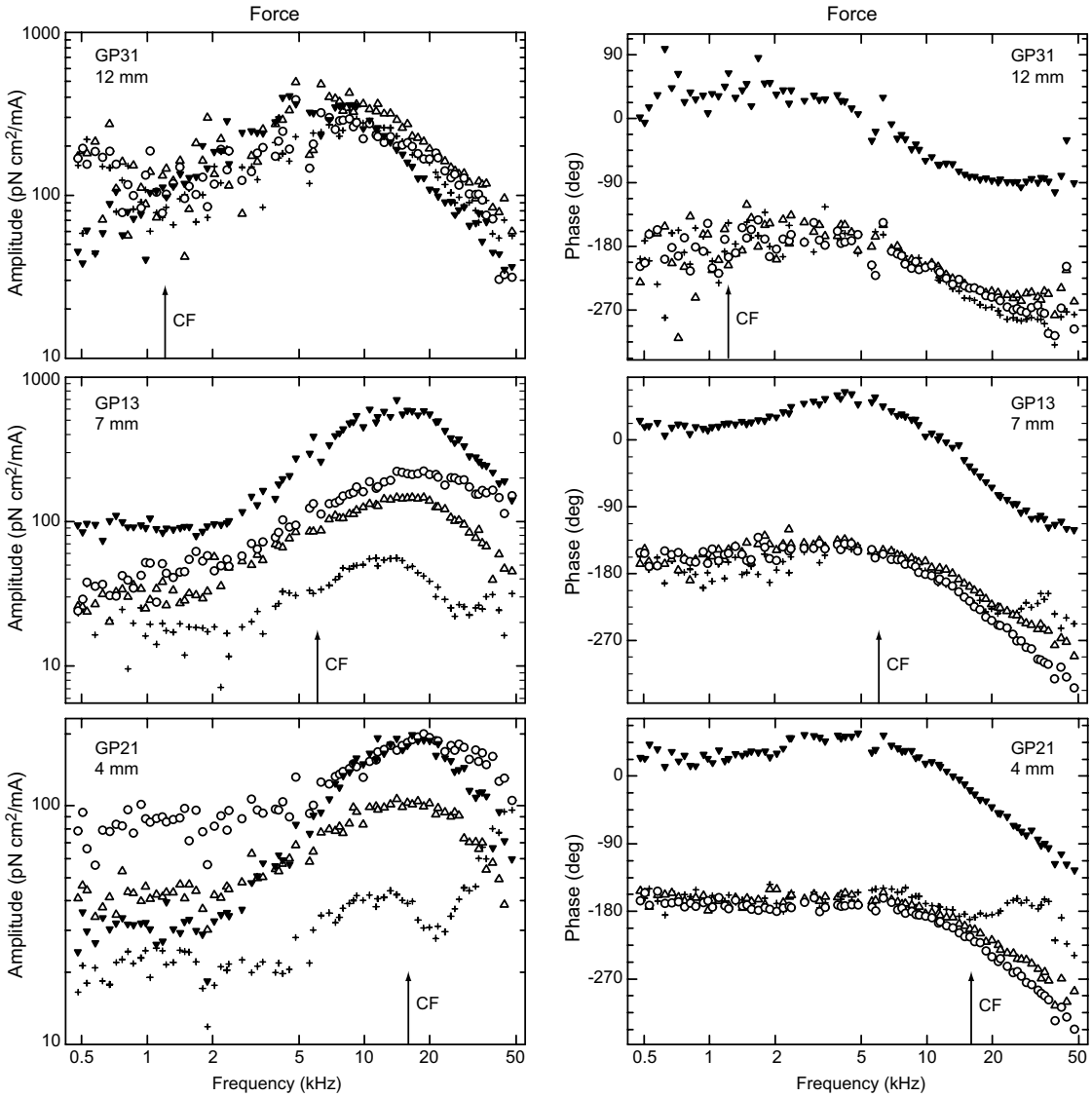

Figure 3.14: *Force amplitudes (left) and phases (right) for three preparations. Upper panel: $x = 12$ mm ($CF \approx 1.2$ kHz); middle panel: $x = 7$ mm ($CF \approx 5.8$ kHz); lower panel: $x = 4$ mm ($CF \approx 15.2$ kHz). Filled triangles: IHC; open circles: 1st row OHC; open triangles: 2nd row OHC; crosses: 3rd row OHC. Arrows: CF calculated from the tonotopic map of Tsuji and Liberman [182]. The maximum is most pronounced for the IHC. Above the frequency of the maximum, amplitudes and phases correspond to a low-pass filter of order between one and two (Table 3.7).*

3.4.2 Third row OHC

Force spectra at the 3rd row OHCs were different to those at the 1st and 2nd row OHCs in the following respects: 1) in most cases amplitudes were 5 to 10 dB smaller, 2) in the 1st and 2nd cochlear turn, $\Delta\varphi$ was never more negative than -90° while in the 3rd turn there were three subpopulations with $\Delta\varphi$ grouped around -90°, -270°, and -450°. 3) Two amplitude peaks, separated by a dip, occurred in about 70% of the data. In most cases (23 of 25) low-frequency velocity, and thus force, at the 3rd row OHCs was in phase with those at the 2nd row OHCs[2]. The exceptions were two measurements in the 1st cochlear

[2]Please note that the velocity measurements used for the force calculation are a subset of all measurements evaluated in Sec. 3.3.

	x (mm)	N	A (dBpN)	f_p (kHz)	s (dB/oct)	$\Delta\varphi$ (deg)	Q_{3dB}	$r_p(dB)$
1st OHC	3.8–4.5	7	35.3 ± 7.6	17.0 ± 3.0	-3.5 ± 2.3	-129 ± 33	0.7 ± 0.2	5.1 ± 3.4
	7–8	11	39.1 ± 6.7	12.8 ± 3.3	-7.3 ± 2.9	-180 ± 45	0.7 ± 0.1	7.3 ± 4.4
	11.5–13	10	40.2 ± 5.1	12.6 ± 4.6	-5.2 ± 2.0	-96 ± 41	0.6 ± 0.1	8.1 ± 5.0
2nd OHC	3.8–4.5	12	28.2 ± 6.1	17.4 ± 2.8	-4.7 ± 2.3	-127 ± 58	0.8 ± 0.2	9.0 ± 4.3
	7–8	18	34.1 ± 5.3	12.5 ± 2.5	-8.4 ± 2.4	-144 ± 65	0.8 ± 0.1	10.6 ± 4.8
	11.5–13	10	35.1 ± 8.7	9.5 ± 2.9	-5.4 ± 1.6	-152 ± 99	0.6 ± 0.2	10.1 ± 5.5
IHC	3.8–4.5	15	20.9 ± 11.3	13.3 ± 2.5	-10.2 ± 2.1	-198 ± 43	0.8 ± 0.1	20.0 ± 5.9
	7–8	14	31.2 ± 8.4	11.3 ± 2.1	-8.0 ± 3.0	-167 ± 89	0.8 ± 0.1	14.8 ± 3.6
	11.5–12.5	9	37.2 ± 8.3	7.8 ± 1.0	-4.6 ± 1.4	-94 ± 35	0.7 ± 0.1	15.0 ± 3.6

Table 3.7: *Parameters extracted from the force spectra at the 1st and 2nd row outer hair cells (OHC) and inner hair cells (IHC). The longitudinal distances from the round window, x, were pooled in regions corresponding to the 1st, 2nd and 3rd cochlear turn. The actual range of x, from which preparations were included in the statistics, is given in column two. N is the number of measurements in this x-range; A the average low-frequency amplitude (at 0.48–1 kHz) normalized to current density in the chamber, given in units of dBpN := dB re 1 pN/(mA/cm^2); f_p the peak frequency; s the asymptotic high-frequency amplitude slope; $\Delta\varphi$ the total phase shift between 0.48–50 kHz; Q_{3dB} the quality factor, defined as f_p over the 3-dB width of the peak; r_p the amplitude at f_p relative to the low-frequency amplitude. Values are given as mean ±standard deviation.*

turn, where the forces at these two positions were in counterphase.

3.4.3 IHC

Force responses at the IHCs were very similar to those at the 1st and 2nd row OHCs, with a broad amplitude maximum, except that the maximum was more pronounced: the peak amplitude was 10–20 dB above the low-frequency values of 10-70 pN cm^2/mA. With values of 0.7–0.8, Q_{3dB} was the same as at the 1st and 2nd row OHCs. The peak frequency, f_p, decreased from 13.3 to 7.8 kHz from the 1st to 3rd cochlear turn. It was slightly below that at the 1st row OHCs (Figs. 3.14 and 3.15). Nevertheless, it was similar to CF in the basal cochlear turn and several octaves above CF in the 2nd and 3rd turn. Over the whole frequency range, the phase of the IHC-force was 180° shifted with respect to the 1st row OHCs. s and $\Delta\varphi$ corresponded also to a system of order between one and two (Table 3.7).

3.4.4 Outer tunnel

At low frequencies, force at the outer tunnel was in phase with that at the IHCs; that is, in counterphase to that at the 1st row OHCs. The total phase shift $\Delta\varphi$ was around -180° in the 1st cochlear turn and increased to much larger values of -270 to -540° in the 3rd turn. Low-frequency force amplitudes were smaller than at the OHCs: around 10 pN cm^2/mA. At higher frequencies, the force amplitude spectra showed one or two amplitude peaks or dips. In general, force at the outer tunnel was less reproducible than at the OHCs.

3.4.5 Hensen's cells

At Hensen's cells, at low frequencies, the force phase fell into two groups: one around 0° and the other around -180°. The total phase shift was grouped around -180° with exceptional values of up to -500°. Low-frequency force amplitude was 1-10 pN cm^2/mA. At higher frequencies, the force amplitude spectra showed one or two amplitude peaks or dips. In general, force at Hensen's cells was less reproducible than at the OHCs.

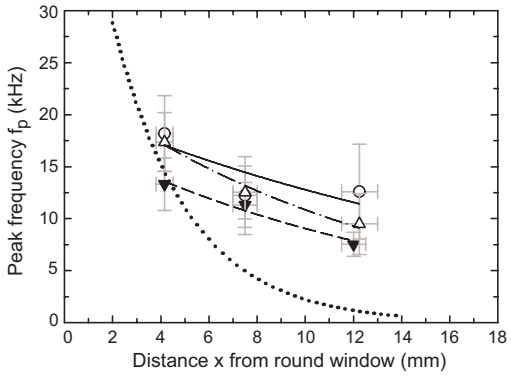

Figure 3.15: *Average peak frequencies of the force amplitude for three radial positions and three longitudinal regions. Filled triangles and dashed line: IHC; open circles and solid line: 1st OHC; open triangles and dash-dotted line: 2nd OHC. Horizontal error bars give the range of longitudinal positions, x, included in the calculation of the average f_p, vertical error bars the standard deviation of f_p. The numbers of measurements from which each average was determined were in the range 31–40. Exponential regression lines and Pearson's correlation coefficients, r, are: IHC: $f_p = (18.1 \pm 1.7) \times 2^{-x/(10.0\pm1.8)}$, $r = -0.9959$ (significant); 1st OHC: $f_p = (21.0 \pm 5.6) \times 2^{-x/(14.0\pm10.0)}$, $r = -0.7780$ (not significant); 2nd OHC: $f_p = (23.6 \pm 2.0) \times 2^{-x/(8.9\pm1.4)}$, $r = -0.9735$ (significant). The dotted line gives the characteristic frequency according to the map of Tsuji and Liberman [182]: $CF = 54.7 \times 2^{-x/2.2}$.*

Chapter 4. Discussion

The experiments described here were targeted at the following questions: 1) is the cantilever theory presented by Sader [152] sufficiently accurate to describe the vibration of atomic force cantilevers in fluid above their first resonant frequency? 2) Is the dynamic mechanical behavior of the organ of Corti governed by elastic, viscous, or inertial forces at a certain frequency? 3) Does the organ of Corti exhibit a – possibly place specific – resonance, which could serve as a second filter to sharpen the envelope of the travelling wave? 4) What is the shape of the deformation of the organ of Corti when the OHCs are active? 5) What is the bandwidth of the electrically evoked deformation? 6) Does the mode of deformation depend on frequency? 7) What is the frequency response of the electromotile force? 8) How is the OHC force coupled to other places within the organ? The answers which my experiments provide to these questions are discussed in the following with respect to cochlear function.

4.1 Validation of the cantilever theory

It was demonstrated that it is possible to apply a quasi-point force to an AFM cantilever in air and in non-polar, non-dissociating fluids, such as CCl_4, while measuring the velocity of deflection of the cantilever. The force can be an arbitrary function of time, the upper frequency limit being restricted by the electronic hardware. In my case, the limit of 67 kHz was set by the sampling rate of the DSP.

The mechanical driving-point impedance was in good agreement with theoretical predictions. The model was based on the work of Sader [152]. For biological applications, fluids other than CCl_4 must be used. The method was therefore attempted in bi-distilled water, but was abandoned because the harmonic distortion was significantly higher than in CCl_4 (10–40 dB, depending on frequency) and the measured impedance did not agree with the theoretical values. Presumably, in dissociating fluids the ions experience the electric field between the cantilever and the electrode, and cause a frequency-dependent electrophoretic drag force on the cantilever. Therefore, the measurement procedure can not be carried out in biologically relevant media. But since I have shown agreement of theory and experiment for Reynolds numbers in the range 0.2–250, the impedance of the cantilever in an infinite fluid can be calculated in any incompressible fluid with the accuracy given in Sec. 3.1.2. The value of the effective lever thickness, T, which is crucial for the calculation, can be derived from any measurement that yields one of the resonant frequencies of the cantilever, be it according to the procedure described here or using thermal excitation spectra [131, 153].

It was also shown that it is possible to measure the mechanical impedance of the cantilever in the proximity of a flat extended surface. The decrease in resonant frequency and increase in impedance amplitude, as compared with the 'infinite' fluid, agree qualitatively with the picture of increased damping in the restricted case. No effort was made to treat this case theoretically.

I did not see a 'forest' of resonance peaks as described by Schäffer *et al.* [158] for this frequency region, but only the lateral resonances of the cantilever. In their paper, the spectrum of resonance peaks depended on the material of the cantilever holder,

indicating that the additional peaks derived from resonances in the holder. In my case the mounting of the cantilever was designed to have eigenfrequencies above the measured frequency range and to act as a mechanical low-pass filter, resulting in 'clean' spectra.

The determination of the cantilever impedance up to high frequencies makes it possible to obtain more precise quantitative results from force modulation AFM compared with the treatment of the cantilever as an ideal, mass- and frictionless spring [132]. When the scan speed is increased in contact or tapping mode AFM, knowledge of the mechanical impedance of the cantilever becomes important to estimate the inertial components of the force exerted by the AFM-tip on the sample. This is relevant whenever the investigated surface is easily altered by interaction with the AFM-tip [62].

4.2 Impedance of the organ of Corti

The impedance measured in this study is the *compressional* impedance of the organ of Corti. It is compressional because the basilar membrane was mechanically clamped, the velocity of the reticular lamina being measured in response to an applied (point) force. These are the first measurements of its kind.

The expression describing the frequency dependence of the impedance (Eq. 3.3) was empirically chosen to reproduce mathematically the data in analytical form. Only the stiffness parameter, k, can be interpreted physically. The other parameters, c_i ($i = 1, \ldots, 5$), define the so-called viscous element of the Voigt-Kelvin model. It should be emphasized, however, that the c_i will not necessarily be defined by viscous material properties alone, but also by other material properties, such as Young's moduli and fluid density, as well as geometry. The usefulness of this empirical description lies in its ability to supply components for and properties of biophysical models of the organ of Corti. For example, one of the salient features of the data, or equivalently of the analytical expression, was that the point impedance is purely viscoelastic; that is, for force applied at a point on the organ of Corti, there is no inertial component of vibration. The biophysical consequence of zero inertia, together with the magnitudes of the viscous and stiffness components, is the subject of Sec. 4.2.3.

A systematic error derives from the fact, that in the impedance measurement, as described in Sec. 2.6.1, the atomic force cantilever causes both a local indentation of the surface (represented by an impedance Z_l) and a global compression of the organ (with impedance Z_g). The total impedance experienced by the cantilever is then $Z_{tot} = (1/Z_l + 1/Z_g)^{-1}$. On the other hand, the force generated by the OHCs acts only on Z_g. Z_{tot}, which is presented here, is a lower bound for Z_g. However, since the cantilever tip has been blunted flat to a diameter of 0.5–2 μm and since the cuticular plates of inner and outer hair cells and the pillar heads are assumed to be mechanically rigid due to a high density meshwork of actin fibers [45, 169, 177], Z_l should be much larger than Z_g and the error consequently is small on both types of hair cells and the pillar heads. However, the error might be significant for the inner sulcus cells and Hensen's cells.

4.2.1 Stiffness

The compressional impedance measured in these experiments should not be confused with the impedance of the cochlear partition, or as it is sometimes called, the impedance of the basilar membrane. That impedance is derived from the displacement (or velocity) of the basilar membrane in response to an applied force (or pressure) at its tympanic surface, without mechanical constraint of the upper (vestibular) surface of the partition. The stiffness component of the cochlear partition impedance has been numerously measured since the original work of von Békésy [189], both *in vitro* [58, 103, 110] and *in vivo* [124, 125]; it appears to derive from the *bending* stiffness of the cochlear partition, as originally

postulated by von Békésy [189]. This stiffness is reduced after removal of the organ of Corti [110]. The compressional stiffness of the organ of Corti decreases by a factor of two from base to apex (Fig. 3.8), whereas the stiffness of the cochlear partition decreases by two orders of magnitude [110, 189]; the two impedances are of similar magnitude only in the apical part of the cochlea. The compressional impedance is an important component of the 'cochlear amplifier impedance' in the work of Nobili and Mammano [118]: these authors predicted that only in the apical region is the compressional stiffness of the organ of Corti comparable in size to the bending stiffness of the cochlear partition. My experiments support this prediction.

The stiffness measured at the 2nd row outer hair cells was a factor 4–10 larger than that of isolated outer hair cells [3, 46, 60, 73]. That is, the mechanical components and structure of the organ of Corti appear to increase the stiffness at the outer hair cells relative to that for the isolated cell.

The stiffness measured at the tunnel of Corti was at least a factor of 40 smaller than the axial stiffness of isolated outer pillar cells estimated from the data of Tolomeo and Holley [179][1], and at least a factor of 400 larger than their measured (midpoint) bending stiffness. Due to the similar microstructure of outer and inner pillar cells [179], their corresponding axial stiffnesses are likely to be comparable. Therefore, the deformation of the triangular structure of the tunnel of Corti by a point load on the pillar heads, as was the situation in my experiments, appears to cause mainly bending of the pillar cells, rather than compression. This is consistent with the more general observation in the literature, that microtubules are almost inextensible, the compliance of cells being due primarily to filament bending or sliding between filaments [53]. Finally, resistance to bending by this triangular structure appears to be greater than for the isolated pillar cells.

4.2.2 Contact versus non-contact impedance measurements

The distance between sample and cantilever in the non-contact case has consequences for the *in-situ* calibration: if it is too large, the hydrodynamics of the fluid surrounding the cantilever will be that of an infinitely extending fluid rather than that with a nearby surface, and the calibration procedure of Sec. 2.6.5 becomes obsolete. On the other hand, as the cantilever approaches the sample surface, fluid coupling between the two increases gradually rather than abruptly, so that the impedance (and I looked especially at the phase) changed only gradually from the non-contact value to the contact value. This meant that according to the continuous monitoring of impedance phase, there was no definite point of contact. Indeed, the contact condition was defined visually as the point at which the surface was depressed approximately 1 μm by the cantilever tip (see Sec. 2.6.4). For the purpose of determining the non-contact impedance, I found that a distance of about 13 μm between sample surface and cantilever tip yielded a fluid coupling that was strong enough for the *in-situ* calibration, but small compared with the coupling in the contact case.

The question arises as to what extent the pre-stress of the preparation due to the presence of the cantilever tip (1-μm compression) has significant consequences for the

[1] These authors found the outer pillar cell to be composed of approximately equal numbers of cross-linked microtubules and actin filaments extending along the length of the cell. Based on 2000 microtubules, on average, with inner and outer diameters, respectively, of 17 nm and 30 nm, they estimate Young's modulus from bending experiments to be about 2 GPa for the microtubules. Assuming that the microtubules are isotropic and uncoupled, obey Hooke's law, with each extending along the entire length of the cell (92 μm) and undergoing equal axial strain, then I estimate that a compressive uniaxial force experiences an axial stiffness of 21 N/m. This estimate may be taken as a lower limit for the axial stiffness. Inclusion of an equal number of actin filaments, with a diameter about one-fifth that of microtubules [179] and Young's modulus of about 3 GPa [53], would contribute an additional 2 N/m. Cross-linking might further increase the axial stiffness.

results. To resolve this issue, I conducted a series of measurements at different distances from the sample. The result was that once a reliable contact had been established, a further approach (meaning stronger pre-stress) of up to 3 μm did not change the measured impedance. This suggests that the experiments were conducted under linear mechanical conditions. Further evidence for linearity derives from the velocity spectra: second and higher order harmonics were always at least 30 dB below the fundamental amplitude and disappeared in the noise for most frequencies. Linear conditions are also consistent with the small standard deviations of the stiffness estimates and the small standard deviations of the stiffness populations at given radial and longitudinal positions. The latter are not shown in Fig. 3.8, because in most cases they were smaller than the radius of the plot symbols. Finally, with a total sample thickness[2] of about 100 μm in the 1st cochlear turn, a compression of 1 μm yields a strain of 1 %. From experiments with isolated outer hair cells, inner and outer pillar cells, and Deiters' cells, I have found that these cells do not exhibit buckling for strains up to at least 10% (data from a separate set of experiments, not illustrated here). Furthermore, when the cantilever tip is retracted, the upper surface of the organ returns to its original position. It is, therefore, unlikely that this relatively small pre-stress of the organ of Corti caused buckling or strain-hardening. In summary, I can safely conclude that the required pre-stress was sufficiently small to ensure linear mechanical conditions and that the measured impedances represent those of the unloaded organ of Corti.

4.2.3 Biophysical significance for cochlear amplification

It is noteworthy that the imaginary part of the impedance almost never became positive, not even at the highest frequency of 50 kHz. This means that the inertial component in the transverse direction was overwhelmingly dominated by the stiffness and/or by the negative imaginary part of the viscosity, so that most of the organ of Corti moved like a purely viscoelastic material at all physiologically relevant frequencies. The only exceptions to this rule were the outer tunnel region and Hensen's cells in the 3rd turn of the cochlea.

This has important consequences for cochlear amplification: displacement x of the cuticular plates is related to the electromechanical force F generated by the outer hair cells by $x = F/(i\omega Z)$, where Z is the impedance of the organ of Corti, which I have presented here. If Z were dominated by an inertial term due to mass, m, at high frequencies $Z \approx i\omega m$, then for constant force stimulation the displacement amplitude would decrease in proportion to ω^{-2}, or equivalently with 12 dB/oct. However, if the load impedance driven by the electromechanical force of the outer hair cells is purely viscoelastic, then $Z \approx \mu$ at high frequencies. Since μ decreased only slightly above 6 kHz (1.2 dB/oct), this means that the displacement amplitude decreases by only 4.8 dB/oct.

Indeed, for the basal region of the cochlea, where frequency selectivity and sensitivity are greatest (for review see Ref. [139]), I found that between 0.48–50 kHz the magnitude of the complex compliance $1/(i\omega Z)$, which is the transfer function between force and displacement, decreased by only 20 dB and the phase shifted from about -25° to only -70° for all rows of outer hair cells (calculated as the phase of Z using Eq. 3.3, with parameters from Table 3.1). That is, without tectorial membrane, the mechanical load on the outer hair cells causes only a ten-fold decrease in their electromechanical displacement responses between low and high frequencies.

The tectorial membrane constitutes an additional point load on the stereocilia of the outer hair cells. What effect does this have on the interpretation of my results? To answer this I note that this load will be elastic at low frequencies and either frictional or

[2] Using confocal microscopy of unfixed preparations, I found distances between basilar membrane and reticular membrane at the tunnel of Corti of about 100 μm both in the 1st and 2nd turn, and 180 μm in the 3rd turn. This distance increases towards Hensen's cells in the 2nd and 3rd turns.

inertial at high frequencies. For the 2nd cochlear turn of the gerbil *in vivo*, Zwislocki and Cefaratti [206] find[3] a transverse stiffness of a 200-μm long piece of tectorial membrane of 0.125 N/m. The load is inertial above its resonant frequency – about 2.5 kHz in the transverse direction for the 2nd cochlear turn of the gerbil[4]. In this turn of the gerbil cochlea, the characteristic frequency is 3–8 kHz [104], implying that the transverse impedance of the tectorial membrane is inertial for the frequency selective region of basilar-membrane motion. Moreover, due to the flat geometry of the tectorial membrane, the fluid forces acting upon it in the transverse direction will be much larger than in the radial direction. Therefore, using this gerbil data as an indicator and the fact that the density of the tectorial membrane and the surrounding fluid are similar, it is conceivable that for frequencies of cochlear amplification the tectorial membrane follows the motion of the surrounding fluid in the transverse direction. Consequently, if the pressure on the tectorial membrane towards scala tympani is in phase with a contractile force of the outer hair cells, the impedance of the organ of Corti could be (partially) compensated by the force of the tectorial membrane on the stereocilia of the outer hair cells.

The finding that in the first two cochlear turns the real part of the impedance is larger than the imaginary part at the characteristic frequency nicely concurs with the viscoelastic model proposed by Nobili and Mammano [118] for cochlear amplification. Their hypothesis is that the attenuation and phase delay of the receptor potential relative to stereocilia displacement, and consequently of the electromechanical force, caused by the electrical time constant of the basolateral membrane of the outer hair cell, is compensated by the combined viscoelastic action of the outer hair cell and its supporting Deiters' cell. Indeed, the Mammano group [92] has since shown that the electromechanical action of the outer hair cell causes motion of its supporting Deiters' cell (together with its nearest neighbors). In order to compensate for the electrical time constant, their model requires that the viscous force be greater than the elastic force at the characteristic frequency; the required ratio is about 33 at the 4.5-mm point, 16 at the 7.5-mm point and 8 at the 12-mm point[5].

Experimentally, I found the real part of the impedance to be about twice the imaginary part at the characteristic frequency in the first two cochlear turns; they were approximately equal in the 3rd turn. The discrepancy between experiment and model is mainly due to the model values of stiffness assumed for the combination of outer hair cell and Deiters' cell being about an order of magnitude smaller than my experimentally observed stiffness values for the organ of Corti. Thus, using their assumed values of cochlear-partition viscosity, $h(x)$, with $h_m(x) \approx h(x)/1.33$, I calculate viscosities of 0.27×10^{-5} Ns/m at all points along the cochlea; this is a factor of 2-3 smaller than my measured values (mean c_2-data at the 2nd row outer hair cell in Fig. 3.8). Fluid vis-

[3] I only consider a stiffness defined by the ratio of force to transverse displacement of the whole tectorial membrane *in situ*, attached to the spiral limbus, and detached from the stereocilia. Zwislocki and Cefaratti [206] consider their previous results [204] as "qualitative". Abnet and Freeman [1] measured the longitudinal and radial, but not the transverse stiffness. In the results of von Békésy [189] the physiological state of the tectorial membrane is questionable, because it is known to be sensitive to the ionic environment [39, 48, 90, 166].

[4] The inertial impedance of a cuboid piece of tectorial membrane of length 200 μm, width 112 μm, and thickness 22 μm [206], with a density of 1 g/cm^3 (if the gel matrix is neglected [47]), was set equal to the elastic impedance of a spring of stiffness 0.125 N/m, to calculate the resonant frequency.

[5] I calculated these ratios as follows. First, using the notation of Ref. [118], denote the combined viscosity of the outer hair cell and its Deiters' cell by $h_m(x)$, and their combined stiffness by $k_m(x)$. The resulting mechanical filter is high-pass with 3-dB (radial) frequency of $\omega_m(x) = k_m(x)/h_m(x)$. The electrical filter, whose time constant is to be compensated, is low-pass with 3-dB (radial) frequency denoted by $\omega_c(x)$. The dependence of this latter frequency on cell-length was determined directly by Preyer *et al.* [130] from the frequency spectrum of the whole-cell receptor potential in response to displacement of the stereocilia; it decreases by 0.058 oct/μm cell-length, beginning with a value of 546 Hz for a length of 20 μm. Finally, I invoke the assumption made by Nobili and Mammano [118] that $\omega_m(x) = \omega_c(x)$; that is, the high-pass filter completely compensates the low-pass filter. Then, at the characteristic frequency the magnitude ratio of the viscous force to the elastic force must be equal to CF/f_c, where $f_c = \omega_c/(2\pi)$. Using the tonotopy measured by Tsuji and Liberman [182], the required ratios at the 4.5-mm, 7.5-mm and 12-mm points are, respectively, 33, 16 and 8.

cosity within the organ of Corti, which was not included in their model, might account for the difference between theory and experiment. The stiffness values derived from the assumption[5] that $\omega_m(x) = \omega_c(x)$, with $k_m(x) = \omega_m(x)h_m(x)$, are factors of 9 and 17 smaller than my measured values at the 7.5-mm and 4.5-mm points, respectively (mean k-data at the 2nd row outer hair cell in Fig. 3.8). Again, embedding of the cells within the structure of the organ of Corti might explain this difference, the experimentally observed stiffness at the OHC *in situ* being larger than expected from model calculations with an isolated combination of outer hair cell and Deiters' cell.

Given all the assumptions involved in the theoretical and experimental analyses of this complicated system, the agreement between theory and experiment is encouraging; namely, that viscoelasticity at the characteristic frequency is of paramount importance for cochlear amplification.

4.3 Force generation in the organ of Corti

4.3.1 Driving force for the force

In general, an electric current through the bath medium will be accompanied by a net electrophoretic fluid flow, thereby exerting a mechanical force on the preparation. However, I was able to confirm the negligibility of this fluid motion by measuring the velocity at the end of a cotton fiber (40 μm diameter, held 3 mm away from its end) at the position of the sample during electrical stimulation: it was below noise level (<-30 dB).

Another means by which the preparation might sense the electric field is via surface charges on the cell membranes, leading to mono- or multipole forces on parts of the preparation. However, it is difficult to conceive why the apical surface of the IHCs and Hensen's cells should carry a charge opposite to that of the OHCs as the observed phase reversals on the reticular lamina would then suggest.

Finally, the reversible pharmacological inhibition (Figs. 3.13 and 3.12), the deterioration of the motile response with time, and the phase reversals across the reticular lamina, refute the assumption of motion being induced by an electrophoretic fluid drag or by surface charges. Therefore, I conclude that in my experimental configuration the activity of the motor molecule prestin in the OHC lateral wall is the cause for the measured deformation of the organ upon external electrical stimulation.

As it is obvious from the data, the force generated by the OHCs is not subject to low-pass filtering above the corner frequency of the cell membrane RC-filter which has been estimated to be 50-500 Hz [65, 130]. Furthermore, since there was no mechanical stimulus, neither of the three mechanoelectrical transduction mechanisms known for OHCs was activated here: the transducer channel in the stereocilia [21, 42, 71, 130, 149], the stretch induced charge transfer by the prestin [51, 72, 78, 157], and the stretch sensitive pore in the lateral plasma membrane [151]. Therefore, the external electrical field and/or the associated extracellular ionic current (which are in phase due to the Ohmic nature of the bath medium) must provide a wide band stimulus for conformational changes of the prestin molecules.

From the applied stimulus voltage, the measured current, and the chamber geometry, extracellular current densities were estimated to be 1–2 mA/cm^2 (depending on frequency) and extracellular voltage gradients to be 18–36 μV/μm, oriented in parallel to the OHC's central axis due to the symmetry. Then, for cells of length 30 and 90 μm, the voltage drop along the cell amounts to 0.5–1 mV and 1.6–3.2 mV, respectively. This is less than half of the physiological range for the receptor potential (7 mV [23]). These estimates provide upper bounds because they do not account for possible restrictions imposed on current flow by the presence of the organ.

The inability of the blockers for the apical conductances to affect electromotility indicates that the ionic current through the transducer channels is negligible. If an OHC is exposed to an external voltage gradient it is conceivable, therefore, that current is flowing through the lateral plasma membrane into the apical part of the cell and out out of the basal part (and vice versa). The OHC plasma membrane can be modelled as a parallel combination of the membrane resistance and capacitance, respectively. Although there will be a continuous distribution of current along the cell, for simplicity it is modelled in the following with only two distinct parts. Each of these parts presents an electrical impedance to the current, so that the cell is a series combination of the apical and basal impedances, Z_a and Z_b; that is, it forms a voltage divider. The intracellular voltage, U_{ic}, is consequently determined by the ratio of the impedances:

$$U_{ic} \propto \frac{1}{1 + Z_a/Z_b} \tag{4.1}$$

It is important to realize that the frequency response of U_{ic} is flat regardless of the (arbitrary) choice of the relative length of the two parts: both Z_a and Z_b are parallel combinations of the membrane capacitance, C_m, and resistance, R_m, so that $Z_{a,b} = (1/R_{m,a,b} + i\omega C_{m,a,b})^{-1}$. If constant specific capacities and resistances are assumed along the cell, R_m is inversely proportional to area, and thus length $L_{a,b}$ of the respective part of the cell (apical or basal), and C_m is directly proportional to $L_{a,b}$, so that

$$\frac{Z_a}{Z_b} = \frac{L_b}{L_a}\,. \tag{4.2}$$

Even if C_m decreases with frequency [155], Eq. 4.2 still holds[6]. If the cell interior is not iso-potential, due to the electric and/or hydrodynamic properties of the subsurface cisternae [61, 133], the voltage divider scheme could still be valid to a first approximation.

Due to the relative magnitude of resistive and capacitive components [130], the capacitive currents dominate above about 0.5 kHz. Therefore, over the frequency range used here, the intracellular voltage is governed by capacitive charge transfer across the OHC plasma membrane. Since about 40% of the membrane capacitance is contributed by the motor molecule [6, 155], this charge transfer, driven by the extracellular field, directly causes a change in prestin conformation.

If the conclusion is true, that in my setup it is predominantly the capacitive current which drives the motor molecule, then the frequency independent amplitude attenuation by salicylate, 9-AC, and cocktail B (cation channels) cannot be mediated via blocking of an ionic current, but is most likely due to a direct interference of the respective agents with the prestin molecule. This view is supported by the inhibitory effect of salicylate and niflumic acid, another chloride-channel blocker, on voltage-dependent capacitance [63, 123, 151].

4.3.2 Properties of the force

The force I presented here is the Norton equivalent force which has to act on the measured equivalent impedance between the clamped basilar membrane and the upper side of the organ to produce the observed velocity. As it was pointed out in Sec. 4.2, the impedance measured here is a lower bound for the global deformational impedance of the organ. Consequently, the force is a lower bound for the true force. However, the error is small (see Sec. 4.2) on hair cells and pillar cells.

If the transmembrane voltage is estimated from the voltage drop along the cell and a voltage divider ratio of one is assumed (see previous section), then the generated forces

[6] In vivo, this reduction in C_m (by a factor of 3 from 0.3 to 3 kHz) will lead to a corresponding increase of the corner frequency of the low-pass filter, which is, however, insufficient to solve the RC-problem. It is noteworthy in this context that the 'R' is not the membrane but the transducer resistance.

are on the order of 30–200 pN/mV. However, since the transmembrane voltage is only an approximate upper bound, the normalized forces could be larger. Nevertheless, they agree with published values of 0.01–700 pN/mV for isolated OHCs, where the more recent values are 50–100 pN/mV [46, 60, 73, 74, 108]. Since in my preparation several OHCs are mechanically coupled, the force presented here is an upper bound for isolated OHCs.

Prestin is not an ideal capacitor. Instead, it occupies two or more energy levels[7]. Transition between these levels will be limited by transition rates and, following a change in state probability, equilibrium will be reached exponentially only after a certain relaxation time τ_p. Therefore, prestin by nature is a lossy capacitor – it is a series combination of a loss resistance and the capacitance, forming a low-pass filter with time constant τ_p. This is the intrinsic frequency limit of the motor. Indeed, my force data is compatible with a first-order low-pass filtering in the high-frequency limit (Table 3.7), with a corner frequency around 50 kHz at room temperature[8]. This is in agreement with the frequency limit found by Refs. [46]. It is likely that the transition rates of the prestin states are strongly dependent on the structure of the molecule, so that genetic variations in prestin between species should lead to different 'speeds' of the motor. This might account for the higher bandwidth of the motor required in echolocating bats, for example.

If the stimulus for the motor molecule is really frequency independent, then the generated force exhibits a broad resonance at 7–20 kHz depending on longitudinal position. This is in agreement with theoretical results by Refs. [171, 192], who predict an electro-mechanical resonance of the OHC in this frequency range, which is caused by the piezoelectric properties of the cell's lateral wall.

The broad maximum significantly extends the frequency amplitude response of the organ deformation: whereas for a constant force, displacement amplitudes would drop above 4 kHz due to the viscoelastic impedance of the organ (lines in Fig. 3.9), the increased force above 4 kHz compensates this and leads to the observed broad frequency response of the electromotility (symbols in Fig. 3.9).

4.4 Electrically evoked deformation of the organ of Corti

4.4.1 Reticular-lamina displacement

For the first time, I provide experimental data showing that the reticular lamina is not moving as a rigid plate upon electrical stimulation but like a double lever with two pivots. Most importantly it has been shown [119, 161] that the vibration pattern of the reticular lamina observed here remains the same when the basilar membrane is not clamped but free-swinging and when the tectorial membrane is in its physiological position (attached to the OHC stereocilia). In the intact system, this active (electrically induced) deformation of the organ adds vectorially to its passive 'rotating wedge' motion observed in vitro [137, 185] upon fluid-induced deflection of the basilar membrane. The phase of the active deformation relative to basilar-membrane deflection is determined by the sum of 1) the phase of the receptor potential relative to basilar-membrane deflection

[7] Note that the experimentally found relation between transferred charge of the molecular motor and transmembrane potential can be excellently fitted by functions other than the commonly assumed two-state Boltzmann function. One example is the Brioullin function describing quantum mechanical paramagnetism [184]. It gives the expectation value for the orientation of a dipole in an external field where the dipole can be in one of two or more states with equidistant energy levels. If there are only two levels, the Brioullin function is identical to a two-state Boltzmann function. In the classical case of infinitely many states, the Brioullin function asymptotes to the Langevin function.

[8] With the corner frequency being defined by the intersection of linear regression lines to the low-frequency (0.48–1 kHz) and high-frequency (50–67 khz) extremes.

and 2) the phase of the deformation of the organ relative to the receptor potential, as presented here.

The double lever vibration pattern of the reticular lamina requires a significant force transfer from the OHCs to the rest of the organ of Corti. The nature of this mechanical coupling can be a solid-solid structure interaction via the junctions between the individual cells or a solid-fluid-solid interaction via the fluid filling the spaces within the organ. Especially the conservation of fluid volume should lead to a significant hydrodynamic pressure on IHCs and HeCs when the OHCs change their length at acoustic frequencies. The relevance of fluid motion is supported by the observation of a measurable longitudinal flow along the tunnel of Corti in response to electrically evoked OHC activity [81]. The two types of interaction could in principle be distinguished by observing the radial displacement pattern in response to a DC stimulus: while a solid-solid coupling transfers the same force at DC and AC stimulation, a *radial* fluid coupling is effective only at high frequencies, because the organ of Corti is quasi open in the longitudinal direction and fluid inertia and viscosity will oppose longitudinal flow only for fast transients (thereby closing the fluid compartment). However, since my configuration was optimized for high acoustic frequencies, DC and very low-frequency displacements of the order of one nanometer disappeared completely in the noise floor. Nevertheless, if solid radial coupling is assumed, it is difficult to conceive how a phase jump at the outer tunnel might occur. Furthermore, the stronger increase in force with frequency on the IHCs compared with the OHCs is indicative of fluid coupling. Therefore, I suggest that fluid coupling is predominant.

A puzzling observation was the counterphasic motion of 2nd and 3rd row OHCs near the base of the cochlea. It seems unlikely that there are two different kinds of OHCs, with different directions of electromotility, because to my knowledge experiments on isolated OHCs always show a contraction upon depolarization. Furthermore, the phase reversal between 3rd row OHCs and HeCs in the mid and apical region of the cochlea point to a strong mechanical coupling within the organ of Corti. I therefore conclude that, in the base of the cochlea and with clamped basilar membrane, the force generated by 1st and 2nd row OHCs is sufficient to move 3rd row OHCs as a whole in the direction opposite to the displacement of their cuticular plates relative to their apex.

4.4.2 Implications for cochlear amplification

It has been shown that intra-cochlear current injection generates motion of the basilar membrane, the reticular lamina, and the tectorial membrane, basilar-membrane travelling-waves, and otoacoustic emissions [55, 57, 67, 101, 107, 121, 122, 126, 135, 136, 194–196, 198, 201]. Most likely, these vibrations are induced by the concerted force generation of a large number of OHCs through their somatic electromechanical transduction mechanism. Since in my case the tectorial membrane was removed, I infer that somatic motility of OHCs is sufficient to produce deformation of the organ up to high frequencies, provided that the transmembrane voltage is adequate. If the stereocilia generate force during their transduction process, it will be coupled into the cochlear partition in addition to the somatic force, but not exclusively.

I found that the double lever deformation pattern of the reticular lamina was independent of frequency. In particular, due to the frequency response of the purely viscoelastic impedance of the organ (Sec. 3.2) and the broad maximum in force amplitude, no displacement resonances of the organ of Corti appeared below 50 kHz. This leads to the conclusion that the localized amplification of the basilar-membrane travelling-wave cannot be accounted for by a place-specific resonance of the organ of Corti as suggested by Neely and Stover [115]. Therefore, an important assertion derived from my data is that a putative second resonance providing local amplification to the basilar-membrane travelling-wave can, if at all, only occur at the tectorial-membrane level. Furthermore,

the phase opposition in auditory nerve fiber responses of IHCs and OHCs suggested by Zwislocki [203] concurs nicely with the counterphasic motion of these cells at the level of the reticular lamina.

Since the organ of Corti (apart from the pillar cells) is an order of magnitude softer than the basilar membrane [40, 58, 84, 110, 119, 160, 161] it is conceivable that it supports its own mode of wave propagation (this has been confirmed theoretically by the sandwich model of de Boer [30]), possibly together with the tectorial membrane [4, 205]. That is, a deformation of the organ or a deflection of the tectorial membrane could propagate along the cochlea as a second travelling wave more or less independently of that on the basilar membrane. In this concept, interference of the two travelling waves leads to localized, frequency-dependent amplification [66, 68, 69]. The data presented here strongly suggest that the arrangement of OHCs is ideally suited for amplification of such a wave, provided that the OHC somata generate force with the proper phase. Furthermore, my data and the one of Ref. [119] indicate that the radial vibration pattern of the reticular lamina might play a role. In the case of a tectorial-membrane travelling-wave, the observation of this interference at a single longitudinal position could probably be interpreted as a tectorial-membrane resonance [57, 205].

In support of this view, firstly, Khanna *et al.* [84] showed that upon acoustical stimulation of an isolated temporal bone preparation, 1) the reticular-lamina vibration at the OHC region is tuned, 2) at its best frequency displacement amplitudes on the reticular lamina are more than an order of magnitude stronger than those on the basilar membrane, and 3) in this preparation the basilar-membrane vibration was not tuned. However, in these measurements a uniform displacement of the reticular lamina across its entire width (from IHCs to Hensen's cells) was found and, consequently, implemented in the associated sandwich model [30]. This (passive) mode of vibration will superpose with the active mode (double lever) described here.

Secondly, it has been shown by Karavitaki and Mountain [81] that *in-vitro* electrically induced activity of the OHCs induces longitudinal flow in the tunnel of Corti with a space constant larger than the travelling wave. Consequently, Refs. [69] and [68] modelled the organ of Corti as an elastic tube sustaining a mode of wave propagation. This slow wave interacts with the basilar-membrane travelling-wave, leading to local amplification. The time domain responses of this model are able to reproduce several important features of measured basilar-membrane responses. The radial coupling observed here, if it is indeed fluid mediated, agrees with the description of the organ of Corti as a flexible tube.

Thirdly, Steele and Kim [173, 174] theoretically found two travelling-waves propagating along the duct when they included two degrees of freedom for the cochlear partition in their model. One is the classical sharply tuned wave and the other is lower in amplitude, broadly tuned, and has a maximum further to the apex.

Fourthly, Guinan *et al.* [56] showed *in vivo* that stimulation of the medial olivocochlear efferents (reducing OHC activity) inhibited the first of several peaks in the firing rate of auditory nerve fibers in response to acoustic clicks. Since the earliest peak in the basilar-membrane response appears to be independent of OHC activity [134], they concluded that there are two travelling waves, the faster of which (presumably propagating within the organ of Corti and/or on the tectorial membrane) depends on OHC activity.

Finally, de Boer and Nuttall [33] showed that the active part of the basilar-membrane impedance, Z_{act}, which they calculated by means of an inverse solution of a 3D-model for a measured basilar-membrane velocity, is non-causal. This implies [32] that either the basilar-membrane impedance is not a function of a single place x alone, but depends on neighboring places, or that a second filter is applied between basilar-membrane velocity and force feedback. Indeed, they found it possible to reproduce the measured basilar-membrane response by describing the 'active pressure', $p_{act}(x)$, acting at one place x of the basilar membrane as a linear combination of basilar-membrane velocities at more

apical and more basal places with real coefficients. Interestingly, these coefficients turned out to be alternating in sign with a spatial period of 30–50 μm. It appears conceivable that it is a wave at the RL-TM level, which stimulates the OHCs with alternating signs.

4.5 Future experiments

Understanding cochlear amplification is not possible without a clear view of the behavior of and the interplay between the components of the cochlear partition (basilar membrane, cells of the organ of Corti, and tectorial membrane) during travelling-wave motion. In order to complete today's fragmentary picture, experiments elucidating the role of the tectorial membrane and the propagation of waves at different levels (basilar membrane, base of OHCs, inner sulcus, reticular lamina, tectorial membrane) are necessary.

A preparation permitting acoustic stimulation of the cochlea, and simultaneous measurement of the travelling wave at all levels and in the base of the cochlea, would be suitable to address these questions. Furthermore, a new (sensitive) method to detect the motion of the relevant structures within the focus-plane of the microscope, and without reflective beads, is necessary to reconstruct the 3-dimensional motion of the structures in response to electrical or acoustical stimulation.

4.6 Conclusions

It was shown experimentally that the theory of cantilevers in a viscous fluid, which was presented by Sader [152] and extended in this work, is valid for Reynolds numbers in the range 0.2–250. This is the range relevant for atomic force cantilevers in biological solutions at acoustic frequencies.

It was demonstrated that my novel impedance measurement technique works reliably up to at least 50 kHz, yielding reproducible results for a biological structure surrounded by fluid. The technique allows determination of the compressional mechanical impedance of the organ of Corti at all auditory frequencies. An empirical model yielded parameters relevant for a biophysical understanding of cochlear amplification.

In contrast to the common presumption that the reticular lamina behaves as a rigid plate when the OHCs generate electromechanical force, I have shown that it moves in an as yet unknown way, namely as a double lever with two pivots – one at the tunnel of Corti and the other at the outer tunnel. It was shown that this deformation pattern persists up to at least two octaves above the characteristic frequency and that a resonance within the organ can be excluded. Instead, displacement at each radial position exhibits a low-pass filter characteristic with a cutoff frequency of 10–20 kHz. A new substance reversibly blocking electromotility, 9-AC, was identified.

The force acting on a specific point was shown to have a broad maximum at 7–20 kHz which leads to considerable broadening of the displacement frequency-response of the reticular lamina. This maximum is consistent with theoretical predictions about an electromechanical resonance in the OHC lateral wall. In the high-frequency limit, the force approximately followed a first-order low-pass characteristic.

The data is compatible with the concept of a second travelling wave.

Bibliography

[1] C.C. Abnet and D.M. Freeman. Deformations of the isolated mouse tectorial membrane produced by oscillatory forces. *Hear. Res.*, 144:29–46, 2000.

[2] M. Abramowitz and I.A. Stegun. *Handbook of Mathematical Functions.* Dover, New York, 1972.

[3] M. Adachi and K.H. Iwasa. Effect of diamide on force generation and axial stiffness of the cochlear outer hair cell. *Biophys. J.*, 73:2809–2818, 1997.

[4] J.B. Allen. Cochlear micromechanics - a physical model of transduction. *J. Acoust. Soc. Am.*, 68:1660–1670, 1980.

[5] J.F. Ashmore. A fast motile response in guinea-pig outer hair cells: The cellular basis of the cochlear amplifier. *J. Physiol.*, 388:323–347, 1987.

[6] J.F. Ashmore. Forward and reverse transduction in the mammalian cochlea. *Neurosci. Res. Suppl.*, 12:S39–S50, 1990.

[7] L.L. Beranek. *Acoustics.* McGraw-Hill, New York, 1954.

[8] L. Bergmann and C. Schäfer. *Optik*, volume 3 of *Lehrbuch der Experimentalphysik.* de Gruyter, Berlin, 9th edition, 1993.

[9] W. Bialek. Physical limits to sensation and perception. *Annu. Rev. Biophys. Biophys. Chem.*, 16:455–478, 1987.

[10] C. Blanchet, C. Erostegui, M. Sugasawa, and D. Dulon. Acetylcholine-induced potassium current of guinea pig outer hair cells: Its dependence on a calcium influx through nicotinic-like receptors. *J. Neurosci.*, 16:2574–2584, 1996.

[11] K.R. Boff, L. Kaufman, and J.P. Thomas. *Handbook of perception and human performance.* Wiley, New York, 1986.

[12] D. Brass and D.T. Kemp. Analyses of mössbauer mechanical measurements indicate that the cochlea is mechanically active. *J. Acoust. Soc. Am.*, 93:1502–1515, 1993.

[13] W.E. Brownell, C.R. Bader, D. Bertrand, and Y. de Ribaupierre. Evoked mechanical responses of isolated cochlear outer hair cells. *Science*, 227:194–196, 1985.

[14] R. Brunner and I. Nöldeke. *Das Ohr.* Thieme, Stuttgart, 2001.

[15] R.A. Buckingham and G.E. Valvassori. Inner ear fluid volumes and the resolving power of magnetic resonance imaging: Can it differentiate endolymphatic structures? *Ann. Otol. Rhinol. Laryngol.*, 110:113–117, 2001.

[16] H. Cai, C.P. Richter, and R.S. Chadwick. Motion analysis in the hemicochlea. *Biophys. J.*, 85:1929–1937, 2003.

[17] W.A. Catterall. Neurotoxins that act on voltage-sensitive sodium channels in excitable membranes. *Annu. Rev. Pharmacol. Toxicol.*, 20:15–43, 1980.

[18] A.R. Cody and D.C. Mountain. Low-frequency responses of inner hair cells: Evidence for a mechanical origin of peak splitting. *Hear. Res.*, 41:89–99, 1989.

[19] N.P. Cooper. Vibration of beads placed on the basilar membrane in the basal turn of the cochlea. *J. Acoust. Soc. Am.*, 106:L59–L64, 1999.

[20] N.P. Cooper and W.S. Rhode. Basilar membrane mechanics in the hook region of cat and guinea-pig cochleae: Sharp tuning and nonlinearity in the absence of baseline position shifts. *Hear. Res.*, 63:163–190, 1992.

[21] A.C. Crawford, M.G. Evans, and R. Fettiplace. Activation and adaptation of transducer currents in turtle hair cells. *J. Physiol.*, 419:405–434, 1989.

[22] L. Cremer and M. Heckl. *Körperschall – Physikalische Grundlagen und technische Anwendungen*, volume 2. Springer-Verlag, Berlin, 1996.

[23] P. Dallos. Membrane potential and response changes in mammalian cochlear hair cells during intracellular recording. *J. Neurosci.*, 5:1609–1615, 1985.

[24] P. Dallos. Neurobiology of cochlear inner and outer hair cells: Intracellular recordings. *Hear. Res.*, 22:185–198, 1986.

[25] P. Dallos. Overview: Cochlear neurobiology. In P. Dallos, A.N. Popper, and R.R. Fay, editors, *The Cochlea*, pages 1–43, Berlin, 1996. Springer Verlag.

[26] P. Dallos. Organ of corti kinematics. *J. Assoc. Res. Otolaryngol.*, DOI: 10.1007/s10162-002-304:1–18, 2003.

[27] P. Dallos, B.N. Evans, and R. Hallworth. Nature of the motor element in electrokinetic shape changes of cochlear outer hair cells. *Nature*, 350:155–157, 1991.

[28] H. Davis. An active process in cochlear mechanics. *Hear. Res.*, 9:79–90, 1983.

[29] E. de Boer. Auditory physics. physical principles in hearing theory. i. *Phys. Reports*, 62:89–174, 1980.

[30] E. de Boer. Wave propagation modes and boundary conditions for the Ulfendahl-Flock-Khanna (UFK) preparation. In P. Dallos, C.D. Geisler, J.W. Matthews, M.A. Ruggero, and C.R. Steele, editors, *The Mechanics and Biophysics of Hearing*, pages 333–339, Berlin, 1990. Springer Verlag.

[31] E. de Boer. Auditory physics. Physical principles in hearing theory III. *Phys. Reports*, 203:125–231, 1991.

[32] E. de Boer. Classical and non-classical models of the cochlea. *J. Acoust. Soc. Am.*, 101:2148–2150, 1997.

[33] E. de Boer and A.L. Nuttall. Properties of amplifying elements in the cochlea. In A.W. Gummer, editor, *Biophysics of the Cochlea*, pages 331–342, Singapore, 2003. World Scientific.

[34] T. Van den Abbeele, P.T.B. Huy, and J. Teulon. Modulation by purines of calcium-activated non-selective cation channels in the outer hair cells of the guinea-pig cochlea. *J. Physiol.*, 494:77–89, 1996.

[35] G.M. Dick, K.K. Bradley, B. Horowitz, J.R. Hume, and K.M. Sanders. Functional and molecular identification of a novel chloride conductance in canine colonic smooth muscle. *Am. J. Physiol*, 275:C940–C950, 1998.

[36] R.J. Diependaal, E. de Boer, and M.A. Viergever. Cochlear power flux as an indicator of mechanical activity. *J. Acoust. Soc. Am.*, 82:917–926, 1987.

[37] R.J. Diependaal, M.A. Viergever, and E. de Boer. Are active elements necessary in the basilar membrane impedance? *J. Acoust. Soc. Am.*, 80:124–132, 1986.

[38] E.K. Dimitriadis and R.S. Chadwick. Solution of the inverse problem for a linear cochlear model: a tonotopic cochlear amplifier. *J. Acoust. Soc. Am.*, 106:1880–1892, 1999.

[39] R.M. Edge, B.N. Evans, M. Pearce, C.-P. Richter, X. Hu, and P. Dallos. Morphology of the unfixed cochlea. *Hear. Res.*, 124:1–16, 1998.

[40] G. Emadi, C.P. Richter, and P. Dallos. Stiffness of the gerbil basilar membrane: Radial and longitudinal variations. *J. Neurophysiol.*, 91:474–488, 2004.

[41] H. Engström and B. Engström. Structure of the hairs on cochlear sensory cells. *Hear. Res.*, 1:49–66, 1978.

[42] B.N. Evans and P. Dallos. Stereocilia displacement induced somatic motility of cochlear outer hair cells. *Proc. Natl. Acad. Sci. USA*, 90:8347–8351, 1993.

[43] E.F. Evans and R. Klinke. The effects of intracochlear and systemic furosemide on the properties of single cochlear nerve fibres in the cat. *J. Physiol.*, 331:409–427, 1982.

[44] C. Fernández. Dimensions of the cochlea (guinea pig). *J. Acoust. Soc. Am.*, 24: 519–523, 1952.

[45] A. Flock, H.C. Cheung, B. Flock, and G. Utter. Three sets of actin filaments in sensory cells of the inner ear. identification and functional orientation determined by gel electrophoresis, immunofluorescence and electron microscopy. *J. Neurocytol.*, 10:133–147, 1981.

[46] G. Frank, W. Hemmert, and A.W. Gummer. Limiting dynamics of high-frequency electromechanical transduction of outer hair cells. *Proc. Natl. Acad. Sci. USA*, 96: 4420–4425, 1999.

[47] D.M. Freeman, C.C. Abnet, W. Hemmert, B.S. Tsai, and T.F. Weiss. Dynamic material properties of the tectorial membrane: a summary. *Hear. Res.*, 180:1–10, 2003.

[48] D.M. Freeman, K. Masaki, A.R. McAllister, J.L. Wei, and T.F. Weiss. Static material properties of the tectorial membrane: a summary. *Hear. Res.*, 180:11–27, 2003.

[49] A. Fridberger, J. Boutet de Monvel, and M. Ulfendahl. Internal shearing within the hearing organ evoked by basilar membrane motion. *J. Neurosci.*, 22:9850–9857, 2002.

[50] T. Fukazawa, K. Ishida, and Y. Murai. A micromechanical model of the cochlea with radial movement of the tectorial membrane. *Hear. Res.*, 137:59–67, 1999.

[51] J.E. Gale and J.F. Ashmore. Charge displacement induced by rapid stretch in the basolateral membrane of the guinea-pig outer hair cell. *Proc. R. Soc. Lond. [Biol]*, 255:243–249, 1994.

[52] C. Gerthsen, H.O. Kneser, and H. Vogel. *Physik*, volume 16. Springer-Verlag, Berlin, 1992.

[53] F. Gittes, B. Mickey, J. Nettleton, and J. Howard. Flexural rigidity of microtubules and actin filaments measured from thermal fluctuations in shape. *J. Cell Biol.*, 120: 923–934, 1993.

[54] D.M. Green. Auditory intensity discrimination. In W.A. Yost, A.N. Popper, and R.R. Fay, editors, *Human Psychophysics*, pages 13–55, Berlin, 1993. Springer Verlag.

[55] K. Grosh, J.F. Zheng, Y. Zou, E. de Boer, and A.L. Nuttall. High-frequency electromotile responses in the cochlea. *J. Acoust. Soc. Am.*, 115:2178–2184, 2004.

[56] J.J. Guinan, T. Lin, and H. Cheng. Abstract #1001: Medial-efferent stimulation can inhibit the earliest peak of click responses from cat single auditory-nerve fibers. In P.A. Santi, editor, *Abstracts of the 27th annual midwinter research meeting of the ARO*, page 340, Mt. Royal, 2004. Association for Research in Otolaryngology.

[57] A.W. Gummer, W. Hemmert, and H.-P. Zenner. Resonant tectorial membrane motion in the inner ear: Its crucial role in frequency tuning. *Proc. Natl. Acad. Sci. USA*, 93:8727–8732, 1996.

[58] A.W. Gummer, B.M. Johnstone, and N.J. Armstrong. Direct measurement of basilar membrane stiffness in the guinea pig. *J. Acoust. Soc. Am.*, 70:1298–1309, 1981.

[59] P. Hagedorn. *Technische Schwingungslehre*. Springer-Verlag, Berlin, 2nd edition, 1989.

[60] R. Hallworth. Passive compliance and active force generation in the guinea pig outer hair cell. *J. Neurophysiol.*, 74:2319–2328, 1995.

[61] J.A. Halter, R.P. Kruger, M.J. Yium, and W.E. Brownell. The influence of the subsurface cisterna on the electrical properties of the outer hair cell. *Neuroreport*, 8:2517–2521, 1997.

[62] H.G. Hansma. Varieties of imaging with scanning probe microscopes. *Proc. Natl. Acad. Sci. USA*, 96:14678–14680, 1999.

[63] D.Z.Z. He, S.P. Jia, and P. Dallos. Prestin and the dynamic stiffness of cochlear outer hair cells. *J. Neurosci.*, 23:9089–9096, 2003.

[64] W. Hemmert, H.-P. Zenner, and A.W. Gummer. Three-dimensional motion of the organ of corti. *Biophys. J.*, 78:2285–2297, 2000.

[65] G.D. Housley and J.F. Ashmore. Ionic currents of outer hair cells isolated from the guinea-pig cochlea. *J. Physiol.*, 448:73–98, 1992.

[66] A. Hubbard. A traveling-wave amplifier model of the cochlea. *Science*, 259:68–71, 1993.

[67] A.E. Hubbard and D.C. Mountain. Alternating current delivered into the scala media alters sound pressure at the eardrum. *Science*, 222:510–512, 1983.

[68] A.E. Hubbard, D.C. Mountain, and F. Chen. Time-domain responses from a nonlinear sandwich model of the cochlea. In A.W. Gummer, editor, *Biophysics of the Cochlea: from Molecules to Models*, pages 351–358, New Jersey, London, Singapore, Hong Kong, 2003. World Scientific.

[69] A.E. Hubbard, Z. Yang, L. Shatz, and D.C. Mountain. Multi-mode cochlear models. In H. Wada, T. Takasaka, K. Ikeda, K. Ohyama, and T. Koike, editors, *Recent Developments in Auditory Mechanics*, pages 167–173, Singapore, 1999. World Scientific.

[70] A.J. Hudspeth. Mechanical amplification of stimuli by hair cells. *Curr. Opin. Neurobiol.*, 7:480–486, 1997.

[71] A.J. Hudspeth and D.P. Corey. Sensitivity, polarity, and conductance change in the response of vertebrate hair cells to controlled mechanical stimuli. *Proc. Natl. Acad. Sci. USA*, 74:2407–2411, 1977.

[72] K.H. Iwasa. Effect of stress on the membrane capacitance of the auditory outer hair cell. *Biophys. J.*, 65:492–498, 1993.

[73] K.H. Iwasa and M. Adachi. Force generation in the outer hair cell of the cochlea. *Biophys. J.*, 73:546–555, 1997.

[74] K.H. Iwasa and R.S. Chadwick. Elasticity and active force generation of cochlear outer hair cells. *J. Acoust. Soc. Am.*, 92:3169–3173, 1992.

[75] A.F. Jahn and J. Santos-Sacchi, editors. *Physiology of the Ear*. Raven Press, New York, 1988.

[76] F. Jaramillo and A.J. Hudspeth. Localization of the hair cell's transduction channels at the hair bundle's top by iontophoretic application of a channel blocker. *Neuron*, 7:409–420, 1991.

[77] B.M. Johnstone, R. Patuzzi, and G.K. Yates. Basilar membrane measurements and the travelling wave. *Hear. Res.*, 22:147–153, 1986.

[78] S. Kakehata and J. Santos-Sacchi. Membrane tension directly shifts voltage dependence of outer hair cell motility and associated gating charge. *Biophys. J.*, 68: 2190–2197, 1995.

[79] F. Kalinec, M.C. Holley, K.H. Iwasa, D.J. Lim, and B. Kachar. A membrane-based force generation mechanism in auditory sensory cells. *Proc. Natl. Acad. Sci. USA*, 89:8671–8675, 1992.

[80] R.P. Kanwal. Vibrations of an elliptic cylinder and a flat plate in a viscous fluid. *Z. Angew. Math. Mech.*, 35:17–22, 1955.

[81] K.D. Karavitaki and D.C. Mountain. Is the cochlear amplifier a fluid pump? In A.W. Gummer, editor, *Biophysics of the Cochlea: from Molecules to Models*, pages 310–311, New Jersey, London, Singapore, Hong Kong, 2003. World Scientific.

[82] E. Kawasaki, N. Hattori, E. Miyamoto, T. Yamashita, and C. Inagaki. Single-cell RT-PCR demonstrates expression of voltage-dependent chloride channels (CLC-1, CLC-2 and CLC-3) in outer hair cells of rat cochlea. *Brain Res.*, 838:166–170, 1999.

[83] S.M. Khanna and D.G. Leonard. Basilar membrane tuning in the cat cochlea. *Science*, 215:305–306, 1982.

[84] S.M. Khanna, M. Ulfendahl, and A. Flock. Mechanical response of the outer hair cell region of the isolated guinea pig cochlea in vitro. In J.P. Wilson and D.T. Kemp, editors, *Cochlear Mechanisms*, pages 387–392, London, 1988. Plenum Press.

[85] W. Kolmer. Das Gehörorgan. In W. von Möllendorf, editor, *Handbuch der mikroskopischen Anatomie des Menschen*, volume 3, pages 250–478, Berlin, 1927. Springer Verlag.

[86] P.J. Kolston. Comparing in vitro, in situ, and in vivo experimental data in a three-dimensional model of mammalian cochlear mechanics. *Proc. Natl. Acad. Sci. USA*, 96:3676–3681, 1999.

[87] P.J. Kolston. The importance of phase data and model dimensionality to cochlear mechanics. *Hear. Res.*, 145:25–36, 2000.

[88] T. Konishi. Some observations on negative endocochlear potential during anoxia. *Acta Otolaryngol. (Stockh.)*, 87:505–516, 1979.

[89] Deutsches Grünes Kreuz.

[90] A. Kronester-Frei. The effect of changes in endolymphatic ion concentrations on the tectorial membrane. *Hear. Res.*, 1:81–94, 1979.

[91] M. Kössl and M. Vater. Cochlear structure and function in bats. In A.N. Popper and R.R. Fay, editors, *Hearing by Bats*, pages 191–234, Berlin, 1995. Springer.

[92] L. Lagostena, A. Cicuttin, J. Inda, B. Kachar, and F. Mammano. Frequency dependence of electrical coupling in Deiters' cells of the guinea pig cochlea. *Cell Commun. Adhes.*, 8:393–399, 2001.

[93] L.D. Landau and E.M. Lifshitz. *Theory of Elasticity*. Pergamon, Oxford, 1970.

[94] M.C. Liberman, J. Gao, D.Z.Z. He, X. Wu, S. Jia, and J. Zuo. Prestin is required for electromotility of the outer hair cell and for the cochlear amplifier. *Nature*, 419: 300–304, 2002.

[95] D.R. Lide, editor. *CRC Handbook of Chemistry and Physics*. Chapman & Hall / CRC Press, 1999.

[96] D.J. Lim. Cochlear anatomy related to cochlear micromechanics. a review. *J. Acoust. Soc. Am.*, 67:1686–1695, 1980.

[97] D.J. Lim and W.C. Lane. Cochlear sensory epithelium. a scanning electron microscopic observation. *Ann. Otol. Rhinol. Laryngol.*, 78:827–841, 1969.

[98] K.-M. Lim and C.R. Steele. A three-dimensional nonlinear active cochlear model analyzed by the wkb-numeric method. *Hear. Res.*, 170:190–205, 2002.

[99] X.Z. Liu, X.M. Ouyang, X.J. Xia, J. Zheng, A. Pandya, F. Li, L.L. Du, K.O. Welch, C. Petit, R.J.H. Smith, B.T. Webb, D. Yan, K.S. Arnos, D. Corey, P. Dallos, W.E. Nance, and Z.Y. Chen. Prestin, a cochlear motor protein, is defective in non-syndromic hearing loss. *Hum. Mol. Genet.*, 12:1155–1162, 2003.

[100] H. Maier, C. Zinn, A. Rothe, H. Tiziani, and A.W. Gummer. Development of a narrow water-immersion objective for laserinterferometric and electrophysiological applications in cell biology. *J. Neurosci. Methods*, 77:31–41, 1997.

[101] F. Mammano and R. Nobili. Biophysics of the cochlea: Linear approximation. *J. Acoust. Soc. Am.*, 93:3320–3332, 1993.

[102] W. Marcotti and C.J. Kros. Developmental expression of the potassium current ik,n contributes to maturation of mouse outer hair cells. *J. Physiol.*, 520:653–660, 1999.

[103] C.E. Miller. Structural implications of basilar membrane compliance measurements. *J. Acoust. Soc. Am.*, 77:1465–1474, 1985.

[104] M. Müller. The cochlear place-frequency map of the adult and developing mongolian gerbil. *Hear. Res.*, 94:148–156, 1996.

[105] B.C.J. Moore. Frequency analysis and pitch perception. In W.A. Yost, A.N. Popper, and R.R. Fay, editors, *Human Psychophysics*, pages 56–115, Berlin, 1993. Springer Verlag.

[106] D.C. Mountain and A.R. Cody. Multiple modes of inner hair cell stimulation. *Hear. Res.*, 132:1–14, 1999.

[107] D.C. Mountain and A.E. Hubbard. Rapid force production in the cochlea. *Hear. Res.*, 42:195–202, 1989.

[108] D.C. Mountain and A.E. Hubbard. A piezoelectric model of outer hair cell function. *J. Acoust. Soc. Am.*, 95:350–354, 1994.

[109] M.J.P. Musgrave. *Crystal acoustics*. Holden-Day, San Francisco, 1970.

[110] R.C. Naidu and D.C. Mountain. Measurements of the stiffness map challenge a basic tenet of cochlear theories. *Hear. Res.*, 124:124–131, 1998.

[111] R.C. Naidu and D.C. Mountain. Longitudinal coupling in the basilar membrane. *J. Assoc. Res. Otolaryngol.*, 2:257–267, 2001.

[112] S.S. Narayan, A.N. Temchin, A. Recio, and M.A. Ruggero. Frequency tuning of basilar membrane and auditory nerve fibers in the same cochleae. *Science*, 282: 1882–1884, 1998.

[113] S.T. Neely. Mathematical modeling of cochlear mechanics. *J. Acoust. Soc. Am.*, 78:345–352, 1985.

[114] S.T. Neely and D.O. Kim. A model for active elements in cochlear biomechanics. *J. Acoust. Soc. Am.*, 79:1472–1480, 1986.

[115] S.T. Neely and L.J. Stover. Otoacoustic emissions from a nonlinear, active model of cochlear mechanics. In H. Duifhuis, J.W. Horst, P. van Dijk, and S.M. van Netten, editors, *Biophysics of hair cell sensory systems*, pages 64–71, Singapore, 1993. World Scientific.

[116] K.E. Nilsen and I.J. Russell. Timing of cochlear feedback: Spatial and temporal representation of a tone across the basilar membrane. *Nat. Neurosci.*, 2:642–648, 1999.

[117] K.E. Nilsen and I.J. Russell. The spatial and temporal representation of a tone on the guinea pig basilar membrane. *Proc. Natl. Acad. Sci. USA*, 97:11751–11758, 2000.

[118] R. Nobili and F. Mammano. Biophysics of the cochlea: II. stationary nonlinear phenomenology. *J. Acoust. Soc. Am.*, 99:2244–2255, 1996.

[119] M. Nowotny, H.-P. Zenner, and A.W. Gummer. Abstract #1002: Impact of outer hair cell electromotility on organ of corti vibration - results from an in-situ preparation. In P.A. Santi, editor, *Abstracts of the 27th annual midwinter research meeting of the ARO*, page 340, Mt. Royal, 2004. Association for Research in Otolaryngology.

[120] A.L. Nuttall and D.F. Dolan. Steady-state sinusoidal velocity responses of the basilar membrane in guinea pig. *J. Acoust. Soc. Am.*, 99:1556–1565, 1996.

[121] A.L. Nuttall, M. Guo, and T. Ren. The radial pattern of basilar membrane motion evoked by electric stimulation of the cochlea. *Hear. Res.*, 131:39–46, 1999.

[122] A.L. Nuttall and T. Ren. Electromotile hearing: Evidence from basilar membrane motion and otoacoustic emissions. *Hear. Res.*, 92:170–177, 1995.

[123] D. Oliver, D.Z. He, N. Klocker, J. Ludwig, U. Schulte, S. Waldegger, J.P. Ruppersberg, P. Dallos, and B. Fakler. Intracellular anions as the voltage sensor of prestin, the outer hair cell motor protein. *Science*, 292:2340–2343, 2001.

[124] E.S. Olson. Intracochlear pressure measurements related to cochlear tuning. *J. Acoust. Soc. Am.*, 110:349–367, 2001.

[125] E.S. Olson and D.C. Mountain. In vivo measurement of basilar membrane stiffness. *J. Acoust. Soc. Am.*, 89:1262–1275, 1991.

[126] A.A. Parthasarathi, K. Grosh, J.F. Zheng, and A.L. Nuttall. Effect of current stimulus on in vivo cochlear mechanics. *J. Acoust. Soc. Am.*, 113:442–452, 2003.

[127] R. Patuzzi, B.M. Johnstone, and P.M. Sellick. The alteration of the vibration of the basilar membrane produced by loud sound. *Hear. Res.*, 13:99–100, 1984.

[128] J.O. Pickles. *An Introduction to the Physiology of Hearing.* Academic Press, London, 2nd edition, 1988.

[129] S. Plontke and H.-P. Zenner. Aktuelle Gesichtspunkte zu Hörschäden durch Berufs- und Freizeitlärm. *Laryngo-Rhino-Otol.*, 83:S122–S164, 2004.

[130] S. Preyer, S. Renz, W. Hemmert, H.-P. Zenner, and A.W. Gummer. Receptor potential of outer hair cells isolated from base to apex of the adult guinea-pig cochlea: Implications for cochlear tuning mechanisms. *Aud. Neurosci.*, 2:145–157, 1996.

[131] U. Rabe, K. Janser, and W. Arnold. Vibrations of free and surface-coupled atomic force microscope cantilevers: Theory and experiment. *Rev. Sci. Inst.*, 67:3281–3293, 1996.

[132] M. Radmacher, R.W. Tillmann, and H.E. Gaub. Imaging viscoelasticity by force modulation with the atomic force microscope. *Biophys. J.*, 64:735–742, 1993.

[133] J.T. Ratnanather, A.S. Popel, and W.E. Brownell. An analysis of the hydraulic conductivity of the extracisternal space of the cochlear outer hair cell. *J. Math. Biol.*, 40:372–382, 2000.

[134] A. Recio, N.C. Rich, S.S. Narayan, and M.A. Ruggero. Basilar-membrane responses to clicks at the base of the chinchilla cochlea. *J. Acoust. Soc. Am.*, 103:1972–1989, 1998.

[135] G. Reuter, A.H. Gitter, U. Thurm, and H.-P. Zenner. High frequency radial movements of the reticular lamina induced by outer hair cell motility. *Hear. Res.*, 60: 236–246, 1992.

[136] G. Reuter and H.-P. Zenner. Active radial and transverse motile responses of outer hair cells in the organ of corti. *Hear. Res.*, 43:219–230, 1990.

[137] C.-P. Richter and P. Dallos. Micromechanics in the gerbil hemicochlea. In A.W. Gummer, editor, *Biophysics of the Cochlea: from Molecules to Models*, pages 278–284, New Jersey, London, Singapore, Hong Kong, 2003. World Scientific.

[138] C.-P. Richter, B.N. Evans, R. Edge, and P. Dallos. Basilar membrane vibration in the gerbil hemicochlea. *J. Neurophysiol.*, 79:2255–2264, 1998.

[139] L. Robles and M.A. Ruggero. Mechanics of the mammalian cochlea. *Physiol. Rev.*, 81:1305–1352, 2001.

[140] L. Robles, M.A. Ruggero, and N.C. Rich. Basilar membrane mechanics at the base of the chinchilla cochlea. i. input-output functions, tuning curves, and response phases. *J. Acoust. Soc. Am.*, 80:1364–1374, 1986.

[141] L. Rosenhead. *Laminar Boundary Layers.* Clarendon, Oxford, 1963.

[142] M.A. Ruggero, S.S. Narayan, A.N. Temchin, and A. Recio. Mechanical bases of frequency tuning and neural excitation at the base of the cochlea: Comparison of basilar-membrane vibrations and auditory-nerve-fiber responses in chinchilla. *Proc. Natl. Acad. Sci. USA*, 97:11744–11750, 2000.

[143] M.A. Ruggero and N.C. Rich. Furosemide alters organ of corti mechanics: Evidence for feedback of outer hair cells upon the basilar membrane. *J. Neurosci.*, 11:1057–1067, 1991.

[144] M.A. Ruggero, N.C. Rich, and A. Recio. The effect of intense acoustic stimulation on basilar-membrane vibrations. *Aud. Neurosci.*, 2:329–345, 1996.

[145] M.A. Ruggero, N.C. Rich, A. Recio, S.S. Narayan, and L. Robles. Basilar-membrane responses to tones at the base of the chinchilla cochlea. *J. Acoust. Soc. Am.*, 101:2151–2163, 1997.

[146] I. Russell and C. Schauz. Salicylate ototoxicity: Effects on the stiffness and electromotility of outer hair cells isolated from the guinea pig cochlea. *Aud. Neurosci.*, 1:309–319, 1995.

[147] I.J. Russell, A.R. Cody, and G.P. Richardson. The responses of inner and outer hair cells in the basal turn of the guinea-pig cochlea and in the mouse cochlea grown in vitro. *Hear. Res.*, 22:199–216, 1986.

[148] I.J. Russell and K.E. Nilsen. The location of the cochlear amplifier: Spatial representation of a single tone on the guinea pig basilar membrane. *Proc. Natl. Acad. Sci. USA*, 94:2660–2664, 1997.

[149] I.J. Russell, G.P. Richardson, and A.R. Cody. Mechanosensitivity of mammalian auditory hair cells in vitro [published erratum appears in Nature 1986 Jun 26-Jul 2;321(6073): 888]. *Nature*, 321:517–519, 1986.

[150] I.J. Russell and P.M. Sellick. Low-frequency characteristics of intracellularly recorded receptor potentials in guinea-pig cochlear hair cells. *J. Physiol.*, 338: 179–206, 1983.

[151] V. Rybalchenko and J. Santos-Sacchi. Cl- flux through a non-selective, stretch-sensitive conductance influences the outer hair cell motor of the guinea-pig. *J. Physiol.*, 547:873–891, 2003.

[152] J.E. Sader. Frequency response of cantilever beams immersed in viscous fluids with applications to the atomic force microscope. *J. Appl. Phys.*, 84:64–76, 1998.

[153] J.E. Sader, J.M. Chon, and P. Mulvaney. Calibration of rectangular atomic force microscope cantilevers. *Rev. Sci. Inst.*, 70:3967–3969, 1999.

[154] A.N. Salt, I. Melichar, and R. Thalmann. Mechanisms of endocochlear potential generation by stria vascularis. *Laryngoscope*, 97:984–991, 1987.

[155] J. Santos-Sacchi. Reversible inhibition of voltage-dependent outer hair cell motility and capacitance. *J. Neurosci.*, 11:3096–3110, 1991.

[156] J. Santos-Sacchi and J.P. Dilger. Whole cell currents and mechanical responses of isolated outer hair cells. *Hear. Res.*, 35:143–150, 1988.

[157] J. Santos-Sacchi, W. Shen, J. Zheng, and P. Dallos. Effects of membrane potential and tension on prestin, the outer hair cell lateral membrane motor protein. *J. Physiol.*, 531:661–666, 2001.

[158] T.E. Schäffer, J.P. Cleveland, F. Ohnesorge, D.A. Walters, and P.K. Hansma. Studies of vibrating atomic force microscope cantilevers in liquid. *J. Appl. Phys.*, 80:3622–3627, 1996.

[159] M.P. Scherer, G. Frank, and A.W. Gummer. Experimental determination of the mechanical impedance of atomic force microscopy cantilevers in fluids up to 70 khz. *J. Appl. Phys.*, 88:2912–2920, 2000.

[160] M.P. Scherer and A.W. Gummer. Impedance analysis of the organ of corti with magnetically actuated probes. *Biophys. J.*, 87:1378–1391, 2004.

[161] M.P. Scherer, M. Nowotny, E. Dalhoff, H.-P. Zenner, and A.W. Gummer. High-frequency vibration of the organ of corti in vitro. In A.W. Gummer, editor, *Biophysics of the Cochlea: from Molecules to Models*, pages 271–277, New Jersey, London, Singapore, Hong Kong, 2003. World Scientific.

[162] P.M. Sellick, R. Patuzzi, and B.M. Johnstone. Measurement of basilar membrane motion in the guinea pig using the Mössbauer technique. *J. Acoust. Soc. Am.*, 72: 131–141, 1982.

[163] P.M. Sellick, R. Patuzzi, and B.M. Johnstone. Comparison between the tuning properties of inner hair cells and basilar membrane motion. *Hear. Res.*, 10:93–100, 1983.

[164] P.M. Sellick and I.J. Russell. The responses of inner hair cells to basilar membrane velocity during low frequency auditory stimulation in the guinea pig cochlea. *Hear. Res.*, 2:439–445, 1980.

[165] W.F. Sewell. The effects of furosemide on the endocochlear potential and auditory-nerve fiber tuning curves in cats. *Hear. Res.*, 14:305–314, 1984.

[166] D.M. Shah, D.M. Freeman, and T.F. Weiss. The osmotic response of the isolated, unfixed mouse tectorial membrane to isosmotic solutions: Effect of Na^+, K^+, and Ca^{2+} concentration. *Hear. Res.*, 87:187–207, 1995.

[167] L.R. Shao, R. Halvorsrud, L. Borg-Graham, and J.F. Storm. The role of BK-type Ca^{2+}-dependent K^+ channels in spike broadening during repetitive firing in rat hippocampal pyramidal cells. *J. Physiol.*, 521:135–146, 1999.

[168] Y. Shinomori, D.S. Spack, D.D. Jones, and R.S. Kimura. Volumetric and dimensional analysis of the guinea pig inner ear. *Ann. Otol. Rhinol. Laryngol.*, 110:91–98, 2001.

[169] N. Slepecky and S.C. Chamberlain. Distribution and polarity of actin in the sensory hair cells of the chinchilla cochlea. *Cell Tissue Res.*, 224:15–24, 1982.

[170] N.B. Slepecky. Structure of the mammalian cochlea. In P. Dallos, A.N. Popper, and R.R. Fay, editors, *The Cochlea*, pages 44–129, New York, 1996. Springer.

[171] A.A. Spector, W.E. Brownell, and A.S. Popel. Effect of outer hair cell piezoelectricity on high-frequency receptor potentials. *J. Acoust. Soc. Am.*, 113:453–461, 2003.

[172] K.P. Steel. The tectorial membrane of mammals. *Hear. Res.*, 9:327–359, 1983.

[173] C.R. Steele. Toward three-dimensional analysis of cochlear structure. *ORL J. Otorhinolaryngol. Relat. Spec.*, 61:238–251, 1999.

[174] C.R. Steele and K.M. Lim. Cochlear model with three-dimensional fluid, inner sulcus and feed-forward mechanism. *Audiol. Neurootol.*, 4:197–203, 1999.

[175] C.R. Steele and S. Puria. Analysis of forces on inner hair cell cilia. In A.W. Gummer, editor, *Biophysics of the Cochlea: from Molecules to Models*, pages 359–367, New Jersey, London, Singapore, Hong Kong, 2003. World Scientific.

[176] I. Tasaki and C.S. Spyropoulos. Stria vascularis as source of endocochlear potential. *J. Neurophysiol.*, 22:149–155, 1959.

[177] L.G. Tilney, D.J. DeRosier, and M.J. Mulroy. The organization of actin filaments in the stereocilia of cochlear hair cells. *J. Cell Biol.*, 86:244–259, 1980.

[178] S. Timoshenko and D.H. Young. *Elements of Strength of Materials*, volume 5. D. van Nostrand Co. Inc., New Jersey, 1968.

[179] J.A. Tolomeo and M.C. Holley. Mechanics of microtubule bundles in pillar cells from the inner ear. *Biophys. J.*, 73:2241–2247, 1997.

[180] J.A. Tolomeo and C.R. Steele. A dynamic model of outer hair cell motility including intracellular and extracellular fluid viscosity. *J. Acoust. Soc. Am.*, 103:524–534, 1998.

[181] Druckkammerzentrum Traunstein, 2004.

[182] J. Tsuji and M.C. Liberman. Intracellular labeling of auditory nerve fibers in guinea pig: Central and peripheral projections. *J. Comp. Neurol.*, 381:188–202, 1997.

[183] E.O. Tuck. Calculation of unsteady flows due to small motions of cylinders in a viscous fluid. *J. Eng. Math.*, 3:29–44, 1969.

[184] S.V. Tyablikov. *Methods in the Quantum Theory of Magnetism*. Plenum, New York, 1967.

[185] M. Ulfendahl, J. Boutet de Monvel, and A. Fridberger. Visualizing cochlear mechanics using confocal microscopy. In A.W. Gummer, editor, *Biophysics of the Cochlea: from Molecules to Models*, pages 285–291, New Jersey, London, Singapore, Hong Kong, 2003. World Scientific.

[186] M. Ulfendahl, Å. Flock, and E. Scarfone. Structural relationships of the unfixed tectorial membrane. *Hear. Res.*, 151:41–47, 2001.

[187] N.F. Viemeister and C.J. Plack. Time analysis. In W.A. Yost, A.N. Popper, and R.R. Fay, editors, *Human Psychophysics*, pages 116–154, Berlin, 1993. Springer Verlag.

[188] M.A. Viergever and R.J. Diependaal. Simultaneous amplitude and phase match of cochlear model calculations and basilar membrane vibration data. In E. de Boer and M.A. Viergever, editors, *Mechanics of hearing*, pages 53–61, The Hague, 1983. Nijhoff.

[189] G. von Békésy. *Experiments in Hearing*. McGraw-Hill, New York, 1960.

[190] P. Wangemann. Comparison of ion transport mechanisms between vestibular dark cells and strial marginal cells. *Hear. Res.*, 90:149–157, 1995.

[191] P. Wangemann, J. Liu, and D.C. Marcus. Ion transport mechanisms responsible for k+ secretion and the transepithelial voltage across marginal cells of stria vascularis in vitro. *Hear. Res.*, 84:19–29, 1995.

[192] E.K. Weitzel, R. Tasker, and W.E. Brownell. Outer hair cell piezoelectricity: Frequency response enhancement and resonance behavior. *J. Acoust. Soc. Am.*, 114: 1462–1466, 2003.

[193] S.J. Williamson and H.Z. Cummins. *Light and Colour in Nature and Art*. Wiley, New York, 1983.

[194] S. Xue, D.C. Mountain, and A.E. Hubbard. Acoustic enhancement of electrically-evoked otoacoustic emissions reflects basilar membrane tuning: Experiment results. *Hear. Res.*, 70:121–126, 1993.

[195] S. Xue, D.C. Mountain, and A.E. Hubbard. Electrically evoked basilar membrane motion. *J. Acoust. Soc. Am.*, 97:3030–3041, 1995.

[196] S. Xue, D.C. Mountain, and A.E. Hubbard. Electrically-evoked otoacoustic emissions: Direct comparisons with basilar membrane motion. *Aud. Neurosci.*, 2:301–308, 1996.

[197] E.N. Yamoah, E.A. Lumpkin, R.A. Dumont, P.J.S. Smith, A.J. Hudspeth, and P.G. Gillespie. Plasma membrane Ca^{2+}-ATPase extrudes Ca^{2+} from hair cell stereocilia. *J. Neurosci.*, 18:610–624, 1998.

[198] G.K. Yates and D.L. Kirk. Cochlear electrically evoked emissions modulated by mechanical transduction channels. *J. Neurosci.*, 18:1996–2003, 1998.

[199] H.P. Zenner, U. Zimmermann, and A.H. Gitter. Fast motility of isolated mammalian auditory sensory cells. *Biochem. Biophys. Res. Commun.*, 149:304–308, 1987.

[200] J. Zheng, W. Shen, D.Z.Z. He, K.B. Long, L.D. Madison, and P. Dallos. Prestin is the motor protein of cochlear outer hair cells. *Nature*, 405:149–155, 2000.

[201] Y. Zou, J.F. Zheng, A.L. Nuttall, and T.Y. Ren. The sources of electrically evoked otoacoustic emissions. *Hear. Res.*, 180:91–100, 2003.

[202] E. Zwicker and H. Fastl. *Psychoacoustics.* Springer Verlag, Berlin, 2nd edition, 1999.

[203] J.J. Zwislocki. Phase opposition between inner and outer hair cells and auditory sound analysis. *Audiology*, 14:443–455, 1975.

[204] J.J. Zwislocki. Mechanical properties of the tectorial membrane in situ. *Acta Otolaryngol. (Stockh.)*, 105:450–456, 1988.

[205] J.J. Zwislocki. Active cochlear feedback: Required structure and response phase. In P.Dallos, C.D. Geisler, J.W. Matthews, M.A. Ruggero, and C.R. Steele, editors, *The mechanics and biophysics of hearing*, pages 114–120, Berlin, 1990. Springer-Verlag.

[206] J.J. Zwislocki and L.K. Cefaratti. Tectorial membrane. II: stiffness measurements in vivo. *Hear. Res.*, 42:211–227, 1989.

[207] J.J. Zwislocki and E.J. Kletsky. Tectorial membrane: A possible effect on frequency analysis in the cochlea. *Science*, 204:639–641, 1979.

Acknowledgments

I am deeply grateful for the support, the patience, and the encouragement from my wife Babette Guhl. Furthermore, I am indebted to my parents, Bärbel and Wolf Scherer, for their support.

I also would like to thank Prof. Anthony W. Gummer, Universitäts-HNO-Klinik, for providing the necessary equipment, for allowing me great latitude in implementing my ideas, for very thoroughly reading my manuscripts, and for critical yet constructive discussions and advice.

I sincerely appreciate the support of Prof. Hanns Ruder, Fakultät für Physik, who readily accepted the subject of this work for a dissertation.

In addition, I would like to thank the former and present members of the Sektion Physiologische Akustik und Kommunikation of the Universitäts-HNO-Klinik, Tübingen, for their cooperation and for stimulating discussions. In particular, Dr. Ernst Dalhoff, Manuela Nowotny, Dr. Jutta Engel, and Dr. Gerhard Frank were of great help.

Finally, I recognize the effort of Prof. Hans-Peter Zenner in supporting a fruitful environment for basic auditory research.

I am indebted to the financial support of the Bundesministerium für Bildung und Forschung (Fö. 01KS9602) and the Deutsche Forschungsgemeinschaft, DFG Gu 194/5-1 and SFB 430 TPA4.